Distribution Agreement

In presenting this thesis or dissertation as a partial fulfillment of the requirements for an advanced degree from Emory University, I hereby grant to Emory University and its agents the non-exclusive license to archive, make accessible, and display my thesis or dissertation in whole or in part in all forms of media, now or hereafter known, including display on the world wide web. I understand that I may select some access restrictions as part of the online submission of this thesis or dissertation. I retain all ownership rights to the copyright of the thesis or dissertation. I also retain the right to use in future works (such as articles or books) all or part of this thesis or dissertation.

Signature:

_____ _____

Heather M. Jackson Date

Structural and functional analysis of NADPH Oxidase 4

By

Heather M. Jackson
Doctor of Philosophy

Graduate Division of Biological and Biomedical Science
Biochemistry, Cell and Developmental Biology

_____
J. David Lambeth, M.D., Ph.D.
Advisor

_____ _____

Xiaodong Cheng, Ph.D.
Committee Member

Criss Hartzell, Ph.D.
Committee Member

_____ _____

John Hepler, Ph.D.
Committee Member

Ichiro Matsumura, Ph.D.
Committee Member

Accepted:

_____
Lisa A. Tedesco, Ph.D.
Dean of the James T. Laney School of Graduate Studies

_____

Date

Structural and functional analysis of NADPH Oxidase 4

By

Heather M. Jackson

B.S., John Carroll University, 2004

Advisor: J. David Lambeth, M.D., Ph.D.

An abstract of

A dissertation submitted to the Faculty of the James T. Laney School of Graduate Studies

of Emory University

in partial fulfillment of the requirements for the degree of

Doctor of Philosophy

In

Graduate Division of Biological and Biomedical Science

Biochemistry, Cell and Developmental Biology

2010

Abstract

Structural and functional analysis of NADPH Oxidase 4

By Heather M. Jackson

NADPH oxidases (Nox) are a family of integral membrane oxidoreductases that catalyze the transfer of electrons from NADPH to molecular oxygen producing superoxide anion and secondary reactive oxygen species (ROS). These ROS react with proteins or microbes linking Nox enzymes to important roles in cell signaling and innate immunity. All seven mammalian isoforms (Nox1-5, Duox1-2) are composed of a heme-binding transmembrane domain and an NADPH- and FAD-binding dehydrogenase domain. Unlike the regulatory subunit dependent Nox1-3 or EF-hand containing Nox5 and Duox1/2, Nox4 displays spontaneous activity. We hypothesize that Nox4 provides a likely model for the active conformation of other Nox isoforms.

In an effort to understand the structural features of these enzymes that control activity, we used a combination of computational modeling and molecular evolution analysis to identify regions of the enzymes of possible functional significance and tested these predictions. A Nox4 dehydrogenase domain homology model was constructed using crystal structures of the ferredoxin reductase super-family as templates. This model along with a model of the heme-binding domain predicted the B-loop of the transmembrane domain is in contact with the dehydrogenase domain in the holo-enzyme. We used fluorescence polarization to detect and characterize an interaction between recombinant Nox4 dehydrogenase domain and Nox4 B-loop peptides, consistent with the model prediction. This interaction is also detected in Nox2 and mutations in the B-loop that abolish these interactions also inhibit Nox2 or Nox4 activity, implying a functional role for the B-loop: dehydrogenase domain interaction.

Comparisons between the Nox4 dehydrogenase domain model and similar structures identified important ligand-binding sites and insertions in the Nox/Duox family absent in the other structures. We hypothesize that these differences in the Nox/Duox family sequences mediate the regulatory mechanisms seen with the various Nox/Duox isoforms. Chimera proteins of Nox2 and Nox4 identify the dehydrogenase domain as being the part of the protein responsible for determining subunit-dependent or spontaneous activity. Furthermore, recombinant Nox4 dehydrogenase domain, but not Nox1, Nox2 or Nox5 exhibits constitutive electron transferase activity. This structural and functional analysis of the Nox enzymes improves our understanding of how these enzymes work and provides a framework to aid in specific drug design.

Structural and functional analysis of NADPH Oxidase 4

By

Heather M. Jackson

B.S. John Carroll University

Advisor: J. David Lambeth, M.D., Ph.D.

A dissertation submitted to the Faculty of the

James T. Laney School of Graduate Studies of Emory University

in partial fulfillment of the requirements for the degree of Doctor of Philosophy

in

Graduate Division of Biological and Biomedical Science

Biochemistry, Cell and Developmental Biology

2010

Acknowledgements

There are a few people who I would like to acknowledge as being vital to the completion of this thesis. First, I would like to thank Dr. Tsukasa Kawahara for his patience, counsel, mentorship and support. I worked with Tsukasa during my rotation, and decided then that he endowed all of the traits of the scientist I wanted to be. Second, I am indebted to Dr. Dave Lambeth for his support and respect. The collegial environment that Dave has created in the Lambeth lab is one that promotes scientific growth and independence. I am grateful to the rest of the members of my Lab, Yukio, Becky, James, Susan and Yerun for their discussions, consideration, patience and help. The members of my committee are to be acknowledged for their stimulating scientific discussions and support both in my graduate work and in my career path.

I am grateful beyond expression to my boyfriend, Noel for his patience and encouragement. Noel is truly an inspiration to me both in career and in life. I will forever be grateful to my sisters, Kelly, Erin, Katie and Molly for providing so much support and much needed distractions. Finally, I would like to acknowledge my parents, Jerry and Margie Jackson for their unwavering, unconditional love and support.

Table of Contents

List of Tables and Figures

Chapter 1

Chapter 2

Chapter 3

Chapter 4

Chapter 1

An introduction to the Nox Family of NADPH Oxidases

1.1 NADPH Oxidases and Reactive Oxygen Species

The term reactive oxygen species (ROS) encompasses a wide variety of molecules with varying degrees of reactivity and targets. Superoxide anions, the initial product of most, if not all, NADPH oxidases is converted to hydrogen peroxide either slowly on its own or enzymatically by superoxide dismutase (SOD) (McCord and Fridovich, 1969). Superoxide can release iron from iron/sulfur proteins, and subsequently produce Fe^{2+} for participation in the Fenton reaction with hydrogen peroxide to produce hydroxyl radicals (reviewed (Valko et al., 2007)). Hydroxyl radicals are the strongest oxidizing agents in biological systems showing little specificity towards DNA, proteins and lipids (Buettner, 1993). Hydrogen peroxide, on the other hand does show reactive specificity towards low pKa cysteine residues allowing its use as a signaling molecule (Denu and Tanner, 1998). This ROS, in the presence of chloride ions and myeloperoxidase, forms hypochlorous acid in neutrophils and aids in the killing of invading microbes (Harrison and Schultz, 1976). Superoxide also reacts with nitric oxide causing changes to the cell on two fronts: by producing the highly reactive peroxynitrite molecule and by halting NO-dependent signaling cascades. Peroxynitrite poses a threat to DNA integrity through its reactivity towards guanine bases (Spencer et al., 1996). This molecule is also reactive towards proteins, carbon dioxide and is another source of the toxic hydroxyl radical (Pacher et al., 2007).

Due to the high reactivity of these ROS, living organisms have evolved ways to tightly control their creation and removal. Removal systems are mediated enzymatically by superoxide dismutase (SOD), catalase, peroxiredoxins and glutathione peroxidase (Gpx) or by scavenging compounds, tocopherols (vitamin E), ascorbate (vitamin C),

glutathione, urate or reduced coenzyme Q10 (Valko et al., 2007). Antagonizing these systems are the ROS sources; xanthine oxidase, uncoupled nitric oxide synthase, and uncoupled mitochondrial electron transport chain. However, the major, deliberate source of cellular ROS is from the NADPH oxidases (Winterbourn, 2008).

NADPH oxidases (Nox) are a family of integral membrane enzymes that catalyze the reduction of molecular oxygen producing superoxide anion and secondary ROS. The reactivity of these molecules was originally thought to be detrimental to the cell. However, ROS are now being appreciated as signaling molecules able to target redox sensitivity proteins for the advantage of the cell. NADPH oxidases are found throughout the eukaryotic kingdom. There are seven isoforms expressed in mammals, Nox1, Nox2, Nox3, Nox4, Nox5, Duox1 and Duox2 all from individual genes (Figure 1.1). Fungal Nox isoforms include NoxA, NoxB and NoxC and amoeba contain NoxA and NoxB. A mosquito isoform is called NoxM, while alga contains NoxD. The plant orthologs are called respiratory burst oxidase homologues, (Rboh) of which there are Rboh A-I. Notably, there are as of yet, no known Nox sequences in yeast or bacteria. The common features of all these protein sequences characterizing them in the Nox family are the key components of the core Nox structure (Kawahara et al., 2007). Previously, a molecular evolution analysis was performed on all known Nox/Duox protein sequences and multiple sites within this core region were found to be conserved implying important structural or enzymatic functions (Kawahara et al., 2007).

The core catalytic unit of Nox enzymes is composed of a heme-binding cytochrome b or transmembrane (TM) domain and a dehydrogenase (DH) domain that contains the binding sites for both FAD and NADPH (Segal et al., 1992). Theoretical

approaches such as hydropathy plots and secondary structure prediction programs as well as empirically derived data from epitope mapping point to a structure in which the TM domain consists of six membrane-spanning α-helices connected by five loops, termed loops A-E (Burritt et al., 2001; Imajoh-Ohmi et al., 1992). Loops A, C and E face the extra-cellular or luminal space where oxygen reduction occurs, while loops B and D face the cytoplasmic side of the membrane where the DH domain is also located. Histidine residues located in the third and fifth transmembrane helices coordinate two non-identical b type hemes (called A and B) (Biberstine-Kinkade et al., 2001). Secondary structural prediction programs and significant homology to other flavoproteins indicate that the Nox DH domain consists of two sub-domains; a β-barrel fold that binds FAD connected by a short linker region to an alternating beta strand/helix domain that binds NADPH (Sumimoto et al., 1992; Taylor et al., 1993).

Inhibitors targeting specific redox centers and steady state kinetics of Nox2 support the electron transfer scheme presented in Figure 1.2 (Cross et al., 1984). In this scheme, hydride transfer from NADPH reduces FAD in the DH domain and electrons flow singly through heme A and heme B in the TM domain to molecular oxygen on the opposing side of the membrane. The initial hydride transfer has been proposed as the rate-limiting and activated step by regulatory subunits in Nox2 (Nisimoto et al., 1999). Oxidation of ferrous Nox2, on the other hand, is fast and proportional to the concentration of oxygen (Isogai et al., 1995). Unlike other oxidases, EPR spectroscopy of Nox2 imply a low-spin hexacoordinated heme form suggesting oxygen reduction occurs at the heme edge (Isogai et al., 1995). However, addition of arachidonic acid, a

known activator of Nox2, induces conversion to the pentacoordinated heme state, which would allow ligation with oxygen (Doussiere et al., 1996).

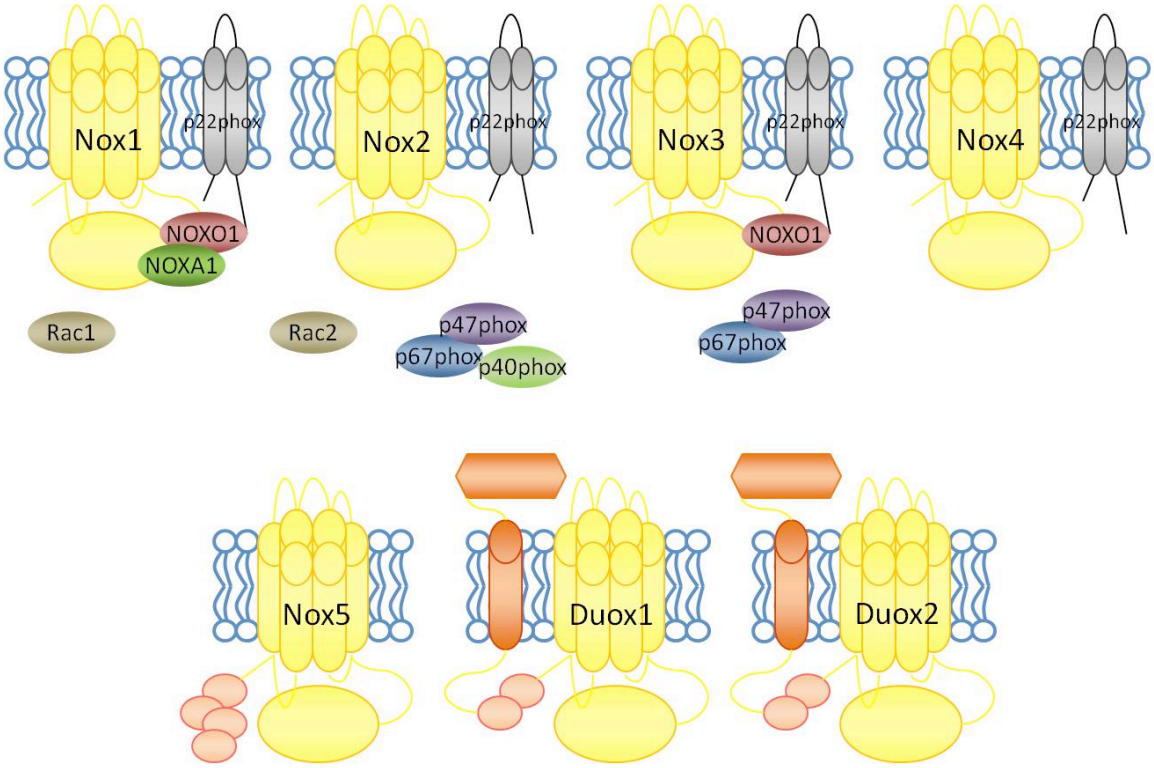

Figure 1.1 Schematic of the Nox/Duox Family.

Nox1-4 heterodimerize with the p22*phox* subunit predicted to contain two transmembrane helices and a long cytoplasmic C-terminal tail. Nox1-3 assemble with cytoplasmic regulatory subunits. Nox1 is regulated by NOXO1, NOXA1 and the small GTPase, Rac1. Nox2 requires assembly with p67*phox*, p47*phox*, p40*phox* as well as Rac1/2. Nox3 is also activated by various combinations of regulatory subunits including p47*phox*/p67*phox* or NOXO1 alone. Nox4 does not appear to require additional cytosolic subunits. Nox5 contains an N-terminal extension composed of four EF-hand motifs depicted as pink circles. Duox1 and Duox2 are predicted to contain two EF-hand motifs, an additional transmembrane helix (orange cylinder) and a peroxidase like domain (orange hexagon) residing on the opposing face of the membrane from the EF-hands and DH domain.

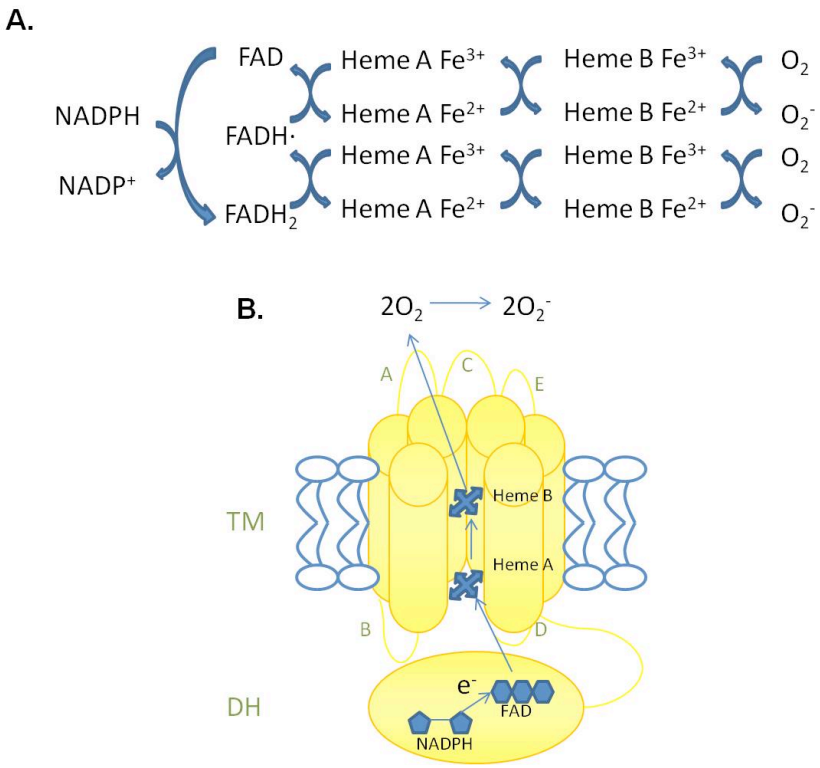

Figure 1.2 Electron transfer scheme of Nox enzymes.

A. A proposed electron transfer scheme within one Nox monomer depicts a hydride transfer from NADPH reducing FAD to the hydroquinone form ($FADH_2$). One electron is then passed from heme A to heme B to the final acceptor, molecular oxygen. One more round of transfer from the semiquinone flavin (FADH) yields a second superoxide molecule. **B.** All Nox/Duox family members are predicted to share the basic structure composed of six transmembrane α-helices connected by extra-cytoplasmic loops A, C and E and two cytoplasmic loops B and D (collectively called the TM domain) extending into cytoplasmic domain. Two heme groups are coordinated by four histidine residues located in transmembrane helices three and five. The large cytoplasmic component forms a dehydrogenase (DH) domain non-covalently binding FAD and NADPH. Blue arrows represent the route of electron transfer through the Nox protein.

1.2 Nox/Duox Enzymes and their roles in Physiology and Pathophysiology

Nox1

Nox1 (Mox1, NOH1) is so named because it was the first described homologue of Nox2 (Banfi et al., 2000; Suh et al., 1999). NCBI lists two splice variants for this gene located on the X chromosome, NADPH oxidase 1 isoform long and long variant. The variant lacks coding sequence for part of the NADPH-binding domain suggesting this protein would not be functional as an electron transferring enzyme. The isoform long is the canonical Nox1 sequence sharing 56% identity with Nox2 (Suh et al., 1999). Nox1 first appears in vertebrata and genes are found in human, chimp, rhesus monkey, guinea pig, cow, mouse, rat, dog, horse, chicken, frog and fish including zebrafish, pufferfish and medaka (Kawahara et al., 2007). Nox1 heterodimerizes with p22*phox* and is activated by Nox-specific regulatory subunits and the small GTPase, Rac1 (see section 1.3 Regulation).

The highest Nox1 expression is found in colon tissue, while lower expression is detected in the prostate, uterus, vascular smooth muscle cells, endothelial cells, pulmonary epithelial cells, hepatocytes and brain tissue including primary microglial cells, astrocytes and neurons (Ago et al., 2005; Banfi et al., 2000; Dai et al., 2006; de Mochel et al., 2010; Goyal et al., 2004; Harrigan et al., 2008; Lassegue et al., 2001; Suh et al., 1999). Lack of reliable antibodies has limited the study of endogenous Nox1 sub-cellular localization. However fusion with a GFP tag showed plasma membrane residence in transfected HEK 293 cells (Helmcke et al., 2009). This report is in agreement with another study demonstrating caveolin co-localization in the plasma

membrane of vascular smooth muscle cells (VSMC) (Hilenski et al., 2004). Nox1 was also localized to intra-cellular vesicles in VSMC (Miller et al., 2007) and microglia (Cheret et al., 2008).

Functions for Nox1 have been implicated in inflammatory pain response in the central nervous system (Ibi et al., 2008), hypoxia signaling in lung cells (Malec et al., 2010), or production of nitric oxide and release of IL-1β in microglia neurotoxicity (Cheret et al., 2008). This isoform is also up-regulated by *Helicobacter pylori* lipopolysaccharide in rodent gut and thought to play a role in host defense (Kawahara et al., 2005a). While these few reports have demonstrated roles for Nox1 in other tissues, this isoform performs multiple roles in the cardiovascular system as well.

Nox1 is expressed in endothelial, smooth muscle and adventitial cells of the vasculature. In endothelial cells, Nox1 mRNA is up-regulated by bone morphogenic protein 4 (BMP4) in response to oscillatory shear stress. Nox1-dependent ROS then stimulates the production of inter-cellular adhesion molecule-1 (ICAM-1) resulting in monocyte adhesion (Sorescu et al., 2004). Nox1 mRNA is also up-regulated by vascular endothelial growth factor (VEGF) in these cells implicating a function of Nox1-ROS in apoptosis and possibly other downstream effects of VEGF stimulation (Kobayashi et al., 2004).

Nox1 expression in vascular smooth muscle cells is up-regulated by a number of stimuli including advanced glycation end products (AGE), aldosterone, Angiotensin II, mechanical stress, low density lipoprotein (LDL), platelet-derived growth factor (PDGF), 12,13-phorbol myristate acetate (PMA), serum, thyroid hormone (T3) and thrombin and

down-regulated by statins (Lassegue and Griendling, 2010). Nox1 knockout mice suggest roles this isoform in extracellular matrix accumulation, proliferation, hypertrophy and migration in VSMC (Gavazzi et al., 2006; Lee et al., 2009). These effects are mediated through signal transduction cascades and it remains to be determined whether this is through direct modulation of redox-sensitive signaling proteins or is the effect of redox controlled transcription.

Nox1 derived ROS are also associated with various disease states. Nox1 message and protein are increased in prostate cancer (Lim et al., 2005) and immortalized keratinocytes (Chamulitrat et al., 2003). Nox1 expression in colon cancer is debatable with some evidence pointing to over-expression, at least in adenomas (Fukuyama et al., 2005; Laurent et al., 2008), while another study showed no significant difference of Nox1 expression between normal and colon cancer tissue (Szanto et al., 2005). A recent study demonstrated that Nox1 is recruited to invadopodia of a colon cancer cell line where it may be involved in extracellular matrix degradation (ECM) (Diaz et al., 2009; Gianni et al., 2009). Depletion of the ECM is a necessary step for cancer cells to migrate and metastasize (Kumar and Weaver, 2009). Invadopodia are rich in tyrosine phosphorylations and it will be interesting to learn whether Nox1-derived ROS modify the kinases and phosphatases that drive this structural formation.

Invadopodia formation is not the only pro-tumor activity of Nox1 in colon cancer. In the colon carcinoma cell line, RKO, exogenous Nox1 inhibited p53 pro-apoptotic transcriptional activity by promoting its deacetylation. Nox1 may also be the source for ROS stimulated cyclin expression and cell cycle progression in Caco-2 cells, a colon adenocarcinoma cell line (Honore et al., 2003). However, this latter study used

diphenylene iodonium (DPI) to show Nox involvement, which is capable of inhibiting all Nox isoforms and Nox4 and Nox5 have also been found in these cells (Cheng et al., 2001).

Nox1 has also been implicated in hypertension, atherosclerosis, aortic dissection, amyotrophic lateral sclerosis (ALS), pancreatitis and osteoporosis (Lambeth et al., 2008). Targeting Nox1 may provide a novel therapeutic option for some of these diseases. Indeed, a recent study showed inhibition of Nox1 blocked Src-induced invadopodia formation and ECM degradation in colon cancer cells (Gianni et al., 2010).

Nox2

Nox2 was not only the first NADPH Oxidase cloned. This isoform is expressed in chordates including humans, chimps, rhesus monkey, mice, rats, dogs, horse, cow, opossum, platypus and frogs (Kawahara et al., 2007).

The initial observation that led to the discovery of ROS producing enzymes was that neutrophils exhibit a large oxygen consumption when exposed to bacteria (Baldridge and Gerard, 1932). This consumption, termed the respiratory burst, would soon be appreciated as a lethal attack on microorganisms by the immune system (Segal, 1981). Clues as to the ROS source came from the discovery that some patients presenting a defective respiratory burst exhibited certain deletions in their X- chromosomes. These patients were diagnosed with chronic granulomatous disease (CGD), characterized by recurrent bacterial and fungal infections leading to abscess and granuloma formations of the liver or intestine (Thrasher et al., 1994). Mapping these deletions of CGD patients to locus Xp21.1 led to the cloning of the gene, CYBB (Royer-Pokora et al., 1986). Around

the same time, researchers were purifying a cytochrome b from the vacuoles of neutrophils that was distinct from those of the ER and mitochondria (Parkos et al., 1987; Segal and Jones, 1978). This cytochrome b was made up of two membrane bound proteins, a ~91 kDa (β subunit) that was heavily glycosylated and a smaller 22 kDa (α subunit) (Parkos et al., 1987). It was then determined that CYBB gene encoded the heavier membraneous protein (Dinauer et al., 1987; Teahan et al., 1987). This cytochrome b became the target of profuse work in the 1970's and 80's leading to its characterization as a terminal oxidase flavoprotein that uses NADPH as a substrate (Babior and Kipnes, 1977). It was subsequently found to be activated by cytosolic 47 kDa and 67 kDa proteins along with a small GTPase (Rac2) (Clark et al., 1990; Knaus et al., 1991). To this day, Nox2 remains the most biochemically characterized Nox protein because of its abundance in neutrophils and high activity stimulated by phagocytosed microorganisms.

Nox2 has multiple aliases that describe some of its physical features such as gp91*phox* for glycosylated protein that migrates at ~91 kDa on a protein gel. The Nox2-p22*phox* heterodimer was first termed cytochrome b_{-245} after its heme midpoint potential at pH 7.0 (later realized to be the average of two hemes with potentials -225 mV and -265 mV). This complex has also been referred to as cytochrome b_{558} for its heme absorption peak at 558 nm (Cross et al., 1981). The name "Nox2" was bestowed to consolidate the nomenclature after the discovery of multiple NADPH oxidase homologues. Nox2 refers to the 91 kDa protein (β subunit) that binds the electron centers and the ~22 kDa component (α subunit) was termed p22*phox*. The active oxidase assembly in

neutrophils is composed of Nox2, p22*phox*, p47*phox*, p67*phox*, p40*phox* and Rac2-GTP (discussed further in Section 1.3).

There are, in fact, multiple forms of CGD including autosomal and X-linked versions. X-linked refers to a defective or null Nox2 component as a result of missense, nonsense or frameshift mutations in the CYBB gene. These mutations result in normal ($X91^{+}$), reduced ($X91^{-}$) or undetectable ($X90^{0}$) amounts of Nox2. Nearly 2/3 of the CGD cases arise from defects in the Nox2 protein (Vignais, 2002). The autosomal form arises from defects in the regulatory subunits, p47*phox*, p22*phox*, p67*phox* and is significantly rarer. Missense mutations resulting in some protein have provided useful tools to probe structure-function relationships of this enzyme complex (Heyworth et al., 2003; Leusen et al., 2000).

Though Nox2 was first discovered though its pivotal role in innate immunity, it has since been found in other cell types where its ROS generation may be linked to cell signaling. In addition to phagocytes, this isoform is also expressed in vascular smooth muscle cells, skeletal muscle, endothelial cells and brain tissue (Infanger et al., 2006; Mofarrahi et al., 2008; Touyz et al., 2002; Van Buul et al., 2005). In endothelial cells, Nox2 derived ROS are important for p38 MAP kinase mediated proliferation and VEGF induced migration (Petry et al., 2006; Ushio-Fukai et al., 2002). In brain tissue, Nox2 is implicated in angiotensin II and NMDA receptor signaling (Sorce and Krause, 2009). Interestingly, there is a high prevalence for cognitive defects in CGD patients that may be independent of the immune disease (Pao et al., 2004). Nox2 is also implicated in multiple disease states of these tissues, including Alzheimer's disease, Parkinson's

disease, ALS, schizophrenia, epilepsy, myocardial infarction and liver ischemia-reperfusion injury (Lambeth et al., 2008).

Nox3

Nox3 was first cloned from commercially available human fetal kidney cDNA (Cheng et al., 2001; Kikuchi et al., 2000). This isoform is 568 amino acids in length and 58% identical to the human Nox2 sequence. Nox3 is the most recent isoform to emerge from the ancestral Nox proteins with its appearance in vertebrates corresponding to around the time of animal transition from water to land. Nox3 genes have been found in chimp, human, monkey, horse, cow, rabbit, mouse, rat, chicken and zebra finch (Kawahara et al., 2007).

Early expression analysis of the Nox3 gene reveals it is located in fetal kidney and to a lesser extent in other fetal tissues including lung, liver, spleen as well as the cell lines HEK 293 (human embryonic kidney) and HepG2 (hepatoma) (Cheng et al., 2001; Kikuchi et al., 2000). Later, Nox3 was found expressed at much higher levels in the inner ear, specifically in the spiral ganglia and organ of Corti (Banfi et al., 2004a). The sub-cellular localization of Nox3 remains to be determined.

Consistent with the emergence of Nox3 during evolution at the time when animals needed the ability to perceive gravity, a function for Nox3 in the development of the otoconia has been revealed. This structure, formed by calcium carbonate, is necessary for the perception of gravity and balance is absent in *het* mutant mice (Paffenholz et al., 2004). The *het* mutation was mapped to defects in the Nox3 protein resulting in the complete absence of a developed otoconia (Paffenholz et al., 2004). These mutant mice

cannot balance, perform abnormally on motor coordination tests, walk with their heads tilted and can only rotate under water rather than swim during the Porsolt force swim test (Paffenholz et al., 2004). A similar phenotype was found with mice carrying mutations mapped to NOXO1 and p22*phox* pointing to a role for these proteins in Nox3 activity and confirming the importance of an active Nox3 complex for the development of this structure (Kiss et al., 2006; Nakano et al., 2008). Though it remains to be determined how Nox3 activity stimulates otoconia development, researchers propose that this enzyme helps to control the pH of the inner ear to create the alkaline environment needed for calcium carbonate crystallization (Nakano et al., 2008). Patients with deletions of chromosome six including the Nox3 gene have hearing impairment among other brain developmental defects suggesting an important role for Nox3 in the inner ear of humans as well (Nagamani et al., 2009).

Nox3 derived ROS have also been implicated in MAP kinase signaling cascades of the hepatoma cell line, HepG2. In these cells, Nox3 mediates insulin induced VEGF expression by SP1 transcription factor activation through p42/44 MAP kinase (Carnesecchi et al., 2006). And through p38 MAP kinase, Nox3 may also lead to palmitate induced insulin resistance (Gao et al., 2010).

Nox4

The fourth Nox isoform was initially called Renox or kidney oxidase (KOX) for its early detection and abundance in kidney tissue (Cheng et al., 2001; Geiszt et al., 2000; Lambeth et al., 2000; Shiose et al., 2001). The gene is located on human chromosome 11 and four splice variants named variants b-e were found in a lung cell line (A549).

However, each of these sequences is missing crucial ligand binding sites, calling into question their feasibility as functional electron transferring enzymes (Goyal et al., 2005). The longest isoform, a, is 578 amino acids in length and is the canonical Nox4 sequence. Aside from the kidney, Nox4 is expressed in endothelial cells, vascular smooth muscle cells, osteoclasts, fibroblasts, keratinocytes, melanoma cells, brain tissue and pancreatic tissue (reviewed (Bedard and Krause, 2007)). Just about every sub-cellular location has been proposed to contain Nox4 including the nucleus, ER, plasma membrane and even the mitochondria (Block et al., 2009; Kuroda et al., 2005; Van Buul et al., 2005; von Lohneysen et al., 2010). While it is possible that Nox4 localizes to multiple compartments and this diversity could be cell type or stimulus dependent, use of over-expression systems and lack of specific antibodies certainly have clouded the issue.

Almost immediately after the discovery of Nox4, the differences between this isoform from the Nox1-3 group became apparent. The Nox4 sequence is more distantly related to Nox2, sharing only about 37% sequence identity (Cheng et al., 2001). Phylogenetic analysis revealed that the Nox4 isoform diverged from ancestral Nox2 prior to the emergence of Nox1 and Nox3 (Kawahara et al., 2007). Nox4 genes appear later in urochordates and are found in human, chimp, monkey, orangutan, horse, cow, rabbit, opossum, dog, platypus, zebra finch, chicken, frog, as well as pufferfish, medaka and sea squirts (Kawahara et al., 2007).

Similar to Nox1-3, Nox4 forms heterodimers with p22*phox* and this in turn mutually stabilizes the two proteins (Ambasta et al., 2004). However, unlike Nox1-3 which are enhanced by or require additional cytosolic regulatory subunits for activity,

Nox4 displays constitutive activity when transfected into HEK 293 or Cos7 (Martyn et al., 2006).

Probably the most peculiar characteristic of Nox4, separating it from the other Nox1-5 isoforms is that researchers can only detect hydrogen peroxide and not superoxide from this enzyme. ROS generation by Nox4 can be measured by hydrogen peroxide detection methods such as amplex red and scopoletin but not with superoxide specific detection methods such as cytochrome *c* and ACP spin trap agent with ESR spectroscopy (Serrander et al., 2007). As of yet, it is unknown why only hydrogen peroxide is detected; either the chemistry is different around the terminal heme binding site allowing direct production of hydrogen peroxide or superoxide dismutation occurs faster than the time it takes for superoxide to react with detection compounds.

The physiological roles of Nox4 differ depending on cell type and stimulus. Multiple lines of evidence suggest Nox4 participation in fibroblast, endothelial and smooth muscle cell proliferation. In fibroblasts, silencing of Nox4 inhibited PDGF induced retinoblastoma protein (rb) phosphorylation (Salmeen et al., 2010). In both fibroblasts and smooth muscle cells, Nox4 mRNA is increased under hypoxia and knockdown of Nox4 decreases proliferation (Ismail et al., 2009; Li et al., 2008). Silencing of Nox4 also reduces BrdU incorporation in the endothelial cell line EaHy929 and cell number in microvascular endothelial cells (Datla et al., 2007; Petry et al., 2006). Conversely, in response to resveratrol, Nox4 appears to induce cell senescence in human umbilical vein endothelial cells (HUVEC) (Schilder et al., 2009). Likewise, transfection of Nox4 decreased growth in fibroblast NIH 3T3 cells (Geiszt et al., 2000; Shiose et al., 2001).

Nox4 is also implicated in both pro- and anti-apoptotic pathways. The presence of Nox4 is needed for 7-ketocholesterol induced apoptosis in smooth muscle cells (Pedruzzi et al., 2004), while silencing of the protein induces apoptosis in pancreatic cancer cells (Mochizuki et al., 2006).

This isoform may function in non-growth cellular pathways as well. Nox4 is thought to play a role in migration of cancer epithelial cells MCF-7 co-cultured with fibroblasts (Tobar et al., 2010) and VSMC in response to insulin-like growth factor 1 (Meng et al., 2008). Nox4 is important for the differentiation of cardiac cells from mouse embryonic stem cells (Li et al., 2006) and myofibroblasts from cardiac fibroblasts (Cucoranu et al., 2005). Differentiated VSMC cells require Nox4 to maintain expression of differentiation markers, smooth muscle MHC, α-actin and calponin (Clempus et al., 2007).

Because of its vast repertoire of participation in cellular processes, it is not surprising that Nox4 is also implicated in multiple disease states such as renal cancer, diabetic nephropathy and pulmonary fibrosis and hypertension (Lambeth et al., 2008).

Nox5

The human Nox5 gene is located on chromosome 15 and multiple splice variants were deposited in the Genbank database. The first report of Nox5 proposed a sequence of 565 amino acids in length, similar to the Nox1-4 isoforms (Cheng et al., 2001). Shortly thereafter, two more sequences were reported, a 737 amino acid Nox5α expressed in spleen tissue and a 719 amino acid Nox5β expressed in the testis (Banfi et al., 2001).

These two variants differ in start codon and have different promoter regions, likely controlling their differential tissue expression.

Nox5 shares about 27% sequence identity with Nox2 and evolved early in eukaryotes. Nox5 first appears in protosomes and deuterosomes and is found in human, chimp, monkey, opossum, chicken, horse, dog, cow, platypus, frog, sea urchin, zebrafish, puffer fish, medaka, fruit fly, honeybee and mosquito genomes (Kawahara et al., 2007; Sumimoto, 2008). The Nox5 gene was lost in rodents preventing the use of knockout rodent model systems for physiological studies. Therefore, much of what is known about Nox5 function comes from studies in mammalian cell and tissue culture systems with the exception of one study performed in fruit flies. This study used RNA interference in fruit flies to establish a role for a Nox5 ortholog (a.k.a. dNox) in smooth muscle contraction (Ritsick et al., 2007).

In mammalian systems, Nox5 is expressed in endothelial cells, vascular smooth muscle cells, spleen, testis lymph tissue and lower expression is found in ovaries, pancreas and placenta (Banfi et al., 2001; Cheng et al., 2001). This isoform has been localized to both the ER and plasma membrane (BelAiba et al., 2007; Kawahara and Lambeth, 2008). Two distinct lines of evidence in endothelial and smooth muscle cells point to a role for Nox5 in cell proliferation. In human aortic smooth muscle cells, silencing of Nox5 abrogated PDGF-induced proliferation via a JAK/STAT signaling pathway (Jay et al., 2008). Transfection of Nox5 in human microvascular endothelial cells (HMEC-1) increased BrdU incorporation, while silencing the gene reduced incorporation (BelAiba et al., 2007). Nox5 also mediates thrombin induced formation of

capillary-like structures in these cells suggesting an additional role in angiogenesis (BelAiba et al., 2007).

Nox5 is also implicated in various ROS mediated disease states. Evidence from the prostate cancer cell line DU 145 suggests Nox5 is important for proliferation, and inhibition of this protein triggers apoptosis (Brar et al., 2003). These same effects are also seen with the short form of Nox5 in Barrett's esophageal adenocarcinoma (Si et al., 2007).

Duox1 and Duox2

Duox1 (a.k.a. ThOX1) and Duox2 (a.k.a. $p138^{Tox}$, ThOX2) were cloned shortly after Nox1 from thyroid cDNA (De Deken et al., 2000; Dupuy et al., 1999). These two isoforms are closely related, sharing 77% identity with respect to their human sequences. These large human Duox1 and 2 genes are both encoded on chromosome 15 and are 1551 and 1548 amino acids in length, respectively (De Deken et al., 2000). Duox1 is expressed in lung and thyroid tissue and to a lesser extent in pancreas, heart, placenta, testis and prostate, while Duox2 is found in the thyroid, as well as kidney, liver, lung, pancreas, prostate, testis and along the intestinal tract (Edens et al., 2001; El Hassani et al., 2005). The structural differences between these proteins and the rest of the Nox family, defining them as Dual Oxidases, lie in the large N-terminal addition consisting of two EF-hand motifs, a transmembrane helix and peroxidase-like domain (Figure 1.1) (Lambeth et al., 2000).

Duox1 or Duox2 genes have been found in human, chimp, monkey, cow, boar, mouse, rats, boar, dog, opossum, platypus, zebra finch, frog, nematodes, chicken, zebra

finch, fugu, medaka, zebra fish, puffer fish, fruit fly, mosquito, honey bee and sea urchin, while sea squirts have four isoforms termed Duox A-D (Kawahara et al., 2007).

Though the Duox peroxidase domains share considerable homology to other peroxidases, lack of conserved heme-ligating residues in the mammalian isoforms questions the feasibility of its functioning as such in mammals (Meitzler and Ortiz de Montellano, 2009). Nevertheless, mutations within this domain correlate with decreased Duox function suggesting some kind of importance for the peroxidase domain whether it be structural or catalytic (Chavez et al., 2009; Vigone et al., 2005). While the function of the peroxidase domain of the mammalian enzyme remains debated, Duox derived ROS can couple with tissue specific peroxidases, supplying hydrogen peroxide substrates for various biochemical reactions. During sea urchin fertilization, a Duox ortholog (Udx1) provides ROS to ovoperoxidase for use in the formation of the fertilization envelope, a necessary egg barrier that blocks polyspermy (Wong et al., 2004). In human thyroid tissue, Duox2 co-localizes with thyroperoxidase (TPO) at the apical membrane of thyrocytes and supplies hydrogen peroxide for the synthesis of thyroid hormones (De Deken et al., 2000; Moreno et al., 2002). Human Duox1 and Duox2 both co-localize with lactoperoxidase (LPO) on mucosal surfaces and may participate in host defense in the lung and intestine (Geiszt et al., 2003).

There are multiple examples of Duox function in lower organisms. The nematode Duox ortholog is important for cross-linking tyrosine residues in cuticle formation (Edens et al., 2001) and in immunity (Vigone et al., 2005). The single Duox gene expressed in zebrafish is found in intestinal epithelial and is important for host defense (Flores et al., 2010). The mosquito Duox ortholog in conjunction with immunomodulatory peroxidase

through protein cross-linking is involved in the midgut immune response (Kumar et al., 2010). And Duox is necessary for fruit fly survival during infection (Ha et al., 2005).

1.3 Activity Regulation of the Nox/Duox Enzymes

Deliberate production and utilization of reactive molecules by organisms comes with the price of ensuring adequate regulation so as to prevent unnecessary damage. In the case of the Nox/Duox family, this regulation is materialized as protein assemblies, ion binding, and post-translational modifications. The proteins that act to directly modify Nox/Duox activity are a collection of common domains that work together to specify not only amount but location of ROS production (Figure 1.3 and Figure 1.4). As enzymes, Nox activity is also dependent on the availability of its substrates and co-factors, though these paradigms have not been explored to the same extent as allosteric control.

The mammalian Nox/Duox family can be sub-divided based on the components directly responsible for activity into the p22*phox*-dependent Noxes (Nox1-4) and the EF-hand containing Noxes (Nox5, Duox1 and Duox2). In addition to Nox5 and Duox1/2, plant rbohD, fungal NoxC and amoeba NoxC all contain EF-hand motifs (Kawahara et al., 2007). Regulatory subunits are encoded in every species known to express Nox1-3 homologues including fungal and amoeba genomes which contain p67*phox* homologues that may participate in regulating NoxA and NoxB (Kawahara and Lambeth, 2007).

p22-phox dependent Nox Sub-family

Nox1, Nox2, Nox3 and Nox4 all form stable heterodimers with the membraneous subunit, p22*phox* (Ambasta et al., 2004; Parkos et al., 1987; Ueno et al., 2005). This interaction is mutually beneficial as increases or decreases in the expression of either the

Nox unit or p22*phox* affects the expression of the other (Ambasta et al., 2004; Yu et al., 1997). Of the p22*phox*-dependent subfamily, Nox1-3 require additional regulatory subunits, while Nox4 exhibits a basal level of constitutive activity in the absence of additional known subunits.

Regulatory subunit-dependent Nox1-3

Nox1, Nox2 and Nox3 form a closely related subgroup of the Nox/Duox family characterized by their sequence similarity and dependence on non-membraneous subunit interactions for activity. These regulatory subunits have specific roles acting to either organize other subunits and sub-cellular localization termed "organizers", or promote electron transfer within the Nox unit termed, "activators". Together with the small GTPase Rac, these organizers and activators complete the Nox1-3 complex promoting ROS production.

Organizers subunits

The organizer subunits are defined by their role in "organizing" the activator subunits at specific sub-cellular locations with a Nox(1-3)-p22*phox* membrane complex. These subunits consist of p47*phox* and its homologues, NOXO1, Tks4/5 or p40*phox*. These subunits all have in common an N-terminal *phox* (PX) domain and 1-5 src-homology 3 (SH3) domains (Figure 1.3). P47*phox* and NOXO1 are closely related organizers with similar domain content and order. Indeed, NOXO1 is thought to have come from a gene duplication of p47*phox* at the time vertebrates began to emerge (Kawahara and Lambeth, 2007). Both proteins possess a PX domain, tandem SH3 domains and a C-terminal proline-rich region (PRR). The PRR of p47*phox*/NOXO1

interacts with the C-terminal SH3 domain of either p67*phox* or NOXA1 (Finan et al., 1994). A crystal structure of the PRR peptide of p47*phox* in complex with the SH3 domain of p67*phox* shows the interaction is mediated by both the PxxP motif and two immediately following helices in p47*phox* (Kami et al., 2002). P47*phox* is necessary for p67*phox* translocation as it is not detected in the membrane of CGD patients without p47*phox* (Heyworth et al., 1991).

Small angle x-ray scattering of p47*phox* suggest this protein exists in multiple conformations; a globular, inactive state and an elongated, active state (Yuzawa et al., 2004). The most recent model of the inactive state conformation is characterized by the autoinhibitory region (AIR) folded over the tandem SH3 domains and the PX domain in contact with the first SH3 domain (Marcoux et al., 2010). The common binding motif, PxxP for SH3 domains is lacking in the AIR presenting a novel interaction strategy for this domain (Groemping et al., 2003). Two crystal structures of truncated p47*phox* containing the tandem SH3 domains and AIR describe this interaction in detail (Groemping et al., 2003; Yuzawa et al., 2004). The N-terminal part of the AIR forms a polyproline II helix that lies in the groove between the two SH3 domains (Groemping et al., 2003). Not only are both SH3 domains necessary to bind the AIR, but they in fact create a "superSH3 domain" that is superior to a single SH3-PxxP interaction both in binding specificity and affinity (Groemping et al., 2003). Two serine residues lying at the distal end of the binding groove together with a third serine of the AIR, greatly contribute to this closed conformation. Phosphorylation of these serines and others by PKC (mimicked *in vitro* by glutamic acid residues) trigger the release of the AIR from the SH3 domains unveiling a binding site for the C-terminal PRR of the p22*phox* (Ago et

al., 1999). A crystal structure of the tandem SH3 domains of p47*phox* in complex with a p22*phox* PRR peptide suggests very similar binding strategy as the AIR-$(SH3)_2$ interaction (Groemping et al., 2003). This docking site for p47*phox* in p22*phox* mediates membrane localization for p47*phox* and its binding partner, p67*phox*. The most significant difference between p47*phox* and NOXO1 is the absence of the AIR and serine phosphorylation sites in NOXO1, allowing unabated p22*phox* binding and constitutive membrane localization (Banfi et al., 2003; Nisimoto et al., 2008).

In conjunction with the p22*phox* docking site, PX domains also promote membrane localization of organizer subunits. PX domains are lipid binding modules first described by their presence in *phox* subunits and have since been found in a variety of other signaling and adaptor proteins (Ponting, 1996). The N-terminal PX domains of NOXO1 and p47*phox* recognize different phosphatidyl inositol (PtdIns) lipids conferring specific sub-cellular localizations in response to active phosphoinositide kinases. P47*phox* strongly binds PtdIns(3,4)P_2 (Kanai et al., 2001) enriched in phagosomal membranes prior to phagosome sealing, while NOXO1 recognizes PtdIns(3,5)P_2, PtdIns(4)P or PtdIns(5)P allowing plasma membrane localization in HEK 293 cells (Cheng and Lambeth, 2004). Investigation of p47*phox* PX domain mutants that impair PtdIns binding, showed decreased plasma membrane but not phagocytic Nox2 activity in response to specific stimuli, suggesting this domain may actually mediate plasma membrane localization in neutrophils (Li et al., 2010). The PX domain of p47*phox* has also been reported to bind phosphatidic acid, phosphatidylserine, moesin and cytosolic phospholipase A2 which may also play a role in p47*phox* localization or regulation and thus, oxidase assembly (Shmelzer et al., 2008; Stahelin et al., 2003).

The p40*phox* protein contains an N-terminal PX domain, a central PB1 domain and C-terminal SH3 domain (Figure 1.3). Recent crystallization of full length p40*phox* revealed a folded conformation whereby the PB1 domain interacts with the PX domain in an "autoinhibited" state (Honbou et al., 2007). The PX domain recognizes PtdIns(3)P on phagosomal membranes contributing to regulatory subunit assembly with Nox2. The events that trigger relaxing of this autoinhibited state allowing PX-PtdIns(3)P binding remain to be determined. A crystal structure of the p40*phox* PX domain in complex with PtdIns(3)P identifies multiple basic residues in direct contact with the lipid (Bravo et al., 2001). The PB1 domain interacts with another PB1 domain of p67*phox* in a 1:1 ratio. Crystal structures of the type I PB1 domain of p40*phox* and type II PB1 domain of p67*phox* provide detailed information about their heterologous dimerization (Wilson et al., 2003). This interaction appears to be important for stabilizing the p40*phox* subunit as CGD patients deficient in p67*phox* have no detectable p40*phox* expression (Tsunawaki et al., 1994). Though the functional significance is not known, the C-terminal SH3 domain shows weak binding to p47*phox* (Massenet et al., 2005).

Tyrosine kinase substrates (Tks4 and Tks5) are the most recent additions to the Nox organizer group and are comparatively less well characterized with respect to Nox assembly (Kawahara and Lambeth, 2007). These proteins consist of an N-terminal PX domain and four (Tks4) or five (Tks5) SH3 domains (Figure 1.3). Tks4/5 binds to NOXA1 through at least one of its SH3 domains (Gianni et al., 2009). The PX domain recognizes PtdIns(3,4)P_2 mediating invadopodia localization in fibroblasts and is necessary for Nox1 activation in this structure (Gianni et al., 2009).

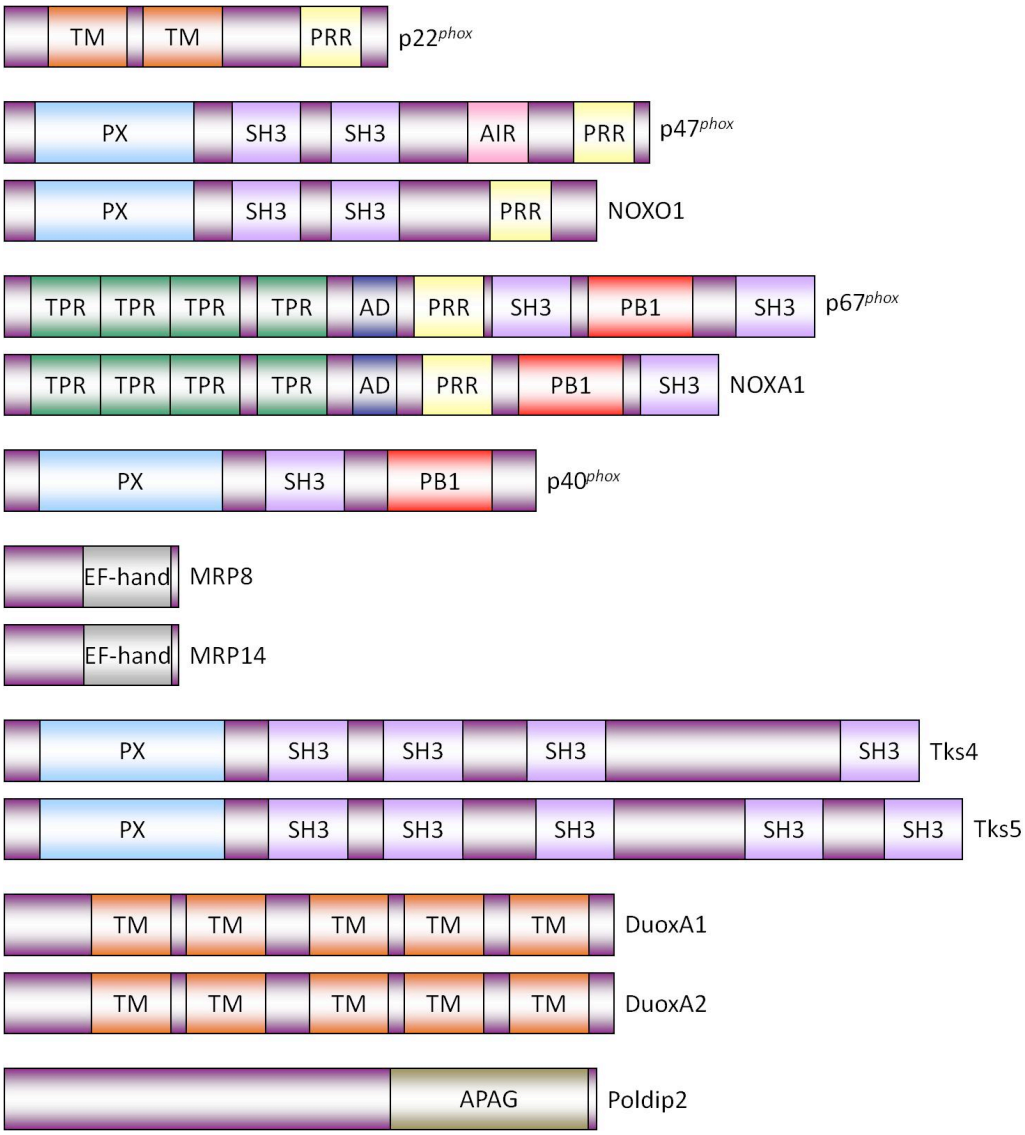

Figure 1.3 Nox/Duox Regulatory Subunits

The Nox/Duox regulatory subunits contain multiple different protein-protein and protein-lipid interacting domains. TM, transmembrane domain; PX, *phox* domain; SH3, src homology 3; AIR, autoinhibitory region; PRR, proline rich region; TPR, tetratricopeptide repeat; AD, activation domain; PB1, *phox* and bem1; apaG, similar to apaG bacterial protein.

Activator subunits

The regulatory subunit proteins that contain an activation domain and are indispensable to Nox1 and Nox2 activation are the activators, p67*phox* and NOXA1. The domain organization between these homologues are well conserved with N-terminal tetratricopeptide repeats (TPR), followed by the activation domain (AD), a central PRR, PB1 and C-terminal SH3 domain (Lambeth, 2004; Sumimoto, 2008; Vignais, 2002). The biggest difference between the homologues is the presence of an additional, central SH3 domain in p67*phox* (Banfi et al., 2003). Due in part to the decades long head start researchers had with p67*phox* before the cloning of NOXA1, most of the biochemical characterization of these activators was done with p67*phox*, although their high sequence homology suggests similar functions for NOXA1.

The TPR domain provides a binding site for the small GTPases, Rac1 and Rac2. Each TPR is composed of two anti-parallel α-helices connected by loops. An insertion is found in the p67*phox* TPR domain relative to other TPR-containing proteins, and is folded into β-hairpin (Lapouge et al., 2000). A crystal structure of the TPR domain in complex with a constitutively GTP-bound Rac1 mutant (Rac1Q61L) shows the β- hairpin insertion between TPR1/2 and TPR3/4 is in direct contact with the N- and C-terminal regions of Rac including part of switch I (Lapouge et al., 2000). The residues involved in direct binding to Rac are conserved in NOXA1 and fungal NoxR (Kawahara and Lambeth, 2007; Sumimoto, 2008).

A ten residue stretch just C-terminal to the TPR domain identified in p67*phox* as an activation domain (AD) is necessary but not sufficient for Nox2 activation (Han et al.,

1998; Mizrahi et al., 2006). Specifically, Val204 and Val205 through mutational analysis were shown to be indispensable for Nox2 activity, while maintaining interactions with p47*phox* and Rac (Han et al., 1998). Subsequent analysis of this domain suggests FAD reduction in Nox2 is impaired with p67*phox* mutated in this region. Using kinetic deuterium isotope effects, the calculated Kd for NADPH remained very similar in the presence of wild type versus Val205 mutated p67*phox* (Nisimoto et al., 1999). These results suggested the AD is important for regulating the hydride transfer from NADPH to FAD within Nox2, rather than pyridine nucleotide binding. Val204 is conserved in NOXA1 orthologs and fungal NoxR (Kawahara and Lambeth, 2007). One of the proposed functions of the Rac-p67*phox* interaction is to induce an active conformation in the AD (Sarfstein et al., 2004).

Though the exact function of the central SH3 domain of p67*phox* remains to be determined, its importance is evidenced by a reduction in ROS production in a Nox2 assembly with the SH3-deleted p67*phox* construct compared with wild type p67*phox* (Maehara et al., 2009). Consistent with the absence of this domain in NOXA1, neither Nox1 nor Nox3 activity was affected by this truncated p67*phox* (Maehara et al., 2009). Therefore, whatever function this central SH3 domain plays in oxidase activation, it is specific for the p67*phox*-Nox2 complex.

Small GTPases

Members of the Rho-family of small GTPases, RhoA, Rac and Cdc42 are involved in many cellular signaling pathways leading to migration, adhesion, mitosis, survival and innate immunity (Bokoch, 2005; Tybulewicz and Henderson, 2009). Three

highly homologous Rac isoforms, Rac1, Rac2 and Rac3 (but not other Rho-family GTPases) assemble at the membrane and promote Nox activation (Miyano et al., 2009). GTPases are regulated by proteins that catalyze GTP-GDP exchange (guanine nucleotide exchange factor, GEF), stimulate GTP hydrolysis (GTPase activating protein, GAP) or sequester the protein in its GDP-bound form (guanine nucleotide dissociation factor, GDI). The signaling events that control these three types of proteins bestow additional complexity to the regulation of Rac dependent Nox enzymes.

Rac binds to its effectors, p67*phox* or NOXA1 and has been proposed to both organize the activator protein in the oxidase assembly and promote direct Nox2 activation (Diebold and Bokoch, 2001; Gorzalczany et al., 2000; Kreck et al., 1996). While the later is debatable since this role has been assigned to the activator subunits, it is undisputed that Rac-GTP is necessary for p67*phox* to activate Nox2. The Rho-family differs from other GTPases by the presence of an insertion helix. Point mutations in this region of Rac1 significantly increased the EC_{50} for Nox2 superoxide production (Freeman et al., 1996; Nisimoto et al., 1997). However removal of this insertion (Mizrahi et al., 2006) or replacement of this sequence with that of Ras showed little disturbance to Nox1, Nox2 or Nox3 activity (Miyano et al., 2009), calling into question the significance of this insertion for Nox function. In order to participate in oxidase assembly, Rac must be present at the membrane. Membrane association of Rac is achieved by both a poly basic region and C-terminal geranylgeranylation (Mizrahi et al., 2006). Rac translocation to the oxidase complex is separate from that of p47*phox*/p67*phox*/p40*phox* as evidenced by retained membrane localization of Rac in neutrophils of CGD patients lacking these *phox* subunits (Heyworth et al., 1994).

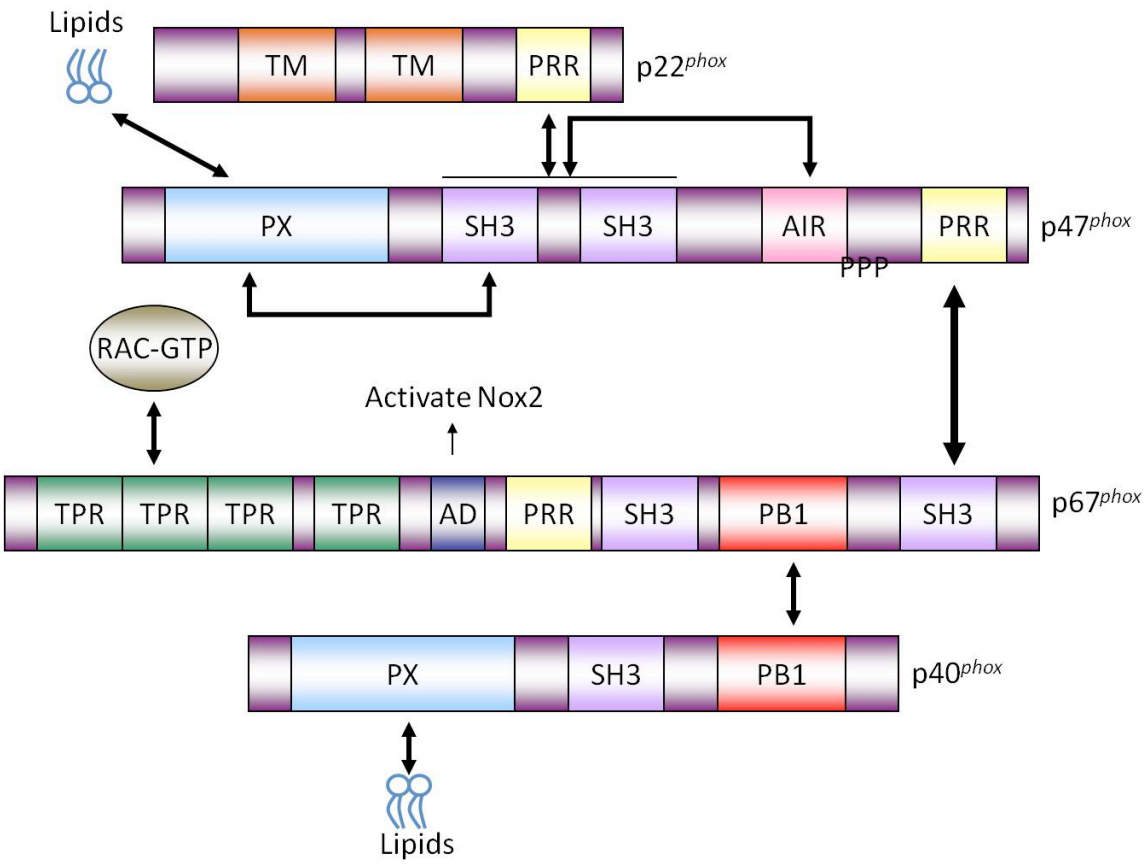

Figure 1.4 Nox2 regulatory subunit protein interactions.

The Phagocytic Nox2 complex is a network of protein-protein and protein-lipid interactions composed of the Nox2 catalytic unit and regulatory subunits. Black arrows indicate interactions between components. P indicates phosphorylation.

Oxidase Assembly

The Nox1-3 regulatory subunits discussed above assemble in combinations of at least one organizer, an activator and a small GTPase to complete oxidase assembly and promote Nox1 or Nox2 ROS production. Heterologous combinations of p47*phox*/p67*phox* or NOXO1/NOXA1 with Rac1 or Rac2 are able to reconstitute Nox1, Nox2 or Nox3 activity in transfected cell systems (Cheng et al., 2004) suggesting overlapping or redundant functions within these proteins, but the physiological oxidase assemblies are cell type, localization and stimulus specific.

The phagocytic Nox2 system was the first described and subsequently best characterized Nox assembly. The current model for this process proposes that in response to invading microbes (mimicked *in vitro* by the phorbol ester, PMA or fMLP peptide), phagocytes initiate signaling cascades leading to the formation of Nox2-p22*phox* containing phagosomes. This cascade includes elevating calcium levels triggering calcium regulated kinases both for the phosphorylation of p47*phox* (and perhaps other subunits) to relieve its autoinhibitory conformation and for the phosphorylation of PtdIns to create lipid binding sites recognized by the PX domains of p40*phox* and/or p47*phox*. Consequently, p47*phox* shuttles p67*phox* in complex with p40*phox* to the membrane for assembly with Nox2-p22*phox*. Rac2 dissociates from its GDI, translocates to the membrane and is held there via its poly basic region and prenylation moiety. Rac2 is then loaded with GTP and binds p67*phox* triggering the AD to stimulate hydride transfer in Nox2, resulting in superoxide production fed into the phagosome interior. In this setting multiple triggers are necessary to assemble a functional Nox2 complex; 1. PI3K activation for lipid modification, 2. PKC activation to

phosphorylate p47*phox* and translocation to the membrane and, 3. Rac2 GTP loading and translocation.

Neutrophils also express two EF-hand containing proteins myeloid related protein, MRP8 and MRP14 that are able to enhance Nox2 activity in the presence and absence of p47*phox*/p67*phox*/p40*phox*/Rac2 complex (Berthier et al., 2003). Though it is not quite clear how these proteins fit into the model described above, they may present yet another mechanism by which calcium promotes superoxide production.

P47*phox*, p67*phox*, p40*phox* are also found in other cell types that express Nox2 (Bedard and Krause, 2007). In these cells, Nox2 assembly is likely similar to the complex in phagocytes with the exception of the Rac isoform involved. Rac1 is ubiquitously expressed, Rac2 is highly expressed hematopoietic cells, while brain tissue express Rac3 (Haataja et al., 1997).

The highest expression of Nox1 is found in the colon, which also expresses NOXA1, Rac1 and organizers, NOXO1, Tks4 and Tks5. Due to the absence of an AIR in NOXO1, this subunit bound to both NOXA1 and p22*phox* is constitutively found at the plasma membrane of a colon cancer line, Caco2 cells localized with Nox1 (Nisimoto et al., 2008). In this paradigm, dissociation of Rac1 from its GDI, translocation to the membrane and exchange for GTP supply the triggering mechanism to turn on Nox1 activity. VSMC on the other hand do not express NOXO1 and instead contain p47*phox*. In these cells, the Nox1-p22*phox* heterodimer activity is dependent on p47*phox*, NOXA1 and Rac1-GTP (Lassegue and Griendling, 2010). Nox1 activity in this scenario is regulated by both the signaling cascades that promote p47*phox* and Rac1 translocation to

the membrane. Newly characterized organizers, Tks4 and Tks5 are expressed in the human DLD1 colon cancer cell line where they assemble with Nox1 (and likely NOXA1 and Rac1) to promote invadopodia localized ROS (Gianni et al., 2009). Interestingly, over expression of NOXO1 in these cells decreases the invadopodia formation suggesting these organizers confer location specific ROS production by Nox1.

Together with Nox3, the regulatory subunits, p22*phox*, NOXA1 and p47*phox* were also found expressed in the inner ear (Banfi et al., 2004a). NOXO1 mRNA is expressed in mouse embryonic inner ear tissue but is subsequently reduced later in development (Kiss et al., 2006). Identification of the regulatory subunits that support Nox3 activity was investigated in a transfected cell system. Nox3 activity in HEK 293 cells can be enhanced with the addition of an organizer (p47*phox*/NOXO1/Tks4/5) and an activator (p67*phox*/NOXA1) and enhancement is seen with either NOXO1 or p67*phox* alone (Banfi et al., 2004a; Cheng et al., 2004; Ueno et al., 2005). The small GTPase, Rac1 also appears to regulate Nox3 activity (Ueyama et al., 2006). The expression analysis suggests the combination of p47*phox* /NOXA1, NOXO1/NOXA1 or NOXO1 alone may be the physiological regulatory subunits for Nox3 at least in the embryonic inner ear.

Constitutively Active Nox4

Due to the observed spontaneous ROS production in Cos-7 or HEK 293 cells transfected with Nox4 (p22*phox* expression is endogenous), this isoform is said to be constitutively active. Indeed, a tetracycline inducible Nox4 expression system in HEK 293 cells showed ROS production as a direct function of tetracycline concentration

(Serrander et al., 2007). These results suggest two possibilities, either the Nox4-p22*phox* complex alone exhibits some activity, in which case Nox4 regulation may be predominately at the level of transcription, or unidentified, constitutively active regulatory subunits are present in excess in these cells.

Recently, DNA polymerase delta interacting protein 2 (Poldip2) was found to enhance Nox4 activity in VSMC cells through an interaction with p22*phox* (Lyle et al., 2009). This protein is predicted by Expasy proteomics server to contain an apaG domain, which is found in the bacterial apaG protein and eukaryotic F-box proteins and is proposed to mediate protein-protein interactions (Gasteiger et al., 2003). Biochemical analysis is needed to determine whether this protein has a direct effect on Nox4 activity, stabilizes the oxidase or affects its localization. Indeed, a Nox4 regulator would explain some experimental evidence that suggests stimulated Nox4 activity. For example, insulin stimulates ROS production in adipocytes within one minute of treatment. This ROS production is thought to be Nox4 dependent as Nox1 and Nox2 are not expressed in these cells and C-terminal deletion constructs of Nox4 blunt this effect (Mahadev et al., 2004).

Stimulated Nox4 activity has also been proposed to be mediated by direct binding to a TLR-4 receptor activated by LPS. In mesangial cells, possible Nox4 derived ROS was measured by cytochrome *c* in response to angiotensin II treatment in a Rac1-dependent manner. However, these data are inconsistent with other reports suggesting Nox4 spontaneous activity is not affected by Rac1 in transfected Cos-7 or HEK 293 systems (Martyn et al., 2006), nor is Nox4 derived ROS detected by cytochrome c (Serrander et al., 2007).

EF-hand regulated Nox Subfamily

Nox5

The longer Nox5 variants differ from the shorter Nox5 and Nox1-4 sequences with the addition of four N-terminal EF-hand motifs (Figure 1.2). These motifs confer a calcium dependency for Nox5 superoxide production. While the exact mechanism for calcium activation of Nox5 is unclear, researchers have demonstrated that elevated calcium levels induce a conformation change in the EF-hand motifs and induce EF-hand interactions with the DH domain (Banfi et al., 2004b). The relatively high IC_{50} for calcium activation of Nox5 (~ 1μM) is sensitized by phosphorylation of the DH domain by protein kinase C (Jagnandan et al., 2007) or through binding of calmodulin (Tirone and Cox, 2007). These data suggest a multi-step activation process for Nox5 involving amino acid modifications combined with structural rearrangements.

Nox5 localization also appears to be regulated in *cis* via a poly basic region. Indeed this region located between the fourth EF-hand motif and first transmembrane helix interacts with PtdIns(4,5)P_2 enriched in the plasma membrane (Kawahara and Lambeth, 2008). Not only does this interaction target Nox5 to the plasma membrane but it also confers a means by which PtdIns(5) kinase can control superoxide production.

Duox1 and Duox2

Duox1 and 2 contain two canonical EF-hand motifs N-terminal to the conserved Nox core structure (Figure 1.2). These motifs likely account for the observed calcium stimulation of ROS production in thyroid tissue (Dupuy et al., 1992) and ionomycin induced ROS production in Duox1 and Duox2 expressed HEK 293 cells (Ameziane-El-

Hassani et al., 2005). Like, Nox5 it is not at present completely clear how these calcium binding motifs control Duox1/2 activity. One study performed prior to the cloning of Duox1/2 showed that protease treatment of thyroid tissue produced calcium independent ROS production (Dupuy et al., 1992). It's possible, therefore, that the calcium induced EF-hand arrangement relieves an autoinhibitory conformation rather than stimulates an active conformation, although more studies are needed to resolve this issue.

Consistent with the theme observed in the regulatory subunits of Nox1-3 and Nox5, phosphorylation also appears to play a role in Duox regulation. Duox1 is phosphorylated by PKA in response to elevated cAMP levels (induced by forskolin) and Duox2 is phosphorylated by PKC in response to PMA (Rigutto et al., 2009). Forskolin and PMA treatment enhanced ROS production in Duox transfected cells in the presence and absence of ionomycin, suggesting the phosphorylation is an activating signal.

While phosphorylation and calcium appear to be responsible for Duox activity, maturation factors are responsible for Duox localization with possible involvement in activity as well (Morand et al., 2009). These maturation factors, DuoxA1 and DuoxA2 are found in a head to head gene arrangement with Duox1 and Duox2 suggesting dual expression with a bidirectional promoter. DuoxA1/A2 are predicted to contain multiple membrane-spanning helices localizing to both the ER and plasma membrane (Grasberger and Refetoff, 2006; Morand et al., 2009). Co-expression of these factors with Duox1 and Duox2 is necessary for Duox release from the ER and plasma membrane localization (Grasberger and Refetoff, 2006).

1.4 Scope of Dissertation

The Nox/Duox family is an extremely important group of enzymes due to their production of highly reactive, potentially destructive molecules and broad involvement in important cellular and organismal processes. The majority of research involving this family since their discovery a decade ago has been geared towards understanding their physiological functions. This research has suggested these enzymes may provide novel, targets for disease intervention. But before we can begin to manipulate proteins for our purposes, we must first understand how they work. The overall goal of this work is to understand the structural features of Nox enzymes that are important for their activity.

A major limitation for the understanding of Nox enzymes is the lack of high resolution structural data. Difficulty in expression, purification and yield has frustrated attempts to obtain this information empirically. In Chapter 2, we describe the creation and analysis of a homology model of the FAD- and NADPH-binding domain of Nox4. Because of the constitutive, basal activity of the Nox4 isoform, this model is used as a prototype to help understand nascent Nox structure.

We have used the results of our previous molecular evolution analysis along with the Nox4 homology model to identify regions of possible importance for Nox function. Chapter 3 describes the investigation of one such region, the B-loop and proposes a role consistent with both evolution data and the homology model. Chapter 4 describes a comparative analysis of Nox DH domains detailing how this domain is responsible for the observed differences in activity and/or regulation displayed by Nox1-4.

Chapter 2

Homology Model of the Nox4 Dehydrogenase Domain

2.1 Introduction

The ever increasing list of diseases associated with Nox enzymes creates a very real need for the discovery of specific inhibitory compounds for these enzymes, both as tools to delineate physiological function and as therapeutic options. The trend in the pharmaceutical field is to include structural information in the design and creation of drugs and drug targets. At present there are no solved complete structures of Nox enzymes, although recent progress has been made towards this end with the deposit of coordinates in the RSCB Protein Data Bank for the x-ray structure of the NADPH-binding domain of Nox2. Structural data on the Nox family of enzymes would provide important information towards the understanding of its regulation, evolution and provide invaluable tools for the development of drugs.

In 1993, Taylor and Segal published a homology model of the Nox2 DH domain using ferredoxin $NADP^+$ reductase from spinach as the single template structure (Taylor et al., 1993). Again in 2003 another homology model of Nox2 was built from corn nitrate reductase (Burritt et al., 2003). While these models have provided information about the Nox2 structure, we believed that a homology model could be improved by including additional, more recent information. First, we now know that Nox2 is among a family of seven isozymes and over 100 sequences of these enzymes are now available to include in sequence alignments (Kawahara et al., 2007). Second, additional 3D structures of related flavoprotein dehydrogenases are now available and some of these structures include bound NADPH, which was crucial information lacking in the earlier models. We chose to build a homology model of the human Nox4 DH domain as this protein has not been modeled previously and it displays constitutive activity, suggesting that all the

necessary components needed for at least a basal level of activity are encoded in the protein sequence.

Dym and Eisenberg have sorted FAD-binding proteins into six structurally conserved families with the two largest and best characterized being those similar to glutathione reductase (GR) and ferredoxin reductase (FR) (Dym and Eisenberg, 2001). Members of the GR sub-family contain a Rossmann fold that binds the FAD moiety while the FR family adopts a β- barrel fold. The sequence of Nox proteins are predicted to fold and share conserved sequence motifs with the FR family. Thus members of this family were chosen as templates to build the Nox4 DH domain model (Rotrosen et al., 1992; Segal et al., 1992; Sumimoto et al., 1992). These proteins include ferredoxin reductases, cytochrome p450 reductase, cytochrome b5 reductases, nitrate reductase, benzoate 1,2 dioxygenase reductase, phthalate dioxygenase reductase and flavohemoglobin.

The structurally homologous proteins, referred to as the basis set, are involved in a wide variety of electron transfer pathways. The ferredoxin $NADP^+$ reductase family catalyzes the reversible electron transfer to $NADP^+$ from ferredoxin or flavodoxin. There are two classes of ferredoxin reductase protein structures: those from plastids and cyanobacteria compose one class (FNR) while structures from eubacteria compose the second class (FPR) (Ceccarelli et al., 2004). The final step of the photosynthetic electron transport chain is catalyzed by plant-type ferredoxin reductase to produce NADPH (Shin and Arnon, 1965). The cytochrome b5 reductases catalyze the transfer of electrons from NADH to cytochrome b5 through FAD, participating in a variety of processes such as fatty acid elongation and desaturation (Keyes and Cinti, 1980), cholesterol biosynthesis

(Reddy et al., 1977), cytochrome p450 reactions (Hildebrandt and Estabrook, 1971) and methemoglobin reduction (Hultquist and Passon, 1971). Nitrate reductases in plants catalyze the reduction of nitrate to nitrite in the first step of nitrogen conversion to ammonia, which is required for plant growth (Beevers, 1969).

In addition to the structurally homologous FAD- and NADPH-binding domains of the basis set proteins listed so far, cytochrome p450 reductase, benzoate dioxygenase, phthalate dioxygenase and flavohemoglobin all bind other electron carriers. Cytochrome p450 reductases also form an FMN-binding domain catalyzing the electron transfer from NADPH through FAD and FMN to cytochrome p450 , heme oxygenase (Schacter et al., 1972) or cytochrome b5 (Enoch and Strittmatter, 1979). Consequently, this enzyme is involved in a variety of microsomal electron transport pathways of both endogenous and exogenous molecules (Wang et al., 1997). Benzoate dioxygenase and phthalate dioxygenase catalyze electron transfer from NADH through flavin to an iron sulfur center (Correll et al., 1992; Karlsson et al., 2002). Phthalate dioxygenase binds FMN rather than FAD, though the ligand binding domain is structurally related to the rest of the basis set. And the final member of the basis set, flavohemoglobin, catalyzes the transfer of electrons from NADH through FAD to an additional heme binding domain (Ermler et al., 1995).

In this section we describe the construction and assessment of a Nox4 DH domain homology model. This model depicts regions that are missing in the distantly related flavoproteins suggesting possible sites for Nox-specific functions. Using this model, we also assigned functions for regions conserved in all known Nox/Duox sequences,

discussed some conserved CGD mutations and explained recently published biochemical studies in the context of a structure.

2.2 Model Construction

Basis Set Proteins

We combined information from several sources to build the Nox4 model including secondary structure prediction from the PredictProtein server (Rost et al., 2004) and Phyre server (Kelley and Sternberg, 2009), alignments of many Nox/Duox sequences (Kawahara et al., 2007) and structures of multiple different FAD and NAD(P)H-binding proteins aligned using the DaliLite server (Holm and Rosenstrom, 2010) including the very recently solved NADPH-binding domain of Nox2. We used the Dali server to create a structure-based sequence alignment (Figure 2.3) of the basis set proteins (Table 2.1) with their RCSB Protein Data Bank code; 1GJR, ferredoxin $NADP^+$ reductase (*Anabaena sp) (Hermoso et al., 2002)*; 1FNB, ferredoxin $NADP^+$ reductase (*Spinacia olderacea*) (Bruns and Karplus, 1995); 2VNH, ferredoxin NADP(H) reductase (*Rhodobacter capsulatus*); 1AMO, cytochrome p450 reductase (*Rattus norvegicus)* (Wang et al., 1997*)*; 1KRH, benzoate dioxygenase reductase (*Acinetobacter sp*) (Karlsson et al., 2002); 1FDR, flavodoxin reductase (*Escherichia coli*) (Ingelman et al., 1997); 2PIA, phthalate dioxygenase reductase (*Burkholderia cepacia*) (Correll et al., 1992); 2EIX, cytochrome b5 reductase (*Physarum polycephalum*) (Kim et al., 2007); 1IB0, cytochrome b5 reductase (*Rattus norvegicus)* (Bewley et al., 2001)*;* 1CNF, nitrate reductase (*Zea mays*) (Lu et al., 1995); 1CQX, flavohemoglobin (*Alcaligenes eutrophus*) (Ermler et al., 1995); 3A1F, Nox2 NADPH-binding domain (*Homo sapiens*) (Unpublished). The human

sequences of Nox1-5 and Duox1/2 were then added to the alignment according to secondary structure predictions and conserved sequence motifs. The following sequences were used; Nox1 accession, NP_008983; Nox2, NP_000399; Nox3, NP_056533; Nox4, NP_058627; Nox5, NP_001171708; Duox1, NP_787954 and Duox2, NP_054799.

The sequence identity between each basis set protein and the human sequence of Nox2, Nox4 and Nox5 as they are aligned in Figure 2.3 were calculated by BioEdit v7.0.5.3 by the similarity matrix: IDENTIFY (Hall, 1999). The overall sequence identity is low among the Nox proteins and the basis set, however, there are multiple sequence motifs highly conserved among the basis set and Nox proteins (see alignment highlighted in yellow) and these regions confer a higher *local* sequence identity. The Nox4 model was built paying close attention to these conserved sequence motifs initially and working from there to build the less well conserved regions. The conserved sequence motifs are characteristic of FAD or NAD(P)H binding proteins as they comprise either the residues in direct contact with these ligands or are structurally crucial for the domain fold. Multiple ferredoxin reductase structures were included in the basis set to obtain a diverse alignment of this protein family; 1GJR from cyanobacteria and 1FNB from spinach are representatives from the plastidic/cyanobacterial class of ferredoxin reductases and 2VNH represents the eubacterial class along with flavodoxin reductase, 1FDR. The closely related 1AMO structure is also an NADPH-utilizing enzyme and the majority of the Nox4 DH domain model was built using structures, 1GJR, 1FNB, 1AMO and 1FDR and the Nox2 crystal, 3A1F (only the NADPH-binding domain). The rest of the basis set structures were used as references but were not actual model templates.

Protein			% Identity			Ligands		Ref.
			Nox2 human	Nox4 human	Nox5 human	In structure	Not in structure	
1GJR	Ferredoxin NADP$^+$ reductase	*Anabaena aequalis*	8.69	10.88	10.97	FAD, NADP$^+$		*(Hermoso et al., 2002)*
1FNB	Ferredoxin NADP$^+$ reductase	*Spinera oleracea*	7.87	8.65	9.95	FAD	NADPH	(Bruns and Karplus, 1995)
2VNH	Ferredoxin NADP(H) reductase	*Rhodobacter capsulatus*	10.65	8.38	9.79	FAD, NADPH		(Bortolotti et al., 2009)
1AMO	Cytochrome p450 reductase	*Rattus norvegicus*	8.38	8.13	8.16	FAD, FMN, NADP^{+*}		*(Wang et al., 1997)*
1FDR	Flavodoxin reductase	*Escherichia coli*	10.51	10.75	9.04	FAD	NADPH	(Ingelman et al., 1997)
1KRH	Benzoate 1,2 dioxygenase reductase	*Acinetobacter sp*	12.46	12.78	11.83	FAD, FES	NADH	(Karlsson et al., 2002)
2PIA	Phthalate dioxygenase reductase	*Burkholderia cepacia*	13.72	12.95	8.59	FMN, FES	NADH	(Correll et al., 1992)
2EIX	Cytochrome b5 reductase	*Physarum polycephalum*	8.83	10.32	9.01	FAD	NADH	(Kim et al., 2007)
1IB0	Cytochrome b5 reductase	*Rattus norvegicus*	8.46	9.97	8.19	FAD, NADH		(Bewley et al., 2001)
1CNF	Nitrate reductase	*Zea mays*	10.21	9.15	7.94	FAD, ADP$^{\neq}$	NADH	(Lu et al., 1995)
1CQX	Flavohemoglobin	*Alcaligenes eutrophus*	11.14	11.28	11.39	FAD	NADH	(Ermler et al., 1995)
3A1F	Nox2	*Homo sapiens*	40.06	18.77	16.33		FAD, NADPH	

Table 2.1 Basis Set Proteins for the Nox4 DH domain Model.

PDB codes for the basis set proteins are listed in the far left column. Sequence identity between Nox2, Nox4 or Nox5 and the basis set proteins was calculated by BioEdit and is expressed as %. Ligands ”in structure” refer to ligands present in the PDB file, while ligands “not in structure” refer to the natural ligands of the protein but are not present in the crystal structure. FAD is flavin-adenine dinucleotide; FMN is flavin mononucleotide; FES is iron sulfur cluster (Fe_2S_2); and NADPH is nicotinamide adenine dinucleotide phosphate. * Though the cytochrome p450 crystal contained bound NADPH, the structure of the nicotinamide moiety is not present. ¥ Nitrate reductase was crystallized with adenine diphosphate (ADP), though NADH is the physiological electron donor.

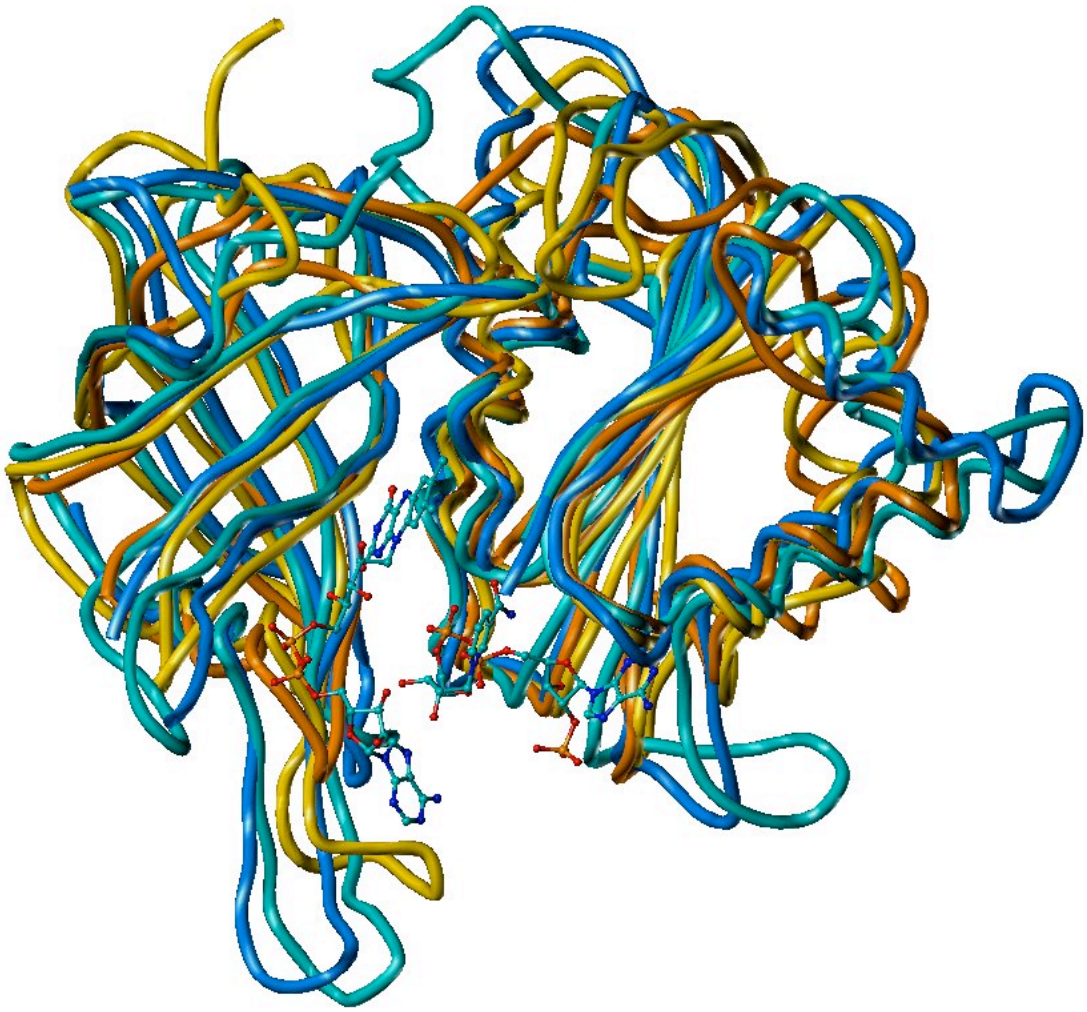

Figure 2.2. The basis set proteins are structural homologues composed of two nucleotide binding domains.

1GJR (cyan), 1AMO (excluding the FMN-binding domain for ease of viewing, blue), 1FDR (orange) and 1IB0 (yellow) were structurally aligned by the Dali Server. FAD and NADPH ligands from the 1GJR structure are displayed as ball and sticks. The FAD-binding domain forms a β-barrel (left) and the NADPH-binding domain is formed by alternating α-helices and β-strands (right).

The Nox4 DH domain model was built using the Homology module of Insight II (Accelerys), which allows manual manipulation of the query sequence assignments. The Nox4 sequence was assigned to sequences of the basis set as structurally conserved regions (SCR), which contain, but are not limited to, secondary structure elements such as β-strands or α-helices, or as designated loops (DL). Loop sequences in Nox4 that do not have homology or share a similar size with any basis set member are searched in the PDB by InsightII for a loop of similar size. This assignment is referred to below as "LOOP SEARCH". The Nox4 preliminary model was then relaxed through iterative rounds of energy minimizations by the Discover module of InsightII. Only the sidechains of sequences assigned as SCR regions are allowed to relax while both the backbone and sidechains are relaxed in regions assigned as DL. The model was then further refined in some regions using Modeller 9v8 at the Emory University BimCore.

FAD-binding domain

The Nox polypeptide chain continues from the sixth transmembrane helix to form first the FAD-binding domain, and then extends into a linker region connecting the NADPH-binding domain. The overall topology of the FAD-binding domain is composed of a β- barrel made up of six alternating β-strands capped by a short α-helix. The first three β-strands (Fβ1, Fβ2, Fβ3) and two interspersed loops of Nox4 were assigned to FDR due to similarity between sequence length of the Nox proteins and 1FDR. Both PredictProtein and the Phyre server predict the first β-strand to begin with Thr310 of Nox4. Though the sixth transmembrane helix was predicted to end near residue Arg304, the six residues between will likely compose a linker region tethering the DH domain to the TM domain. The GQ motif is the first motif in the N-terminus of this domain to

anchor the alignment. This highly conserved motif is found in 1GJR, 1FNB, 1KRH, 1FDR, 2EIX and 1CQX as well as in most Nox/Duox sequences (Kawahara et al., 2007), with the exceptions being that Nox5 and 1AMO conserve a GD in this position and 2PIA and 1CNF only conserve the glycine. The glycine residue forms a type II turn at the domain interface in the ferredoxin reductases and this turn allows close approximation of the two domains (Bruns and Karplus, 1995).

	SCR Fβ1	Loop	SCR Fβ2	Loop	SCR Fβ3
Nox4	TISSVIS	HPSD	VMEIRMV	KENFKARP	GQYITLH
FDR	WVTGKVT	WTDA	LFSLTVH	APVLPFTA	GQFTKLG

Residues extending from the previous β-strand (Fβ3) form a loop that is different in size and sequence than the basis set proteins, so this sequence was searched in the PDB database using InsightII and assigned to a loop structure of the same size. The polypeptide chain continues into the fourth β-strand of this domain. This region is highly conserved in all flavin binding proteins as these residues make direct contact with the ligand (see section 2.3.1). Though this β-strand could have been modeled after any of the basis set proteins due to the sequence conservation of the group, we chose to model it after 1AMO due to the size of the loop following this strand. All of the basis set proteins conserve an arginine at this first position in Fβ4, however the Nox/Duox family conserve a histidine (Kawahara et al., 2007; Shatwell et al., 1996). The second position of this strand can accommodate various amino acids as the side chain points away from the flavin, while its backbone hydrogen bonds with the ligand. The third position is conserved in the entire basis set proteins as an aromatic residue, helping to align the Phe of Nox/Duox proteins, while the fourth position of this motif conserves either a serine or

threonine. The following ten residues form a long loop leading into the fifth β-strand of this domain.

```
           SCR        DL
           Fβ4
Nox4       HPFT       LTMCPTETKA
1AMO       RYYS       IASSSKVHPN
```

The fifth β-strand of this domain was modeled after 1FNB due to significant sequence homology. The anchoring position in this strand is the final, highly conserved basic residue, Lys372 (Nox4), which is not only conserved in the basis set proteins, but is also either a lysine or arginine in most known Nox/Duox sequences (Kawahara et al., 2007). This residue extends across the NADPH-binding domain to interact with the diphosphate of either $NADP^+$ in ferredoxin reductases (Hermoso et al., 2002), NADH in cytochrome b5 reductases (PDB: 1IB0 (Bewley et al., 2001)) or ADP of nitrate reductase (Lu et al., 1995).

```
           SCR        LOOP SEARCH          SCR
           Fβ5                             Fα1
NOX4       TFGVHLK    IV                   GDWTERFRD
1FNB       SVSLCVK                  1AMO  GVATSWLRA
```

The following loop is very short in Nox4 so that the GXXT/SXXL motif would align between Nox4 and 1AMO. This motif is found in the FAD-binding domain's single α-helix in all of the basis set proteins and residues within this helix either directly interact with the phosphates of FAD or position other residues important for ligand binding (Dym and Eisenberg, 2001; Sridhar Prasad et al., 1998). Two interesting consequences arise from placement of this motif as shown above; 1. the short preceding loop is missing length and an aromatic residue to stack with the adenine ring of FAD and 2. a large insertion follows this helix. The previous Nox2 homology model built by

Taylor et. al. is different than our Nox4 model in this area as they aligned residues GCDKQEFQ (Nox2 370-377) with the helix motif shown above in 1AMO (or in Figure 2.2) (Taylor et al., 1993). Placement of these residues as the helix does allow formation of a longer preceding loop that contains an aromatic residue to stack the adenine. However, this alignment was made prior to cloning of the first Nox isoforms so it was not known at the time whether this region in Nox2 is conserved in other Nox/Duox proteins, nor was this motif known to be conserved in other flavin binding proteins at the time. A multiple sequence alignment of over 100 Nox/Duox sequences (Kawahara et al., 2007) shows this GXXS/TXXL motif is conserved in Nox/Duox enzymes and is upstream of the Nox2 GCDKQEFQ region. Glycine residues are often found as the C-terminal cap of helices, explaining the high conservation of this residue in the helix motif (Richardson and Richardson, 1988). The serine/threonine residue makes a side chain hydrogen bond to the residue two positions downstream of the conserved arginine/lysine in Fβ5 in the basis set proteins, helping to position this basic residue to contact the NAD. In addition to satisfying the conserved sequence constraints of the basis set, this region in Nox4 is predicted to be helical by secondary structure prediction programs. Therefore, the current alignment of the motif in Nox4 shown above was used. This helix was modeled after 1AMO due to slightly higher homology than with the other basis set proteins. Another consequence of this assignment unique to the Nox4 model is that it places Trp576 in location to stack with His352, positioning this residue to bind the FAD. This tryptophan residue in the Nox4 sequence is conserved as either a tryptophan or phenylalanine (fungal NoxA or NoxB) in the Nox/Duox family demonstrating the importance of the aromaticity of this residue.

The residues following this helix are an insertion compared with the other basis set proteins and secondary structure prediction programs do not predict secondary structure in this region for Nox4. Due to the very little information available to model this insertion, we used an automated model of Nox4 DH domain generated by the I-TASSER protein structure prediction server to serve as the template in this region (Roy et al., 2010; Zhang, 2008, 2009). This model of the Nox4 DH domain was overall similar to the topology of our model but differed in the specific side chain conformations of ligand-contacting residues. The I-TASSER model displays these residues as a large loop with a small helix.

```
Nox4 LLLPPSSQDSEILPFIQSRNYP
```

The final β-strand (Fβ6) and loop of the FAD-binding domain was assigned to 1FNB. The loop contains a proline, kinking the carbon backbone in most of the basis set proteins including 1CNF, 1KRH, 2PIA, 1CQX, 1GJR and 1FNB. The conservation of this motif in Nox4 anchors the alignment with a high degree of confidence.

```
           SCR        DL
           Fβ6
Nox4       KLYID      GPFG
1FNB       EVKLT      GPVG
```

Continuing along the polypeptide chain is the formation of the linker region connecting the two domains. The Nox2 crystal structure begins at this region with a helix, which is unique among the basis set proteins, with the exception of a single turn present in 1FDR. A helix in this region would significantly shorten the length of the linker creating a very close approximation of the two domains. Since none of the basis set proteins contain this domain orientation, and the Nox2 crystal lacks the FAD-binding

domain, we did not model Nox4 with a helical linker. There is not a high degree of sequence homology between Nox4 and any of the other basis set proteins, consequently 1AMO was used as the template because of similar length.

```
      DL
Nox4  SPFEESLNYE
1AMO  QFRLPFKSTT
```

NADPH-binding domain

The overall topology of the NAD(P)H-binding domain for the basis set proteins is the classic Rossmann fold, composed of at least three alternating β-strands and helices. This structure is characteristic for nucleotide binding proteins (Rao and Rossmann, 1973) and secondary structure prediction programs predict a fold of at least five alternating β-strands and helices for the Nox proteins. The β-strands all localize to the inside of the protein, so the hydrophobic nature of these regions helps to localize the strands in the Nox4 sequence and gives high confidence for the assignments of these structures. The NADPH-binding domain was originally constructed using the same approach and templates as the FAD-binding domain, however, the recent deposit of structure coordinates for the Nox2 NADPH-binding domain provided important, new information. Some of the Nox4 model was re-assigned to the Nox2 structure where there was significant deviation and these refinements were made with the molecular modeling program, Modeller 9v8 (Sali and Blundell, 1993). This program does not require distinguishing between SCR or Loops, so the assignments described below, when modeled by Modeller and not InsightII, do not indicate these notations.

The first β-strand (Nβ1) and helix (Nα1) of this domain contain a highly conserved sequence motif (underlined) characteristic of many FAD- and NAD(P)H-binding proteins. To ensure a smooth transition from the linker residues into this crucial

region, we assigned the Nox4 sequence to 1AMO. The Nα1 helix varies in size among the different basis set proteins and among the different Nox isoforms with extensions at the C-terminal end. The N-terminal end is fixed by the conserved motif and begins as a 3-10 helix. A loop search was conducted for the following region as none of the basis set proteins contained a loop of similar size. The second β-strand of this domain shares significant homology to 1AMO and was assigned accordingly.

```
     SCR                              LOOP SEARCH    SCR
     Nβ1     Nα1                                     Nβ2
Nox4 VSLCVAGGIGVTPFASILNTLLDD      WKPYKLR         RLYFIWVC
1AMO PVIMVGPGTGIAPFMGFIQERAWI                      ETLLYYGC
```

The next loop contains residues RD of the sequence motif R/KD/E conserved in most Nox proteins and RT in Duox (Kawahara et al., 2007). Neither this motif, nor the following helix share significant sequence homology with the basis set, thus Nox4 was modeled after the Nox2 crystal structure in these regions.

```
                Nα2
Nox4 RDIQS      FRWFADLLCMLHNKFWQE  NRPD
Nox2 RDTHA      FEWFADLLQLLESQMQER  NNAG
```

The following strand (Nβ3) is fairly well conserved in the Nox/Duox sequences consisting of mainly hydrophobic with some alternating polar residues, and these aid in aligning this region to the basis set. The Nox4 sequence was assigned to the 1FNB structure in this region, and as this strand is very similar in 1GJR, 1FDR and 3A1F, Nox4 is modeled essentially the same as the entire structural family.

```
      SCR
      Nβ3
Nox4 YVNIQLYLSQ
1FNB  FRLDFAVSR
```

The next region of the Nox/Duox sequences is an insertion relative to the rest of basis set proteins. Interestingly, there is a significant degree of sequence homology within the various Nox/Duox isoforms (see section 2.3.3 Insertions).

```
     Nβ3                      NIα              NIβ
Nox4 YVNIQLYLSQ     TDG  IQKIIGEKYHALN  S    RLFI       GRP
Nox2 FLSYNIYLTG     W..  ............  Q    KTLY       GRP
```

As this region is an insertion relative to the basis set, the only possible templalte would be the Nox2 structure. However, the Nox2 crystal structure is missing residues D100 – K122 (represented by the dots in the above alignment), corresponding to the turn following Nβ3 and all of insertion helix NIα (see Figure 2.3 Alignment) Even though 1FDR, like Nox2 and Nox4, contains a 6th beta strand, it does not have the inserted helical region between Nβ3 and NIβ. Thus, there is no template for the position of the helix. This region of the model was, therefore, generated in sections. After modeling and extending Nβ3 and the insertion beta strand (NIβ) on the available Nox2 sections, an idealized helical structure was formed for the sequence predicted to be such by secondary structure prediction programs by assigning it a helical structure in the Modeller command file. Modeller was allowed flexibility of the positioning of this helix, (packed near and parallel to Nα2, packed near and parallel to Nα4 or packed in between, nearly to the edge of the beta sheet). It is anticipated that the inserted helix will pack near Nα2, however, with a lack of specific data for a more precise positioning of this helix, the Modeller position was maintained. Nox2 was used as the template to position NIβ and the subsequent turn in order to position the R in GRP towards NADP with its guanidinium group stacking with the base.

The following helix (Nα3) is highly variable among the basis set proteins; while the ferredoxin reductases and 1AMO have two small, almost perpendicular helices creating a turn, 1FDR, 1CNF, 2PIA and the cytochrome b5 reductases contain only one smaller helix. The 1KRH polypeptide is coiled and does not even form a regular helix in this region. Nox2 is different even still, containing one helix, though it does not superimpose well onto the 1FDR-like helices. The Nox/Duox sequences all vary in amino acid composition in this region, though the length remains fairly constant suggesting this helix is likely different from the basis set proteins, but similar among the Nox/Duox family. Therefore, the Nox2 crystal structure was used as the template for the Nox4 model. Nβ4, like the other strands of this domain, superimposes well among the basis set proteins and the high homology of the Nox sequences with these proteins places high confidence in their alignment. Indeed, this strand ends with the invariant CG motif which lies very close to the NADPH-binding site and serves to anchor the alignment. The Nox2 crystal structure provides the template for this strand and the following helix (Nα4), which varies among the different basis set structures. 1GJR, 1FNB, 1AMO, 2EIX and 1CQX have a bifurcated, bent helix, while the other half of the basis set form a single helix similar to the Nox2 structure.

```
     Nα3                  Nβ4             Nα4
Nox4 RWKLLFDEIAKYN  RG   KTVGVFCC  G    PNSLSKTLHKLSNQNN
Nox2 NWDNEFKTIASQH  PN   TRIGVFLC  G    PEALAETLSKQSISNS
```

The final β-strand (Nβ5) of Nox2 stretches in a linear direction in the absence of a ligand or flavin-binding domain. In the other basis set proteins, which are crystals of both the FAD- and NADPH-binding domains and all contain FAD, the β-strand slightly arcs so that the final aromatic residue can interact with the flavin. Nox4 was assigned to 1AMO to model the C-terminus similar to the basis set proteins rather than Nox2.

1AMO was chosen as the template specifically as this polypeptide chain also contains a final serine residue, which is unique in the Nox4 isoform, though some insect Nox/Duox sequences end with a glycine following the final aromatic residue (Kawahara et al., 2007).

	Loop search	SCR
		Nβ5
Nox4	SYGTRFE	YNKESFS
1AMO		YSLDVWS

Coordinates for the FAD and NADPH ligands from the 1GJR structure were added to the Nox4 DH domain model and analyzed for the appropriate contacts. Regions of Nox enzymes important for binding these ligands were previously predicted by comparison with the ferredoxin reductase family (reviewed (Vignais, 2002)). Where ever these residues were not in correct orientation or distance from their respective ligand, we manually torsioned the side chain, while the backbone remained stationary. This was done for residues Lys372, Arg464 and Arg523 using the modeling software, SYBYL8 (Tripos).

The final model was then submitted to PROCHECK to check all Psi/Phi angles and over all geometry of the model (Laskowski, 1993). The percentage of residues in the most favored regions of the Ramachandran plot is 88.1%. All of the main chain residues are within this most favored region. One residue, Ser551 is in the disallowed region. This part of the model used the Nox2 crystal structure as a template to accurately model the conserved CG residues (see Figure 2.3 Alignment) which are just upstream of this serine in a loop connecting Nβ4-Nα4. In an effort to preserve the structure of this important loop, the serine residue was not further optimized. Four other residues have imperfect Psi/Phi angles but as three of these residues are located in the FAD insertion- a

region of low confidence and the fourth is located in another surface loop, the model was not further refined. The results of the overall geometry analysis were within an acceptable range except for a few main chain bond angles, which measured in the unusual range. Most the residues that deviate from ideal positions are located in loops.

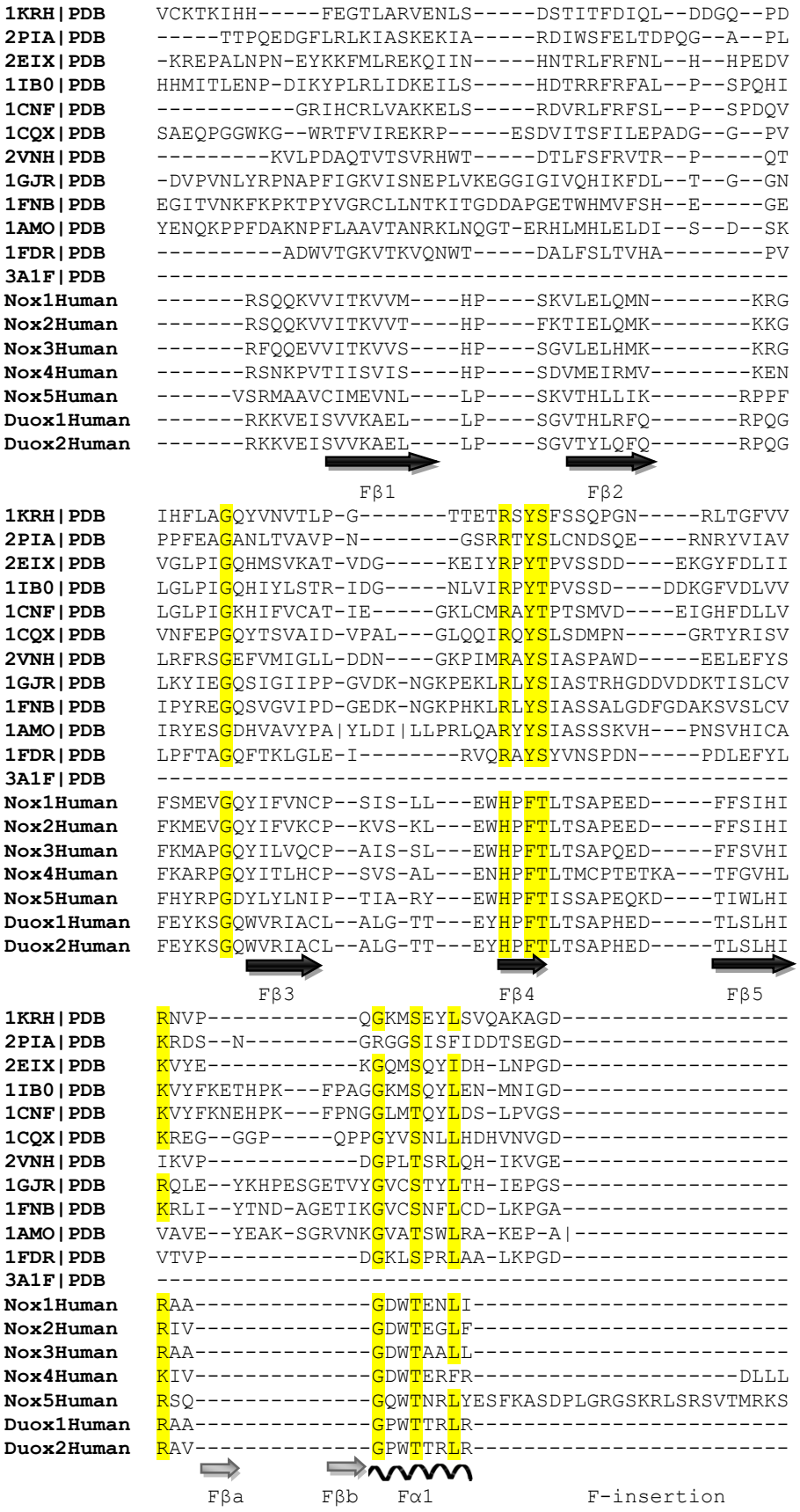
1KRH|PDB VCKTKIHH-----FEGTLARVENLS-----DSTITFDIQL--DDGQ--PD
2PIA|PDB -----TTPQEDGFLRLKIASKEKIA-----RDIWSFELTDPQG--A--PL
2EIX|PDB -KREPALNPN-EYKKFMLREKQIIN-----HNTRLFRFNL--H--HPEDV
1IB0|PDB HHMITLENP-DIKYPLRLIDKEILS-----HDTRRFRFAL--P--SPQHI
1CNF|PDB ----------GRIHCRLVAKKELS-----RDVRLFRFSL--P--SPDQV
1CQX|PDB SAEQPGGWKG--WRTFVIREKRP-----ESDVITSFILEPADG--G--PV
2VNH|PDB ---------KVLPDAQTVTSVRHWT-----DTLFSFRVTR--P-----QT
1GJR|PDB -DVPVNLYRPNAPFIGKVISNEPLVKEGGIGIVQHIKFDL--T--G--GN
1FNB|PDB EGITVNKFKPKTPYVGRCLLNTKITGDDAPGETWHMVFSH--E-----GE
1AMO|PDB YENQKPPFDAKNPFLAAVTANRKLNQGT-ERHLMHLELDI--S--D--SK
1FDR|PDB ----------ADWVTGKVTKVQNWT-----DALFSLTVHA--------PV
3A1F|PDB --
Nox1Human -------RSQQKVVITKVVM----HP----SKVLELQMN--------KRG
Nox2Human -------RSQQKVVITKVVT----HP----FKTIELQMK--------KKG
Nox3Human -------RFQQEVVITKVVS----HP----SGVLELHMK--------KRG
Nox4Human -------RSNKPVTIISVIS----HP----SDVMEIRMV--------KEN
Nox5Human ------VSRMAAVCIMEVNL----LP----SKVTHLLIK-------RPPF
Duox1Human -------RKKVEISVVKAEL----LP----SGVTHLRFQ-------RPQG
Duox2Human -------RKKVEISVVKAEL----LP----SGVTYLQFQ-------RPQG
Fβ1
Fβ2
1KRH|PDB IHFLAGQYVNVTLP-G-------TTETRSYSFSSQPGN-----RLTGFVV
2PIA|PDB PPFEAGANLTVAVP-N--------GSRRTYSLCNDSQE----RNRYVIAV
2EIX|PDB VGLPIGQHMSVKAT-VDG-----KEIYRPYTPVSSDD----EKGYFDLII
1IB0|PDB LGLPIGQHIYLSTR-IDG-----NLVIRPYTPVSSD----DDKGFVDLVV
1CNF|PDB LGLPIGKHIFVCAT-IE-----GKLCMRAYTPTSMVD----EIGHFDLLV
1CQX|PDB VNFEPGQYTSVAID-VPAL---GLQQIRQYSLSDMPN-----GRTYRISV
2VNH|PDB LRFRSGEFVMIGLL-DDN----GKPIMRAYSIASPAWD-----EELEFYS
1GJR|PDB LKYIEGQSIGIIPP-GVDK-NGKPEKLRLYSIASTRHGDDVDDKTISLCV
1FNB|PDB IPYREGQSVGVIPD-GEDK-NGKPHKLRLYSIASSALGDFGDAKSVSLCV
1AMO|PDB IRYESGDHVAVYPA|YLDI|LLPRLQARYYSIASSSKVH---PNSVHICA
1FDR|PDB LPFTAGQFTKLGLE-I--------RVQRAYSYVNSPDN-----PDLEFYL
3A1F|PDB --
Nox1Human FSMEVGQYIFVNCP--SIS-LL---EWHPFTLTSAPEED-----FFSIHI
Nox2Human FKMEVGQYIFVKCP--KVS-KL---EWHPFTLTSAPEED-----FFSIHI
Nox3Human FKMAPGQYILVQCP--AIS-SL---EWHPFTLTSAPQED-----FFSVHI
Nox4Human FKARPGQYITLHCP--SVS-AL---ENHPFTLTMCPTETKA---TFGVHL
Nox5Human FHYRPGDYLYLNIP--TIA-RY---EWHPFTISSAPEQKD----TIWLHI
Duox1Human FEYKSGQWVRIACL--ALG-TT---EYHPFTLTSAPHED-----TLSLHI
Duox2Human FEYKSGQWVRIACL--ALG-TT---EYHPFTLTSAPHED-----TLSLHI
Fβ3
Fβ4
Fβ5
1KRH|PDB RNVP----------QGKMSEYLSVQAKAGD-----------------
2PIA|PDB KRDS--N---------GRGGSISFIDDTSEGD-----------------
2EIX|PDB KVYE----------KGQMSQYIDH-LNPGD-----------------
1IB0|PDB KVYFKETHPK---FPAGGKMSQYLEN-MNIGD-----------------
1CNF|PDB KVYFKNEHPK---FPNGGLMTQYLDS-LPVGS-----------------
1CQX|PDB KREG--GGP-----QPPGYVSNLLHDHVNVGD-----------------
2VNH|PDB IKVP----------DGPLTSRLQH-IKVGE-----------------
1GJR|PDB RQLE--YKHPESGETVYGVCSTYLTH-IEPGS-----------------
1FNB|PDB KRLI--YTND-AGETIKGVCSNFLCD-LKPGA-----------------
1AMO|PDB VAVE--YEAK-SGRVNKGVATSWLRA-KEP-A|-----------------
1FDR|PDB VTVP----------DGKLSPRLAA-LKPGD-----------------
3A1F|PDB --
Nox1Human RAA----------GDWTENLI-------------------------
Nox2Human RIV----------GDWTEGLF-------------------------
Nox3Human RAA----------GDWTAALL-------------------------
Nox4Human KIV----------GDWTERFR--------------------DLLL
Nox5Human RSQ----------GQWTNRLYESFKASDPLGRGSKRLSRSVTMRKS
Duox1Human RAA----------GPWTTRLR-------------------------
Duox2Human RAV----------GPWTTRLR-------------------------
Fβa
Fβb
Fα1
F-insertion


1KRH|PDB ----------KMSFTGPFG-SFYLRD-V-KRPVLMLAGGTG
2PIA|PDB ----------AVEVSLPRNE-FPLDKR--AKSFILVAGGIG
2EIX|PDB ----------FLQVRGPKGQF-DYKPNM-VKEMGMIAGGTG
1IB0|PDB ----------TIEFRGPNGLL-VYQGKG|VKSVGMIAGGTG
1CNF|PDB ----------YIDVKGPLGHV-EYTGRG|ARRLAMICGGSG
1CQX|PDB ----------QVKLAAPYG-SFHIDVDA-KTPIVLISGGVG
2VNH|PDB ----------QIILRPKPVGTLVID---|GKRLWFLATGTG
1GJR|PDB ----------EVKITGPVGKEMLLPDDP-EANVIMLATGTG
1FNB|PDB ----------EVKLTGPVGKEMLMPKDP-NATIIMLGTGTG
1AMO|PDB ----------LVPMFVRKS-QFRLPFKS-TTPVIMVGPGTG
1FDR|PDB ----------EVQVVSEAAGF-FVLD---|CETLWMLATGTA
3A1F|PDB ----------IAVDGPFG-TASEDVFS-YEVVMLVGAGIG
Nox1Human --------RAFEQQYSPIPRIEVDGPFG-TASEDVFQ-YEVAVLVGAGIG
Nox2Human --NACGCDKQEFQDAWKLPKIAVDGPFG-TASEDVFS-YEVVMLVGAGIG
Nox3Human --EAFGAEGQALQEPWSLPRLAVDGPFG-TALTDVFH-YPVCVCVAAGIG
Nox4Human PPSSQDSEILPFIQSRNYPKLYIDGPFG-SPFEESLN-YEVSLCVAGGIG
Nox5Human QRSSKGSEILLEKHKFCNIKCYIDGPYG-TPTRRIFA-SEHAVLIGAGIG
Duox1Human ----EIYSAPTGDRCARYPKLYLDGPFG-EGHQEWHK-FEVSVLVGGGIG
Duox2Human ----EIYSSPKGNGCAGYPKLYLDGPFG-EGHQEWHK-FEVSVLVGGGIG
Fβ6
Nβ1
1KRH|PDB IAPFLSMLQVLEQ----------KGSE--HPVRLVFGV
2PIA|PDB ITPMLSMARQLRA----------EGL--RSFRLYYLT
2EIX|PDB ITPMLQVARAIIK----------NPKEK--TIINLIFAN
1IB0|PDB ITPMLQVIRAVLK----------DPNDH--TVCYLLFAN
1CNF|PDB ITPMYQIIQAVLRD----------QPEDH--TEMHLVYAN
1CQX|PDB LTPMVSMLKVAL----------QAPP--RQVVFVHGA
2VNH|PDB IAPFASLMREP----------EAYEKF--DEVIMMHAC
1GJR|PDB IAPMRTYLWRMFKDAERAAN----------PEYQFK--GFSWLVFGV
1FNB|PDB IAPFRSFLWKMFFEK----H----------DDYKFN--GLAWLFLGV
1AMO|PDB IAPFMGFIQERA---WLRE----------QGKEV---GETLLYYGC
1FDR|PDB IGPYLSILRLG----------KDLDRFKNLVLVHAA
3A1F|PDB VTPFASILKSVWY--KYCNN----------ATNLKL--KKIYFYWLC
Nox1Human VTPFASILKSIWYKFQCA----------DHNLKT--KKIYFYWIC
Nox2Human VTPFASILKSVWYKYCNN----------ATNLKL--KKIYFYWLC
Nox3Human VTPFAALLKSIWYKCSEA----------QTPLKL--SKVYFYWIC
Nox4Human VTPFASILNTLLDD----------WKPYKL--RRLYFIWVC
Nox5Human ITPFASILQSIMYRHQKRKHTCPSCQHSWIEGVQDNMKL--HKVDFIWIN
Duox1Human VTPFASILKDLVFKSSV----------SCQVFC--KKIYFIWVT
Duox2Human VTPFASILKDLVFKSSL----------GSQMLC--KKIYFIWVT
Nα1
Nβ2
1KRH|PDB TQD-CDL-VALEQLD--ALQQ------KL-------PWFEYRTVVAH---
2PIA|PDB RDP-EGT-AFFDELTSDEWRS----------DVKIHHDH---
2EIX|PDB VNE-DDI-LLRTELD--DMAK------KY-------SNFKVYYVLNN---
1IB0|PDB QSE-KDI-LLRPELE--ELRN------EH-----S-SRFKLWYTVDK---
1CNF|PDB RTE-DDI-LLRDELD--RWAA------EY-----P-DRLKVWYVIDQ---
1CQX|PDB RNS-AVH-AMRDRLR--EAAK------TY-------ENLDLFVFYDQ---
2VNH|PDB RTV-AELEYGRQLVE--ALQEDPLIGELV-----E-GKLKYYPTTTR---
1GJR|PDB PTT-PNI-LYKEELE--EIQQ------KY-----P-DNFRLTYAISR---
1FNB|PDB PTS-SSL-LYKEEFE--KMKE------KA-----P-DNFRLDFAVSR---
1AMO|PDB RRSDEDY-LYREELA--RFHK------DG-------ALTQLNVAFSR---
1FDR|PDB RYA-ADL-SYLPLMQ--ELEK------RY-----E-GKLRIQTVVSR---
3A1F|PDB RDT-HAFEWFADLLQ--LLES------QMQERNNA-GFLSYNIYLTG---
Nox1Human RET-GAFSWFNNLLT--SLEQ------EMEELGKV-GFLNYRLFLTGW|-
Nox2Human RDT-HAFEWFADLLQ--LLES------QMQERNNA-GFLSYNIYLTGW--
Nox3Human RDA-RAFEWFADLLL--SLET------RMSEQGKT-HFLSYHIFLTGW--
Nox4Human RDI-QSFRWFADLLC--MLHN------KFWQENRP-DYVNIQLYLSQT--
Nox5Human RDQ-RSFEWFVSLLT--KLEM------DQAEEAQYGRFLELHMYMTSALG
Duox1Human RTQ-RQFEWLADIIR--EVEE------NDHQ-----DLVSVHIYITQLAE
Duox2Human RTQ-RQFEWLADIIQ--EVEE------NDHQ-----DLVSVHIYVTQLAE
Nα2
Nβ3

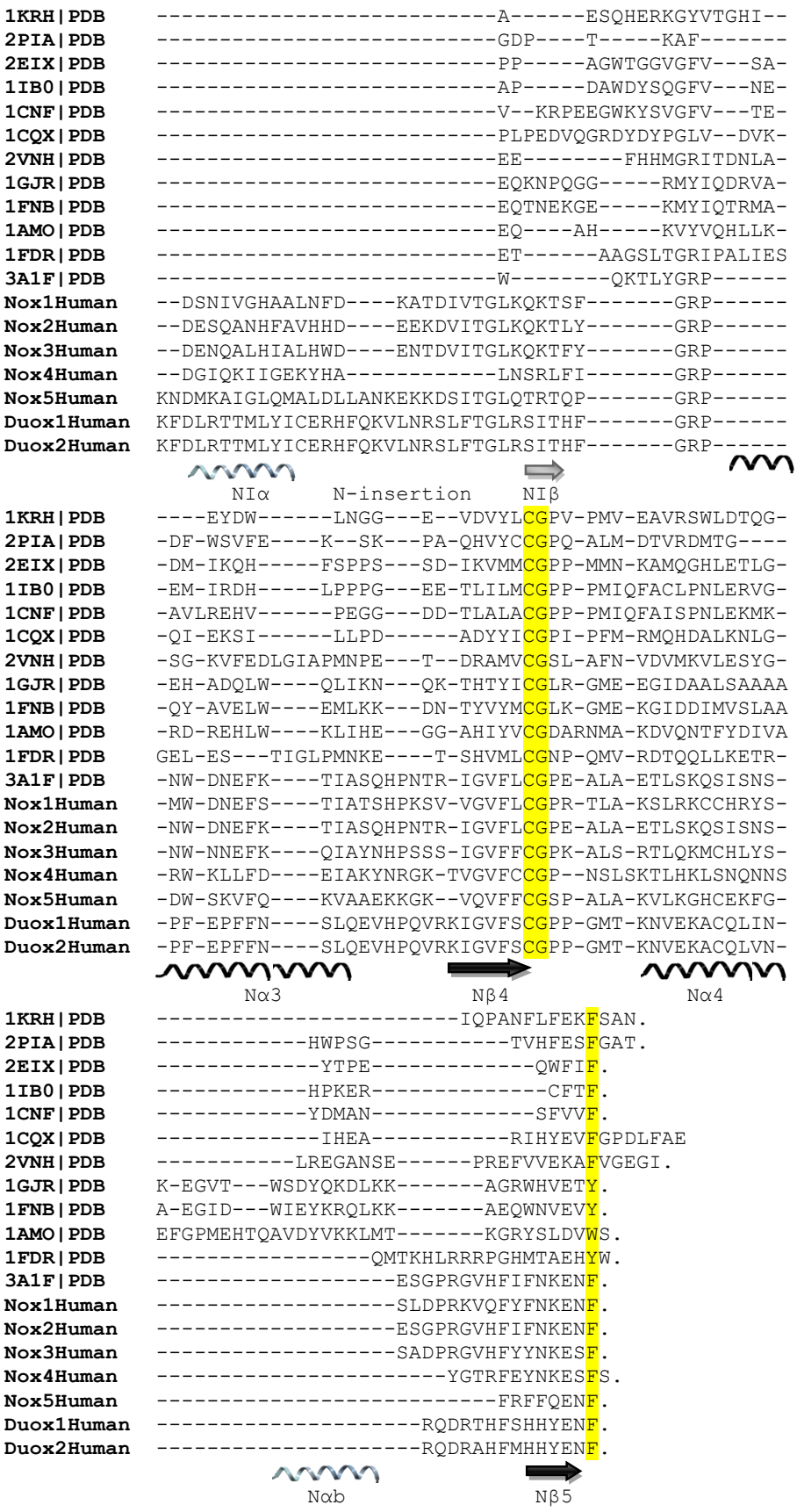
1KRH|PDB ----------A------ESQHERKGYVTGHI--
2PIA|PDB ----------GDP----T-----KAF-------
2EIX|PDB ----------PP-----AGWTGGVGFV---SA-
1IB0|PDB ----------AP-----DAWDYSQGFV---NE-
1CNF|PDB ----------V--KRPEEGWKYSVGFV---TE-
1CQX|PDB ----------PLPEDVQGRDYDYPGLV--DVK-
2VNH|PDB ----------EE--------FHHMGRITDNLA-
1GJR|PDB ----------EQKNPQGG-----RMYIQDRVA-
1FNB|PDB ----------EQTNEKGE-----KMYIQTRMA-
1AMO|PDB ----------EQ----AH-----KVYVQHLLK-
1FDR|PDB ----------ET------AAGSLTGRIPALIES
3A1F|PDB ----------W--------QKTLYGRP------
Nox1Human --DSNIVGHAALNFD----KATDIVTGLKQKTSF-------GRP------
Nox2Human --DESQANHFAVHHD----EEKDVITGLKQKTLY-------GRP------
Nox3Human --DENQALHIALHWD----ENTDVITGLKQKTFY-------GRP------
Nox4Human --DGIQKIIGEKYHA----------LNSRLFI-------GRP------
Nox5Human KNDMKAIGLQMALDLLANKEKKDSITGLQTRTQP-------GRP------
Duox1Human KFDLRTTMLYICERHFQKVLNRSLFTGLRSITHF-------GRP------
Duox2Human KFDLRTTMLYICERHFQKVLNRSLFTGLRSITHF-------GRP------
NIα
N-insertion
NIβ
1KRH|PDB ----EYDW------LNGG---E--VDVYLCGPV-PMV-EAVRSWLDTQG-
2PIA|PDB -DF-WSVFE----K--SK---PA-QHVYCCGPQ-ALM-DTVRDMTG----
2EIX|PDB -DM-IKQH-----FSPPS---SD-IKVMMCGPP-MMN-KAMQGHLETLG-
1IB0|PDB -EM-IRDH-----LPPPG---EE-TLILMCGPP-PMIQFACLPNLERVG-
1CNF|PDB -AVLREHV------PEGG---DD-TLALACGPP-PMIQFAISPNLEKMK-
1CQX|PDB -QI-EKSI------LLPD------ADYYICGPI-PFM-RMQHDALKNLG-
2VNH|PDB -SG-KVFEDLGIAPMNPE---T--DRAMVCGSL-AFN-VDVMKVLESYG-
1GJR|PDB -EH-ADQLW----QLIKN---QK-THTYICGLR-GME-EGIDAALSAAAA
1FNB|PDB -QY-AVELW----EMLKK---DN-TYVYMCGLK-GME-KGIDDIMVSLAA
1AMO|PDB -RD-REHLW----KLIHE---GG-AHIYVCGDARNMA-KDVQNTFYDIVA
1FDR|PDB GEL-ES---TIGLPMNKE----T-SHVMLCGNP-QMV-RDTQQLLKETR-
3A1F|PDB -NW-DNEFK----TIASQHPNTR-IGVFLCGPE-ALA-ETLSKQSISNS-
Nox1Human -MW-DNEFS----TIATSHPKSV-VGVFLCGPR-TLA-KSLRKCCHRYS-
Nox2Human -NW-DNEFK----TIASQHPNTR-IGVFLCGPE-ALA-ETLSKQSISNS-
Nox3Human -NW-NNEFK----QIAYNHPSSS-IGVFFCGPK-ALS-RTLQKMCHLYS-
Nox4Human -RW-KLLFD----EIAKYNRGK-TVGVFCCGP--NSLSKTLHKLSNQNNS
Nox5Human -DW-SKVFQ----KVAAEKKGK--VQVFFCGSP-ALA-KVLKGHCEKFG-
Duox1Human -PF-EPFFN----SLQEVHPQVRKIGVFSCGPP-GMT-KNVEKACQLIN-
Duox2Human -PF-EPFFN----SLQEVHPQVRKIGVFSCGPP-GMT-KNVEKACQLVN-
Nα3
Nβ4
Nα4
1KRH|PDB ----------IQPANFLFEKFSAN.
2PIA|PDB ----------HWPSG----------TVHFESFGAT.
2EIX|PDB ----------YTPE----------QWFIF.
1IB0|PDB ----------HPKER----------CFTF.
1CNF|PDB ----------YDMAN----------SFVVF.
1CQX|PDB ----------IHEA----------RIHYEVFGPDLFAE
2VNH|PDB ----------LREGANSE------PREFVVEKAFVGEGI.
1GJR|PDB K-EGVT---WSDYQKDLKK-------AGRWHVETY.
1FNB|PDB A-EGID---WIEYKRQLKK-------AEQWNVEVY.
1AMO|PDB EFGPMEHTQAVDYVKKLMT-------KGRYSLDVWS.
1FDR|PDB ----------QMTKHLRRRPGHMTAEHYW.
3A1F|PDB ----------ESGPRGVHFIFNKENF.
Nox1Human ----------SLDPRKVQFYFNKENF.
Nox2Human ----------ESGPRGVHFIFNKENF.
Nox3Human ----------SADPRGVHFYYNKESF.
Nox4Human ----------YGTRFEYNKESFS.
Nox5Human ----------FRFFQENF.
Duox1Human ----------RQDRTHFSHHYENF.
Duox2Human ----------RQDRAHFMHHYENF.
Nαb
Nβ5

```
1AMO   |NDSALVNQIGEILGADLDVIMSLNNLDEESNKKHPFPCPTTYRTALTY[1]
       |TNPPRTNVLYELAQYASEPSEQEHLHKMASSSGEGKELYLSWVVEARRHILAILQDYPSLRPPIDHLCE[2]
1AMO   |GENGGRA[3]
1IB0   |KFAIRADKKSNPVVRT[1]
1CNF   |SFVINGKQRNA[1]
2VNH   |ALLP[1]
1FDR   |EVPH[1]
3A1F   |DESQANHFAVHHDEEKDVITGLK[1]
```

Figure 2.3 Alignment of the basis set amino acids sequences with human Nox1-5 and Duox1/2.

The structure-based sequence alignment of the basis set proteins listed by their PDB codes was performed by the Dali server (Holm and Rosenstrom, 2010). The Nox/Duox sequences were added to the alignment based on conserved sequence motifs and secondary structure predictions in the FAD-binding domain and by alignment with the Nox2 crystal structure sequence (3A1F) in the NADPH-binding domain. The secondary structure elements are denoted by arrows for β-strands and curves for α-helices. Black arrows/curves denote secondary structure elements found in all listed proteins (or predicted for Nox/Duox family) and grey images indicate an element only found in some of the listed proteins. F and N listed with the helix or β-strand number denote the FAD-binding domain and NADPH-binding domain, respectively. Secondary structure elements are numbered when conserved in every protein. Elements named a,b are not found in all proteins. Conserved sequence motifs referred to in the text are shown in yellow. Exceptions to the alignment are listed following the alignment and explanations for this are as follows; 1AMO [1,2] These residues were not included in structural alignment as they create the FMN-binding domain; [3] Residues absent in the crystal structure. 1CNF [1], 1IB0[1], 2VNH[1], 1FDR[1] indicate insertions in linker region not included in the sequence alignment figure (for simplicity) but are present in the crystal structures. 3A1F [1] Sequence is not present in X-ray crystal structure

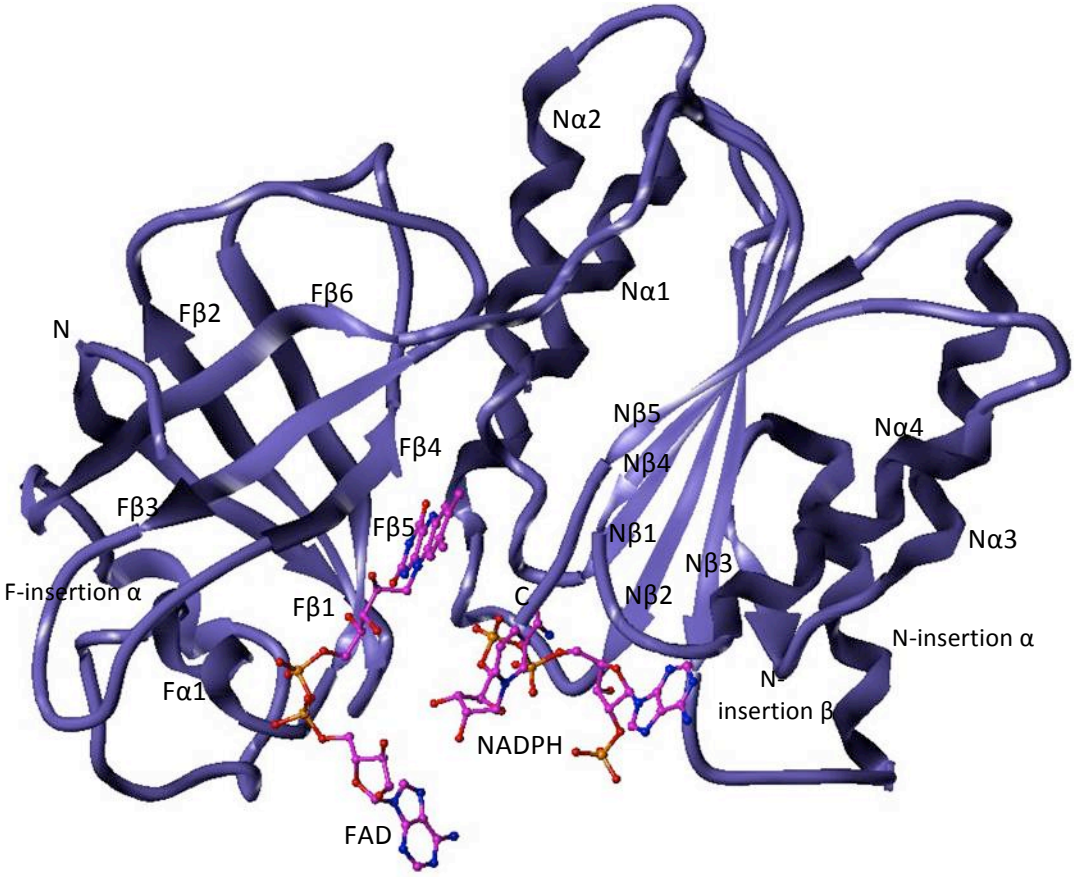

Figure 2.4 The Nox4 Dehydrogenase domain model.

The dehydrogenase unit is composed of two domains, a β-barrel fold capped by a single helix to bind the FAD, followed by a Rossmann fold that binds NADPH. The two ligands are shown as ball and sticks, with carbons in magenta, nitrogens in blue, oxygens in red and phosphates in orange. The overall fold of the model is similar to the basis set structures and includes two insertion sequences, one found in each domain.

2.3 Results and Discussion

2.3.1 FAD and NADPH Binding Sites

The Nox4 model contains the coordinates for the FAD and NADPH ligands from 1GJR. The FAD co-factor is positioned at the domain interface on the internal side of the β-barrel. The majority of the contacts between the protein and ligand are from β-strand Fβ4 and helix Fα1 forming a network of hydrogen bonds, Van der Waals contacts and polar interactions with primarily the isoalloxazine ring, ribityl and phosphates of the FAD. The residues of the Nox4 model that contribute Van der Waals contacts with the ligand are Phe354, Leu371, Gly375, Trp377, Ile433 and Phe577 (Figure 2.5).

All of the basis set proteins superimpose well with respect to the isoalloxazine ring and ribityl portion of FAD whereas the adenosine moiety is found in multiple conformations. The isoalloxazine ring is held in place by hydrogen bonds with Thr355, Thr436 and His370 and stacking interactions with Phe577. All of these residues are conserved in the Nox/Duox family (Kawahara et al., 2007). Thr436 is located in the glycine rich loop of the NADPH-binding domain conserved in all of the basis set structures (see Figure 2.3 alignment). Residues from this loop in all of these structures interact with FAD either through Van der Waals contacts or hydrogen bonding. The Nox4 model is shown with the final aromatic residue, Phe577, stacking with the isoalloxazine ring of FAD. A similar arrangement is seen in 1GJR, 1FNB, 1AMO, 1FDR, 1KRH and 2PIA, where an aromatic residue from the final β-strand of the NADPH-binding domain reaches across to the re-face of the FAD to interact. The other members of the basis set, 2EIX, 1IB0, 1CNF and 1CQX do not show this arrangement in

their crystal structures, though they do all conserve an aromatic residue in the same position.

The highly conserved HPFT motif in Nox/Duox proteins (His352, Pro353, Phe354 and Thr355 in Nox4) is somewhat different than the conserved RXYS/T motif of the basis set located in the fifth β-strand of the FAD-binding domain. The involvement of this motif in Nox FAD binding is confirmed by two CGD mutations, His338-Tyr and Thr341-Lys (Nox2 numbering, analogous to Nox4 His352 and Thr355), which show diminished ROS production and FAD-binding (Debeurme et al., 2010; Leusen et al., 2000; Yoshida et al., 1998). Histidine 352, although with fewer possible bonding residues than the guanidinium group of arginine, can also hydrogen bond with the phosphate groups of FAD together with Asp376 and Thr378 stemming from the neighboring helix (Fα1). The N-terminal positive dipole of this helix also contributes to binding the pyrophosphates. The second position of the motif points away from the ligand while its backbone hydrogen bonds with the ligand, explaining why this residue is not as well conserved in the basis set proteins. This position is a proline in all known Nox/Duox sequences except for some insect Duox proteins ((Kawahara et al., 2007) and Jackson unpublished results) and this proline indeed forms a backbone hydrogen bond to the ribityl group of FAD. The third position in the motif, a tyrosine in the basis set forms a second hydrogen bond to the ribityl portion of FAD via its side chain hydroxyl group. The Nox/Duox proteins strictly conserve a phenylalanine in this position and this residue forms Van der Waals contacts with the FAD. Since the phenylalanine does not hydrogen bond with the ribityl group, the backbone of His370 performs this function in the Nox4 model fulfilling the two hydrogen bonding requirements seen in the basis set. The last

residue of this motif (Thr355 in Nox4) is highly conserved as either a serine or threonine in both the basis set and Nox/Duox family and forms a backbone hydrogen bond with the isoalloxazine ring.

The remaining contacts with FAD seen in the basis set proteins than are not accounted for in the Nox4 model are interactions with the adenosine group. This moiety is in fact found in a several conformations in the basis set ranging from bent to extended with respect to the isoalloxazine ring. This bent conformation is seen in structures 1FDR and 1KRH. The remaining basis set proteins bind FAD in a more extended conformation. The difference between the two conformations appears to be determined by two conditions; 1. the length of the loop between the β-strand, Fβ5 and helix, Fα1 of the FAD-binding domain and 2. the length of the C-terminus. On the first issue, this loop is long in the extended FAD-binding group and it provides a stacking residue for the adenine ring and in some structures, an additional hydrogen bond. 1FDR and 1KRH both contain a short loop in this region (see Figure 2.2. lower, left loop near adenine). The one member of the basis set that is an exception to this is 2EIX, which contains an extended FAD and short loop. This conformation appears to be stabilized through interactions with the second chain of the crystallized dimer. The Nox4 sequence was modeled with a short loop, suggesting that either its FAD should conform to a bent shape or if it remains elongated (as displayed in the model), it may need to interact with other parts of the enzyme for stability. One candidate region is the FAD-insertion sequence (discussed in section 2.3.3). Though this region is modeled away from the ligand, its structure is not known, so it cannot be ruled out as a point of FAD contact. On the second issue, the bent conformation of FAD in 1FDR and 1KRH structures is stabilized by interactions with the

C-terminus. In the 1FDR structure, back to back tyrosine and tryptophan residues in the C-terminus allow for simultaneous stacking interactions with both isoalloxazine and adenine ring of FAD. The structures of 1KRH and two other ferredoxin reductases from *Azotobacter vinelandii* (Sridhar Prasad et al., 1998) or *Rhodobacter capsulatus* (2VNH) (Bortolotti et al., 2009) all contain a longer C-terminus that contributes either stacking interactions or hydrogen bonds to the bent adenine. The Nox4 C-terminal sequence neither contains an additional aromatic residue to stack with the adenine like 1FDR, nor a longer C-terminus like 1KRH suggesting that a bent conformation may not be stabilized in the Nox4 structure. Therefore, the Nox4 model contains coordinates for an extended FAD (see Figure 2.5), although neither conformation can be fully accommodated in the model. It remains to be determined whether and where are the residues responsible for interacting with adenosine moiety of FAD in Nox/Duox structures.

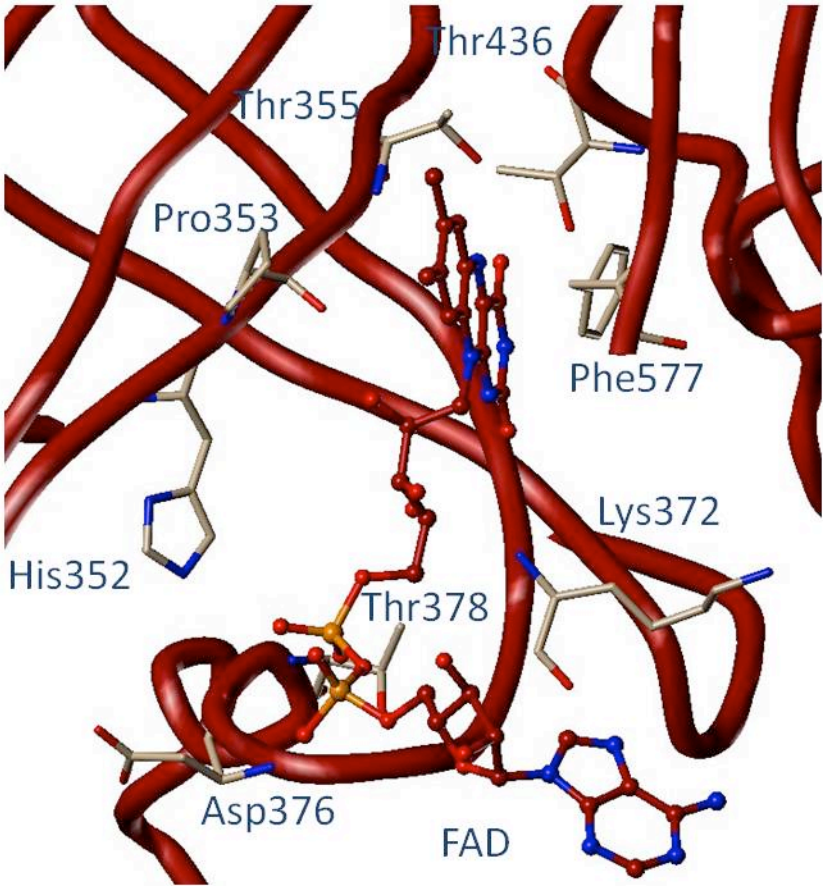

Figure 2.5 FAD-binding site of the Nox4 Model.

FAD sits at the domain interface on the internal side of the β--barrel. The isoalloxazine ring and ribityl group are bound by the neighboring β-strand, while the helix and His352 interact with the phosphates. Phe577 from the C-terminus stacks with the isoalloxazine ring. Important interacting residues are shown as sticks with the carbons in grey, nitrogens in blue and oxygens in red. FAD is shown with carbons in maroon, nitrogens in blue, oxygens in red and phosphates in orange.

The NADPH-binding site is composed of four loops (1-4) connecting Nβ1-Nα1, Nβ2-Nα2, Nβ3-Nα3 and Nβ4-Nα4 of the NADPH-binding domain. Figure 2.6 depicts these four loops in some basis set proteins grouped by NADPH or NADH specificity. Those residues that form hydrogen bonds, polar interactions or stack with the ligand are also displayed. The general features of all of the basis set proteins for binding the ligand are a hydrogen bonding network primarily to the phosphate groups and hydrophobic interactions. Evidence from studies on ferredoxin reductase suggest the adenine and diphosphate regions are recognized and bound first by the protein while the nicotinamide is more mobile and can move in and out of electron transferring position (Deng et al., 1999).

The Nox4 model can account for most of the important hydrogen bonding residues with the diphosphate region, namely Lys372, Arg 464, Ile 433. Lysine 372 extends from the Fβ5 strand of the FAD-binding domain and is the only residue from this domain to interact with NADPH. Additionally, Gly431 and Ser551 of the Nox4 model are within hydrogen bonding distance to the nicotinamide and adenine ring, respectively. Contacts with the nicotinamide ring are also seen in 1IB0 and 1GJR but it is not known how general these interactions are as none of the other structures contained the nicotinamide portion of the ligand bound in their crystal structures. Gly431 of Nox4 is part of the highly conserved glycine rich motif found in all the basis set proteins and Nox/Duox enzymes (see Figure 2.3 Alignment), suggesting this interaction is likely conserved.

The 1GJR and 1AMO structures show a residue extending from either Nα3 (Gln237 of 1GJR) or Nα4 (Asp639 of 1AMO) to hydrogen bond with the adenine ring.

Helix Nα3 in the Nox4 model is significantly smaller and farther away from the ligand than in the 1GJR structure, and helix Nα4 is closer. Ser551 from helix Nα4 does hydrogen bond with the adenine ring in the Nox4 model, however it is not conserved in the Nox/Duox enzymes and therefore, may not represent a genuine ligand interaction. Indeed, the Nox2 crystal contains an alanine residue in this position and in the present NADPH conformation in the Nox4 model, a backbone hydrogen bond to the ligand is not possible for this position. Placement of the NADPH ligand in the Nox4 model is only an estimation and there are other residues near either helix Nα3 or Nα4 in Nox/Duox enzymes that may provide this hydrogen bond if the NADPH were to sit in a different conformation. Van der Waals contacts are made between residues Val321, Gly432, Phe469, Pro549, Phe577 and Ser578 and the ligand. All of these residues except Ser578 are conserved in the Nox/Duox family (Kawahara et al., 2007) with few exceptions, suggesting these interactions are applicable to the rest of the enzyme family.

The ferredoxin $NADP^+$ reductase family, cytochrome p450 reductases and flavodoxin reductases bind NADP(H), while the cytochrome b5 reductase and nitrate reductase structures recognize NADH. The 1GJR and 1AMO loops contain two crucial arginine or lysine residues in loop 3 and a tyrosine that hydrogen bonds to the 2'phosphate, which is important for achieving specificity for NADPH (Figure 2.6 A.). 1CNF and 1IB0 contain a phenylalanine rather than tyrosine in this position and aspartic acid residues in loop 3, which would repel a negatively charged 2'phosphate group, conferring NADH specificity (Figure 2.6 B.). The Nox4 model contains an arginine residue (Arg523) in loop 3 and an arginine residue (Arg464) in loop 2 that are within or near hydrogen bonding distance of the 2'phosphate of NADPH (Figure 2.6 C). Both of

these positions are invariantly either an arginine or lysine in the Nox/Duox sequences suggesting a critical, conserved role for the basic sidechain (Kawahara et al., 2007). These arginines are present in the Nox2 crystal structure and they are near the modeled ligand when the Nox2 crystal and Nox4 model are superimposed (Figure 2.6C). These observations are consistent with the measured preference of Nox2 and Nox4 (and likely all Nox family members) for NADPH over NADH as a substrate in biochemical analyses (Cross et al., 1984; Nisimoto et al., 2010; Nisimoto et al., 1999).

The final important interaction with NADPH to be accounted for in the Nox4 model is the stacking interaction between an aromatic residue and adenine ring present in many nucleotide binding proteins. 1GJR and 1AMO contain tyrosine residues and 1IB0 contains a phenylalanine in the third loop of the NAD binding site that stack with the adenine ring. Interestingly, 1CNF also contains a phenylalanine in this position but it is flipped outward and is not actually stacking the ring. Loop 3 of the Nox4 model is part of the NADPH-binding domain insertion; consequently this region is an area of low confidence in the model. Nevertheless, the nearest aromatic residue in this region is Trp526. Although this position is highly conserved in most of the Nox/Duox family as either a tryptophan or phenylalanine (Kawahara et al., 2007), it resides too far from the NADPH ligand to effectively interact. This position is a CGD null mutant in Nox2 (Trp516-Arg), so perhaps its strict conservation in the Nox family can be explained by structural stability rather than an effect of ligand binding (Kaneda et al., 1999). In the Nox4 model and Nox2 crystal structure, an arginine residue sits in the same position as the aromatic residues of the basis set proteins and is also present in the 1FDR structure, though this structure does not contain NADPH. Arginine residues can form stacking

interactions through their planar guanidinium group (Flocco and Mowbray, 1994). This is seen in the recently crystallized ferredoxin reductase from *Rhodobacter capsulatus* in which Arg203 interacts with the adenine ring of NADPH (Bortolotti et al., 2009). An arginine residue in this position of Nox4 is also in place to hydrogen bond with the 2'phosphate similar to the tyrosine residues of 1GJR and 1AMO. As modeled, Arg523 is ~4 Å from the 2' phosphate of NADPH as this region was based on the Nox2 pyridine nucleotide-binding domain crystal structure, which did not contain the bound ligand. However, this residue could conceivably be within sufficient hydrogen bonding distance to the NADPH with minimal alterations to the protein backbone.

The adenosine portion of NADPH binds similarly between the various basis set proteins, however the diphosphate and nicotinamide portion can be bound differently even between two members of the ferredoxin reductase family. The disphosphate and nicotinamide portion of the ligand extend away from the protein in the 2VNH structure (ferredoxin reductase from *Rhodobacter capsulatus*), whereas the 1GJR (Ferredoxin reductase from *Anabaena*) binds these regions closer to the protein (Bortolotti et al., 2009). These differences in binding conformation are reflected in their binding affinities with the binding constant being two orders of magnitude stronger in the *Anabaena* structure than in the *Rhodobacter* structure (~2 μM vs. ~200 μM) (Bortolotti et al., 2009; Medina et al., 2001). The Nox/Duox sequences share similarities with both ferredoxin reductases and the measured K_m of NADPH for Nox2 and Nox4 is in between the two binding affinities (30-55 μM range of reported Km values of Nox2 and Nox4), suggesting these enzymes might bind NADPH in an intermediate conformation (Doussiere et al., 1993; Nisimoto et al., 2010). Due to similarities between the C-

terminal tale of 1GJR and the Nox/Duox sequences, the Nox4 model was created with NADPH binding similarly to 1GJR, although conceivably, some features of the alternative binding mode may apply to the Nox family. A crystal structure of a Nox enzyme bound to NADPH is needed to determine the exact binding conformation.

By homology with the ferredoxin reductase and cytochrome p450 reductase structures, three residues in the Nox4 model are predicted to surround the pyridine ring near the site where hydride transfer occurs; Thr352, Cys547 and Glu575. In general, these three residues are proposed to position the FAD and NADPH ligands so as to allow hydride transfer from NADPH to FAD, stabilize the transition states of the isoalloxazine ring or nicotinamide moiety and possibly assist in release of the oxidized $NADP^+$ (Deng et al., 1999; Hubbard et al., 2001). A more detailed electron transfer mechanism awaits further structural and biochemical studies of the Nox/Duox enzymes.

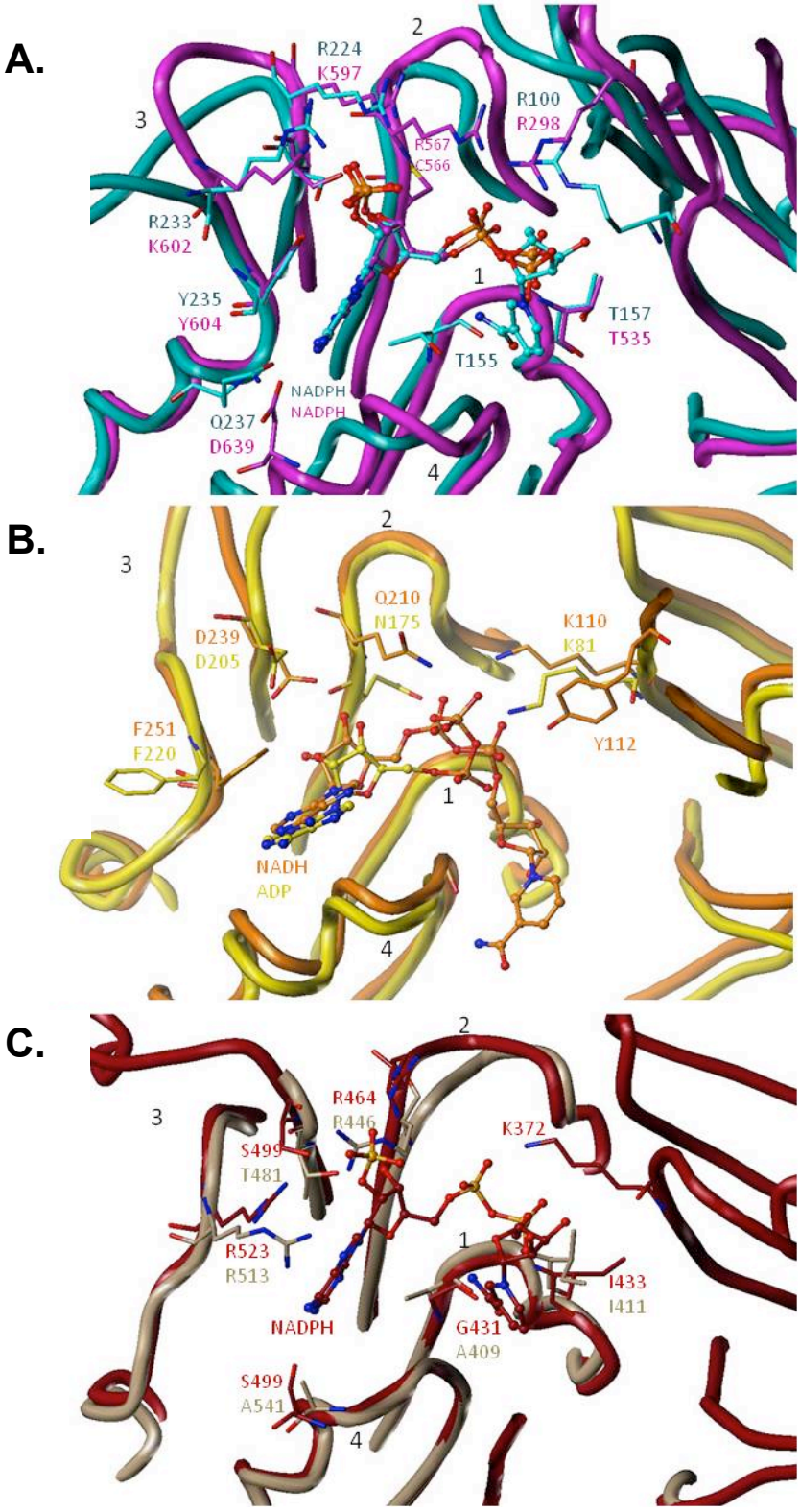
A.
R224
K597
2
R100
R298
3
R567
C566
R233
K602
1
Y235
Y604
T157
T535
T155
NADPH
NADPH
Q237
D639
4
B.
2
3
Q210
N175
D239
D205
K110
K81
F251
F220
Y112
1
NADH
ADP
4
C.
2
R464
R446
3
K372
S499
T481
1
R523
R513
I433
I411
NADPH
G431
A409
S499
A541
4

Figure 2.6 Structures of the NADPH-binding site.

Four loops (labeled 1-4) of the NADPH-binding domain compose the ligand binding cleft. Residues involved in hydrogen bonding, polar or stacking interactions with the ligand are displayed. The ribbon and carbons are color coded for their respective protein. **A**. 1GJR (cyan) and 1AMO (magenta) are depicted with their bound ligand. Both crystals bound NADP(H) however, the nicotinamide portion could not be solved in 1AMO. Residues highlighted in 1GJR are Arg100, Thr155, Thr157, Ser223, Arg224, Arg233, Tyr235 and Gln237 (Hermoso et al., 2002) and in 1AMO are Arg298, Thr535, Cys566, Arg567, Ser596, Arg597, Lys602, Tyr604 and Asp639 (Wang et al., 1997). **B**. 1IB0 (orange) and 1CNF (yellow) are shown with NADH and 5'ADP, respectively. Residues highlighted in 1IB0 are Lys110, Tyr112, Gln210, Asp239, Phe251 and Gly274 (Bewley et al., 2001); and in 1CNF are Lys81, Asp205 and Phe220 (Lu et al., 1995). **C.** The Nox4 model (maroon) and Nox2 crystal structure, 3A1F (gray) are shown with residues predicted to interact with the NADPH ligand. Residues highlighted in Nox4 are Lys372, Gly431, Ile433, Arg464, Ser499, Ser551 and Arg523; and in 3A1F are Ala25, Ile27, Arg62, Thr97, Arg129 and Ala157 (corrected Nox2 numbering in full length sequence are Ala409, Ile411, Arg446, Thr481, Ala541 and Arg513).

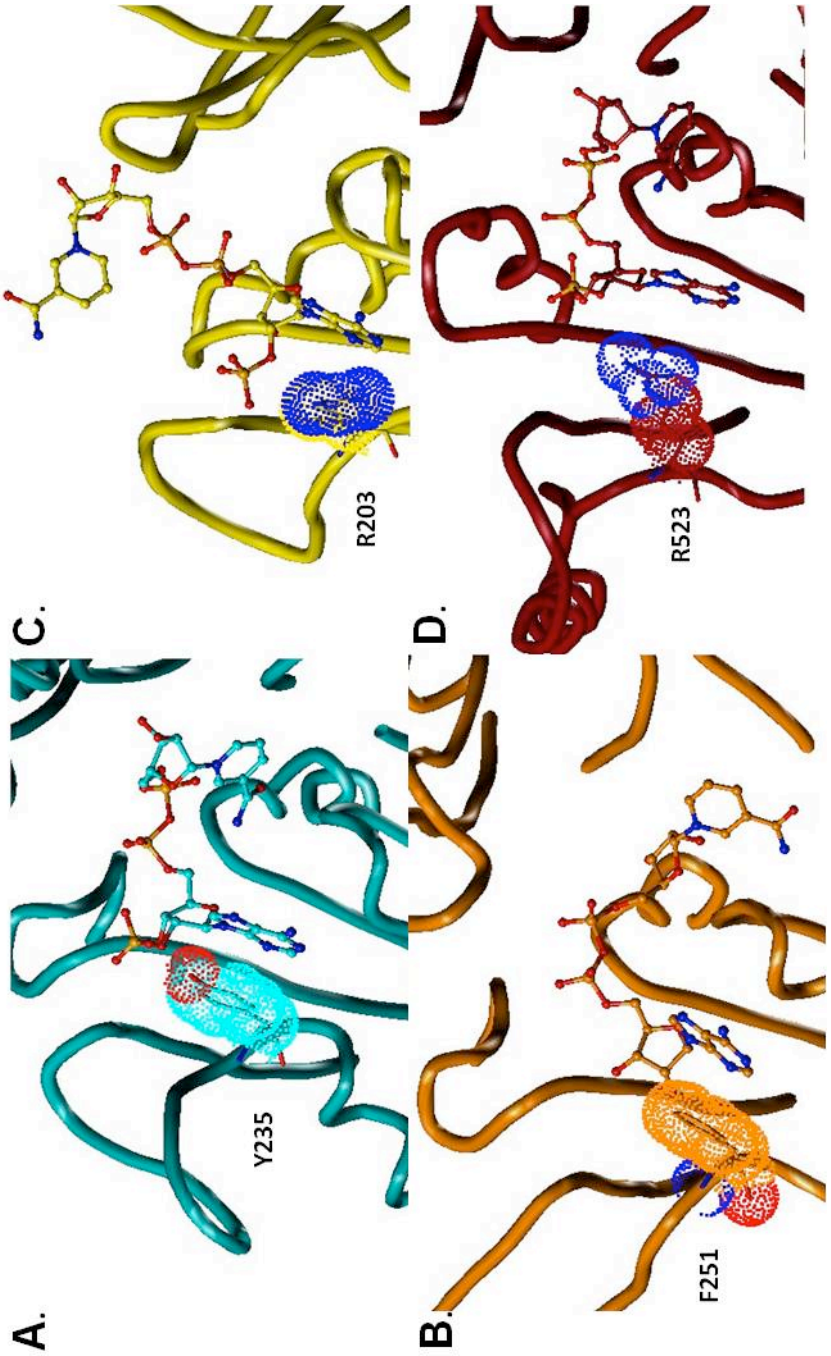
A.
Y235
B.
F251
C.
R203
D.
R523

Figure 2.7 Comparison of NAD adenine interactions in 1GJR, 1IB0, 2VNH and the Nox4 model.

Protein ribbons are displayed with their respective co-crystallized ligand. The Nox4 model is displayed with the ligand from 1GJR. The residue interacting with the adenine ring in each structure is shown with dot surface. Carbons are color coded with the ribbon, nitrogen atoms are shown in blue and oxygen atoms are shown in red. Tyr235 stacks with the adenine ring of $NADP^+$ in 1GJR **A**., while Phe251 performs the same function with NADH in 1IB0, **B.**, Panel **C.** shows Arg203 contacting the adenine ring via cation-π interactions in structure 2VNH. **D.** The Nox4 model contains Arg523 in this position similar to 2VNH.

2.3.2 Conserved Regions in all Nox/Duox Sequences

A molecular sequence analysis of over 100 Nox/Duox proteins from 25 species was conducted previously in the lab and 68 amino acids were found conserved in nearly every sequence (Kawahara et al., 2007). Many of these 68 residues are predicted to be important for FAD- and NADPH- binding, and most of the remaining residues were found grouped into four regions. These regions are referred to as the B-loop, a cytosolic loop connecting transmembrane helix two and three; TM6-FAD, the region between the sixth transmembrane helix and the first FAD-binding residues; VXGPFG, a motif in between the FAD and NADPH-binding sites and the C-terminus (Figure 2.8) (Kawahara et al., 2007). This study also confirmed the importance for Nox2 activity and expression of some of the residues in these regions by mutational analysis.

Five conserved residues are in the TM6-FAD region. These residues are Ile324, Met326, Lys328, Gly336 and Leu341 in Nox4 and they all localize to the β-barrel domain. The first two residues are also conserved hydrophobic residues in the basis set proteins because they reside in β-strand Fβ2 and are buried inside the hydrophobic barrel. A similar arrangement is seen with Leu341 of Fβ3, explaining the hydrophobic selective pressure on this position in Nox/Duox proteins. Gly336 is the first invariant residue of the polypeptide chain found among the Nox/Duox family and all basis set members (see Figure 2.3 Alignment). Its strict conservation is due to this residue being favorable at position i + 2 of type II turns (Wilmot and Thornton, 1988). It has been suggested that this type of turn in the β-barrel of ferredoxin reductases is important for packing with the NADPH-binding domain (Bruns and Karplus, 1995). Kawahara also showed that mutation of this residue to glutamic acid in Nox2 caused complete loss of maturation and

heterodimerization with p22*phox* confirming the importance of this residue in the stability of this domain (Kawahara et al., 2007). The lysine residue (Lys328) is located in a loop (Fβ2-Fβ3) and it is not conserved in the basis set, however, mutation of this residue to glutamic acid did cause significant reduction in Nox2 activity, suggesting that it is important for function, though the precise reason remains to be determined (Kawahara et al., 2007).

The second conserved region, VXGPFG is located at the end of the β-barrel chain extending into the linker region between the two domains. These residues correspond to Ile409, Gly411, Pro412, Phe413 and Gly414 in Nox4. The first position of this region is a conserved hydrophobic amino acid in all Nox/Duox and basis set proteins as it is also buried inside the β-barrel. The GPFG motif is conserved in most of the basis set proteins with the exception of third position which varies (see Figure 2.3 Alignment). The kink in the polypeptide chain caused by the position of the GP residues is also formed by 1FDR, though it does not conserve these residues. This kink in the structure at this position allows the chain to change direction to go on to form the linker region and NADPH-binding domain (Figure 2.8A). Without this kink, the chain would continue away from the FAD and orientation of the two domains, and therefore, ligands would surely be altered. Indeed, mutation of the first glycine of the motif in Nox2 to glutamic acid caused complete loss of protein expression (Kawahara et al., 2007). The aromatic residue at position three of the motif is also conserved in the 1KRH and 1CQX structures. In both of these cases, the aromatic residue packs against the neighboring aromatic residue at the N-terminus of Fβ3. Interestingly, the Nox/Duox family also conserves the aromaticity of this position in Fβ3 and this packing arrangement is also seen in the Nox4 model.

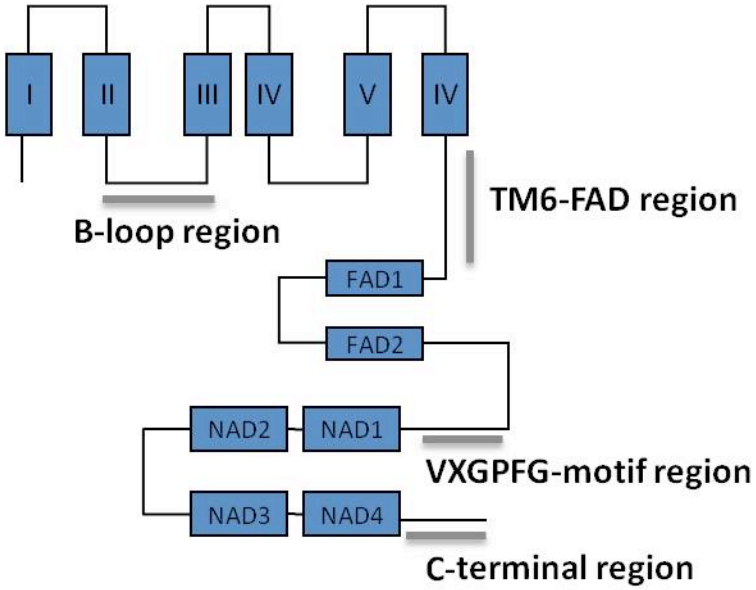

Figure 2.8 Regions conserved in Nox/Duox family.

A molecular sequence analysis of over 100 Nox/Duox proteins from 25 species was conducted previously and four regions were found conserved in nearly every sequence (Kawahara et al., 2007). These regions are referred to as the B-loop, a cytosolic loop connecting transmembrane helix two and three; TM6-FAD, the region between the sixth transmembrane helix and the first FAD-binding residues; VXGPFG, a motif in between the FAD and NADPH-binding sites and the C-terminus (Kawahara et al., 2007).

The final C-terminal region was found to contain four strictly conserved residues in the Nox/Duox family; Leu556, Phe570, Glu575 and Phe577 (Nox4 numbering). The leucine and phenylalanine are also conserved in some of the basis set proteins as a hydrophobic and aromatic residue, respectively. As with the hydrophobic residues in the TM6-FAD region, these amino acids are also buried in protein core suggesting that preservation of protein fold is the driving force for their conservation. The last two conserved amino acids are positioned closer to the domain interface at the site of FAD- and NADPH-binding. Phe577 of Nox4 was previously discussed in the FAD-binding section as this residue stacks with the isoalloxazine ring (see section 2.3.1). Glu575-Arg is a CGD mutation in Nox2 resulting in loss of activity, subunit translocation and FAD binding (Debeurme et al., 2010; Kawahara et al., 2007; Leusen et al., 2000). A function of the glutamic acid residue conserved in most of the basis set proteins was uncovered upon crystallization of the ferredoxin reductase protein co-crystallized with $NADP^+$ in a productive binding mode (Deng et al., 1999). This structure, which contains a mutation of the C-terminal tyrosine residue to serine allows the nicotinamide moiety of NADPH to come into electron transferring position with the isoalloxazine ring of FAD. This conformation is stabilized by a hydrogen bond between the glutamic acid side chain and the carboxamide group of the nicotinamide moiety. It is not completely understood where the C-terminal aromatic sidechain goes when the nicotinamide moiety is positioned with the isoalloxazine ring as this was only observed in the ferredoxin reductase mutant protein. Since Nox4 is not modeled with the isoalloxazine and nicotinamide moieties in electron transferring positions, this function of the glutamic acid

residue is not readily apparent, however, the conservation between the Nox/Duox family and ferredoxin reductases does suggest a similar conformation is achievable.

While the above function explains the loss of activity in the CGD Glu568-Arg mutation in Nox2, it is not so apparent why this substitution results in loss of FAD binding and subunit translocation (Debeurme et al., 2010; Leusen et al., 2000). The somewhat buried position of this glutamate and distance from the other proposed subunit binding sites indicates that it is not likely to directly contact p47*phox* or p67*phox*. And neither is this glutamate predicted to directly bind FAD in the Nox4 model or in ferredoxin reductases or cytochrome p450 reductase (analogous position in aspartate). Therefore, FAD or subunit binding disruption of the mutation may be due to drastic structural changes that occur upon lysine substitution.

In summary, the Nox4 model and comparisons with the structurally homologous basis set proteins has allowed us to assign functions to these regions that were previously reported to be highly conserved in the Nox/Duox family. The TM6-FAD region composes part of the β-barrel domain and evolution has constrained many of these residues to be hydrophobic to accommodate the barrel fold. The VXGPFG region helps to direct the polypeptide chain to help orient the two domains that must be in close enough proximity to allow electron transfer. The C-terminus is crucially important to both bind and help stabilize the electron transferring conformation of the ligands. The final region, the B-loop will be discussed in Chapter 3.

2.3.3 Insertions

The loops within the FAD-binding domain of the Nox/Duox human sequences are mostly within the range of sizes displayed by the basis set proteins, excepting the F-insertion and the small loop between Fβ5 and Fα1. Implications of this small loop were discussed in the FAD-binding site section (see section 2.3.1). The four loops connecting the C-terminus of the β-strands to the N-terminus of the helices in the NADPH-binding domain that compose the ligand binding site are well conserved in sequence length and identity. However, the loops connecting the C-terminus of the helices to the N-terminus of the β-strands, which lie at the opposite side of the domain as the ligand, do vary between the basis set structures and Nox/Duox sequences (Figure 2.9). The loop connecting Nα1-Nβ2 is larger in Nox5 than any other Nox or basis set sequence and it contains a C-terminus polybasic region identified in Nox5 to be important for activity (Kawahara and Lambeth, 2008). Interestingly, residues at the C-terminus of Nα1 were recently proposed as the Rac binding site in Nox2 (Kao et al., 2008). These two independent studies suggest this region could be important for modulating Nox activity. The larger size of loops Nα2-Nβ3 and Nα3-Nβ4 is also characteristic of the Nox/Duox family versus the other basis set proteins, and further studies are needed to determine the significance of this difference.

The Nox/Duox amino acid sequences contain two larger insertions relative to the other basis set members, one located in each domain (Figure 2.9). The presence of an insertion in the NADPH-binding domain (referred to here as N-insertion) was previously discussed by Taylor and colleagues (Taylor et al., 1993), however the presence of the insertion in the FAD-binding domain (F-insertion) has not to our knowledge been

previously acknowledged. In fact, the F-insertion was aligned with the basis set differently between our Nox4 model and the Taylor Nox2 model (see Page 52-53) for further explanation) (Taylor et al., 1993). For the purposes of this discussion, the F-insertion is defined as residues Asp383-Pro405 and the N-insertion is defined as residues Gln500-Phe520 in the human Nox4 sequence. Interestingly, both insertion sequences in the Nox/Duox family show isoform specificity, suggesting these insertions may confer different isoform characteristics such as regulation.

The N-insertion in the Taylor Nox2 model forms a helix that covers the NADPH-binding cleft and it was therefore proposed as a regulated element in Nox2 activation (Taylor et al., 1993). Our Nox4 model used the recently solved Nox2 crystal as a template in this region since it is not present in the other basis set structures. Though the Nox2 crystal does not contain coordinates for the entire insertion region, it shows the direction of the polypeptide chain as heading away from the ligand binding cleft and the residues re-entering the domain form an additional β-strand (NIβ in Figure 2.3) in line with the other strands of the domain. The Nox4 model fills in these missing residues with a helix (Figure 2.8C), which is also predicted in the other Nox/Duox isoforms. So as to preserve the structure of the additional β-strand (NIβ), the insertion helix (NIα) cannot sit over the ligand-binding cleft in the Nox4 model. However, all of the other Nox isoforms have more sequence in the N-insertion than Nox4 and these extra residues might allow for more mobility of the helix (see Figure 2.3 Alignment).

Multiple CGD mutations, deletions and point mutations of Nox2 resulting in deficient subunit translocation and Nox2 activity within this insertion clearly suggest this is a possible docking site for one or more regulatory subunits (Leusen et al., 2000; Li et

al., 2005; Schapiro et al., 1991). Recently, the N-insertion of Nox5 was proposed as a binding site for the EF-hand regulatory domain (Tirone et al., 2010). This interaction could occur in the other EF-hand containing Nox enzymes, Duox1 and Duox2, though this has not yet been directly tested. Interestingly, the Nox4 N-insertion is the smallest of all of the Nox isoforms and this enzyme is the only isoform to display constitutive activity. Recently, two Nox homologues were discovered in *Na. gruberi* that contain a much larger N-insertion, forming an SH3 domain (Sumimoto, 2008). The binding partner of this domain is unknown. However, its presence indicates that this insertion could be an evolutionarily conserved, general region of regulation.

The F-insertion was modeled as a loop with two turns of a helix. However, this region is not predicted with high confidence to have secondary structure by prediction servers (Phyre and Predict Protein) (see Figure 2.9 B). Therefore, its structure in the model is more of a place holder than a strong prediction. Many of the residues composing this insertion are hydrophobic suggesting that it may fold back towards the β-barrel. The residues composing the F-insertion in Nox4 have not been studied, so little is known about their function. However, this region has been investigated in Nox2 and Nox5. The CGD mutation Cys369-Arg displays normal amounts of Nox2 protein, but has diminished ROS production and p47*phox*/p67*phox* translocation to the membrane, a requirement for Nox2 activity (Leusen et al., 2000). Indeed another group has determined that a peptide corresponding to the defined F-insertion of Nox2 can bind p67*phox in vitro* (Edgar Pick, personal communications). These lines of evidence point to this region serving as a docking site for regulatory subunits in Nox2. This hypothesis may also apply to the other subunit-dependent Noxes, Nox1 and Nox3, though this has

not been directly tested and there is only some sequence conservation between Nox2 and Nox3 and even less with Nox1 in this region (see Figure 2.3 Alignment).

Somewhat perplexing is that the CGD Cys369-Arg substitution was recently found to diminish FAD-binding of Nox2 in the transfected X-CGD PLB-985 cell model system (Debeurme et al., 2010). The placement of this insertion after the helix Fα1 is distant from the FAD-binding site. Perhaps this mutation compromises the larger protein structure, indirectly affecting its ability to bind the ligand. Alternatively, it may suggest that this insertion does in fact fold in such a way as to contact the ligand.

Interestingly, several serine/threonine residues located in this F-insertion in Nox5 were shown to be phosphorylated by PKC and this event leads to increased calcium sensitivity of Nox5 superoxide production (Jagnandan et al., 2007). These data suggests the EF-hand regulatory domain of Nox5 must be in physical or energetic contact with this insertion to observe such feedback. This notion along with the proposed subunit interactions with the Nox2 F- and N-insertions conform to a general mechanism: the insertions in Nox sequences relative to the basis set provide the point of contact between these enzymes and their regulatory domains or subunits and may help to induce the catalytically active conformation.

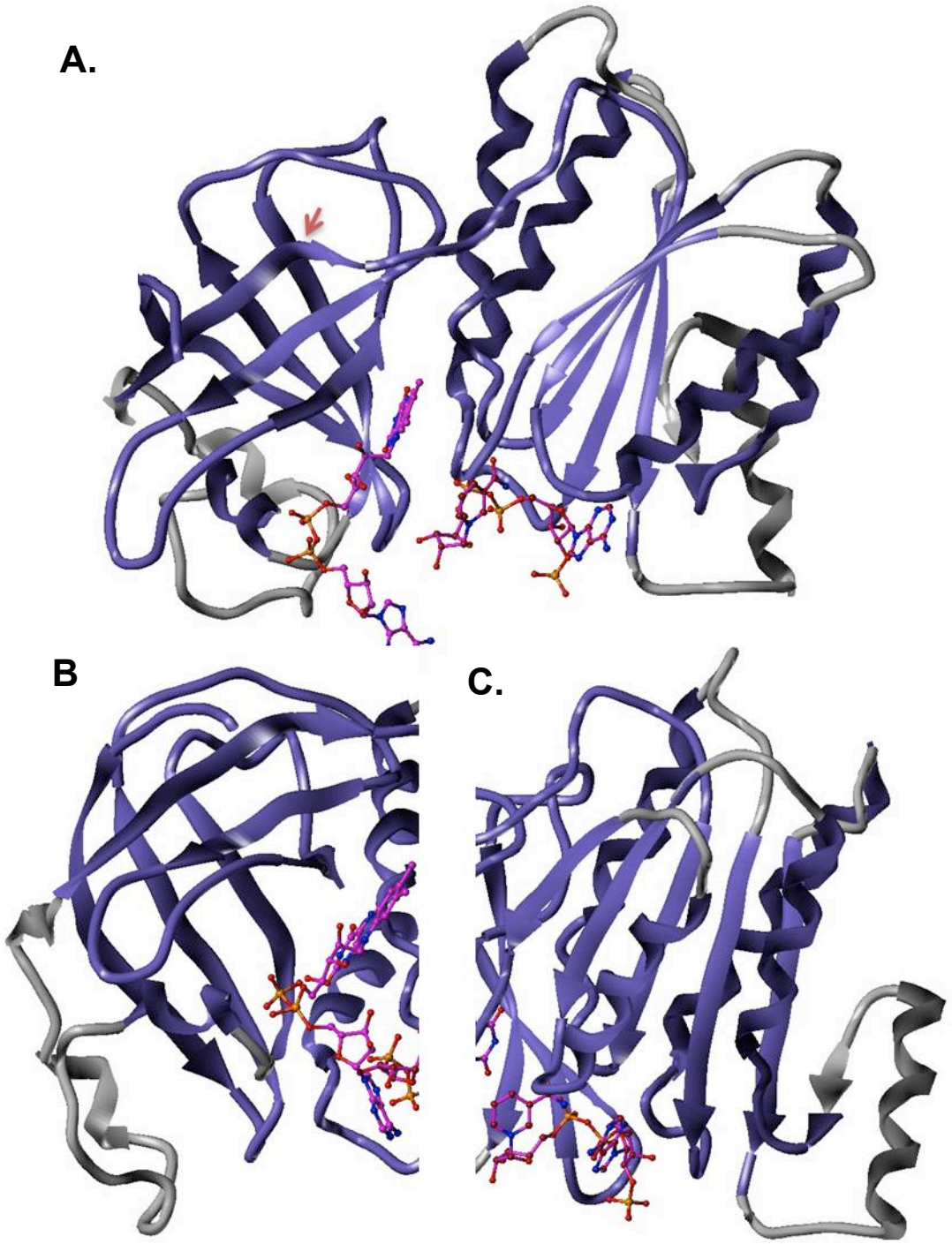
A.
B
C.

Figure 2.9 The Nox4 DH domain model displaying the variable loops.

Panel **A** shows the "front" view of the model with the FAD-binding β-barrel on the left and the NADPH-binding domain on the right. The loops that are different in size from the basis set structures are shown in grey. The region composed of the GPFG motif is denoted with a red arrow referring to the kink in the β-strand. Panel **B** shows the F-insertion and small loop of the FAD-binding domain. Panel **C** shows the loops of varying sizes in the NADPH-binding domain. The N-insertion contains an additional β-strand (NIβ) and helix (NIα) compared with the rest of the basis set.

2.3.4 Homology models of the transmembrane and dehydrogenase domains of Nox4

The Nox/Duox family has been proposed to evolve from the gene fusion of an ancestral cytochrome b and ferredoxin reductase (Sumimoto, 2008). The transmembrane domain of the Nox/Duox proteins is predicted to contain six membrane spanning α-helices connected by five loops. The B- and D-loops face the cytoplasmic side of the membrane while the remaining loops reside in the extracellular space or lumen, depending on the localization of the enzyme. Transmembrane helices three and five contain four histidine residues that coordinate two heme groups referred to as heme A and heme B. Helices two through five are homologous to the transmembrane four helix bundle of the cytochrome bc1 complex, formate dehydrogenase and cytochrome b6f that also bind two heme groups. Dr. Susan Smith constructed the model of the Nox4 transmembrane domain using these proteins as templates.

Hydride transfer occurs between the C4 atom of the nicotinamide ring in NADP(H) and the N5 atom of the isoalloxazine ring of FAD in the ferredoxin reductases (Karplus et al., 1991). The electron transfer route continues in the Nox/Duox family with passage from FAD to heme B, heme A and finally to molecular oxygen. The two models are shown in Figure 2.10 in an orientation that aligns the di-methyl edge of the FAD facing towards heme B. This is an approximate orientation based on the idea that electrons transfer from the C8 atom of FAD to the heme edge as is the case in flavohemoglobin (Ermler et al., 1995). Theoretically, the transmembrane domain may rotate 360 degrees about the y-axis to keep heme B facing towards the FAD. However, as the domains are oriented in Figure 2.10, the B-loop does not sit over the ligand binding pockets allowing oxidized $NADP^+$ to freely exchange with reduced NADPH.

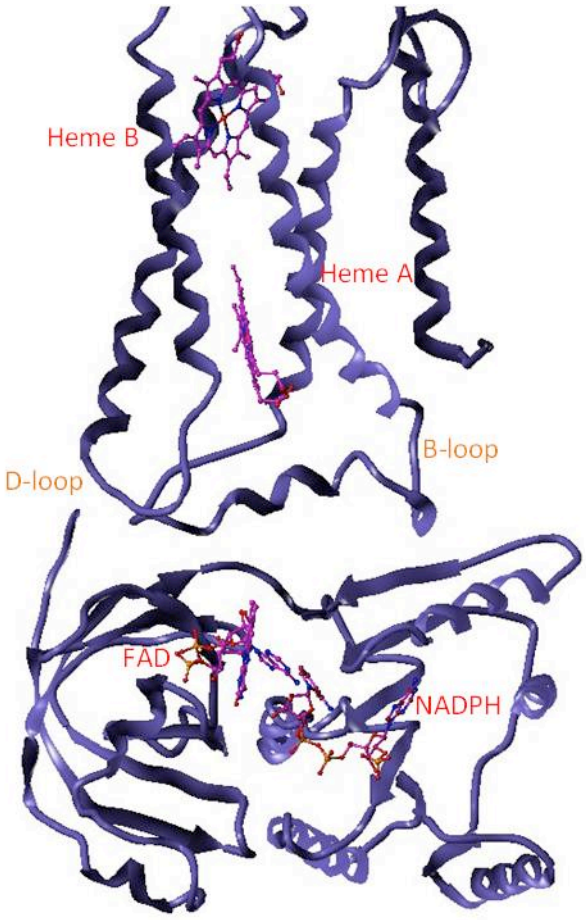

Figure 2.10. Models of the Nox4 transmembrane and dehydrogenase domains.

The transmembrane domain model is shown in an approximate orientation with the dehydrogenase domain model. Two hemes, FAD and NADPH are shown in ball and stick representation. The transmembrane domain model is composed of a four helix bundle (helices 2-5 in the Nox family) binding two heme groups. The first transmembrane helix is not modeled and the sixth transmembrane helix is shown off to the right. The large, un-modeled loops A, C and E are not viewed. The two intracellular loops B and D are labeled. Electrons pass from the NADPH ligand through FAD, heme B, heme A to molecular oxygen.

2.4 Conclusions and Future Directions

The homology model of the Nox4 DH domain is the starting point for a wide variety of structure-function studies on Nox enzymes. This model offers an improvement over the former Nox2 model by including sequence information about the entire Nox/Duox family rather than just Nox2 for alignment with the structural templates. The FAD- and NADPH- binding sites have been re-examined and the contacting residues proposed here are conserved in the majority of the Nox/Duox family. These candidate residues now require mutational studies to directly test their involvement in ligand binding.

Future directions also include docking the transmembrane and dehydrogenase domain models. The two domains are roughly oriented in Figure 2.10. However, more information is needed to accurately dock these two models. Indeed, a model of the holo-Nox4 enzyme would provide a structural platform to understand previous biochemical studies. For instance, mutations in the D-loop of Nox2 caused significant reduction in activity and switching the Nox4 D-loop into a Nox2 backbone caused a significant increase in Nox2 activity (Li et al., 2005). It is unknown how such a small loop could have an effect on activity and certainly a three dimensional model of this loop in the holo-enzyme could provide clues to its function.

The Nox4 models can also be used as templates to build models of the other Nox isoforms. Very little is known about the Nox5 and Duox structures so models of these isoforms would be especially informative. Indeed, the EF-hand motifs in Nox5 and Duox1 were recently modeled (Kawahara et al., 2007) so addition of the other two

domains would complete the Nox5 structure. Models of the Nox1-3 DH domains could provide the structural foundation for docking their regulatory subunits, many of which have had partial structures solved by NMR or x-ray crystallography (Karathanassis et al., 2002; Lapouge et al., 2000). An understanding of the subunit-DH domain interactions would certainly provide clues as to their mechanisms of regulation. Furthermore, a comparison between structures of Nox4 versus the regulated Nox isoforms could help elucidate the mechanism by which Nox4 displays constitutive activity. Additionally, Nox models could aid in the design of isoform or conformational specific antibodies.

The alignment of the two models (shown in Figure 2.10) predicts that the B-loop region should be in close proximity to the DH domain. This loop is also the only remaining highly conserved region that we did not describe a possible function in section 2.3.2. The next chapter addresses both of these issues and directly tests the prediction of these models.

Chapter 3

The Nox4 B-loop interacts with the dehydrogenase domain

3.1 Introduction

Nox4 is unique among the Nox enzymes in that it is constitutively active in the absence of non-membrane-associated regulatory subunits or calcium binding regulatory domains (Ambasta et al., 2004; Kawahara et al., 2005b; Martyn et al., 2006). The constitutive activity of Nox4 suggests that this enzyme exists in or is in equilibrium with an active conformation. Understanding the structural features of Nox4 may, therefore, provide insights into the active conformation of all of the Nox enzymes, which in other Nox enzymes is induced by regulatory domains or subunits.

Most of these regions identified by the molecular evolution analysis performed previously in our lab were assigned functions in Chapter 2 using the Nox4 homology model. However, one region, the cytosolic B-loop, remained to be investigated.

In earlier studies of Nox2, this loop was proposed as a binding site for p47*phox*, as residues corresponding to a region of this loop from a phage display peptide library bound to recombinant p47*phox* (DeLeo et al., 1995). Furthermore, both mutagenesis of arginine residues in the Nox2 B-loop and peptides corresponding to the Nox2 B-loop inhibited Nox2 activity and prevented p47*phox*/p67*phox* translocation to the membrane (Biberstine-Kinkade et al., 1999; DeLeo et al., 1995; Park et al., 1997). However, the Nox2 B-loop shares considerable homology with that of Nox4 (*vide infra*), suggesting a more general role for this loop in Nox function. The TM and DH domain homology models of Nox4, when fit together according to the proposed electron transfer scheme, predict the B-loop to be in close proximity to the DH domain (see Figure 2.9).

The present study was undertaken to investigate the importance of the B-loop in Nox4 function. Using fluorescence polarization, we find that Nox4 B-loop binds to the DH domains of Nox4 and data support a model in which this binding mediates the functionally important interaction between the FAD/NADPH-binding DH domain and the heme-containing TM domain of Nox enzymes.

Fluorescence polarization was first described in 1926 by Perrin and developed further by Weber (Perrin, 1926). The Stokes equation relates rotational rates with molecular size and the Perrin equation relates fluorescence polarization with rotational rates and fluorescence lifetime (reviewed, (Dandliker and De Saussure, 1970)). Combining the two equations gives the basis of fluorescence polarization: size of a fluorescent molecule affects its rotation rate and alters the plane in which the molecule will emit light. In the experimental setup, a fluorophore is excited with plane polarized light and its emission is recording in the parallel and perpendicular planes. The size of the fluorophore and thus how fast it rotates, will dictate how much light is detected in these two planes. Weber was the first to apply fluorescence polarization to measure the binding between two molecules (Weber, 1953). The advantages of using fluorescence polarization for binding studies are that it is quantitative, sensitive, allows for measurement of binding in solution and it not dependent on fluorescence intensity (Jameson and Seifried, 1999). We used this technique to investigate the binding the Nox4 DH domain protein and B-loop peptides.

3.2 Experimental Procedures

B-loop Sequence Alignment- Nox family B-loop and surrounding sequences were aligned using ClustalW2 available online (http://www.ebi.ac.uk/Tools/clustalw2/index.html) from European Bioinformatics Institute (Larkin et al., 2007). Alignments were created using human Nox1 (GenBankTM accession No. NM_007052), rat Nox1 (GenBankTM No. NM_053683), chicken Nox1 (DDBJTM No. BR000265), dog Nox1 (GenBankTM No. XM_549136), mouse Nox1 (GenBankTM No. NM_172203), human Nox2 (GenBankTM No. NM_000397), mouse Nox2 (GenBankTM No. NM_007807), rat Nox2 (GenBankTM No. NM_023965), dog Nox2 (DDBJTM No. BR000269), chicken Nox2 (DDBJTM No. BR000270), human Nox3 (GenBankTM No. NM_015718), mouse Nox3 (GenBankTM No. AY573240), dog Nox3 (DDBJTM No. BR000273), chicken Nox3 (GenBankTM No. XM_426166.1), rat Nox3 (GenBankTM No. NM_001004216), human Nox4 (GenBankTM No. NM_016931.2), mouse nox4 (GenBankTM No. NM_015760), rat Nox4 (GenBankTM No. NM_015760), dog Nox4 (GenBankTM No. XM_542262.2), frog Nox4 (Ensembl No. ENSXETP00000025676), chicken Nox4 (DDBJTM No. BR000274), human Nox5 (GenBankTM No. AF353088), dog Nox5 (DDBJTM No. BR000277), cow Nox5 (DDBJTM No. BR000276), opossum Nox5 (DDBJTM No. BR000304), chicken Nox5 (DDBJTM No. BR000278), frog Nox5 (Ensembl No. ENSXETP00000017078), human Duox1(GenBankTM No. NM_017434), Duox2 (GenBankTM No. NM_014080).

Site-directed Mutagenesis- Nox4 point mutations including Arg84 mutated to Ala (denoted R84A) were generated using site-directed mutagenesis with human Nox4 cDNA with a silent mutation deleting the internal BamH1 site. Amplification used a sense Nox4

full length primer with an N-terminal BamH1 site (Primer 1 = 5'ttttGGATCCGCCACCATGGCTGTGTCCTGGAGGAGCTGGCTCGCCAACGA-3') and anti-sense Nox4 primer with a C-terminal Not1 site (Primer 2 = 5'-ttttGCGGCCGCC TAGCTGAAAGACTCTTTATTGTATTC-3'). Two internal primers were also generated for each point mutation (primer 3 = 5'-AGCAGGAGAACCGAGAGATTGTTGGAT-3' and primer 4 = 5'-ATCCAACAATCTCTCGGTTCTCCTGCT -3') with the R95E substituted codon underlined. PCR reactions amplified Nox4 cDNA using primers 1 & 3, 2 & 4 and the products of these two reactions were amplified by primers 1 & 2 to create full length cDNA containing the appropriate point mutation. PCR products were digested and inserted in mammalian expression vector, pcDNA3 (Invitrogen) and correct sequences were verified by commercial DNA sequencing (Agencourt Bioscience Corp.). A similar strategy was used to create all Nox4 amino acid substitutions. Nox4 C-terminal myc-tagged constructs were created for immunoprecipitation and western blots using sense Primer 1 and anti-sense Primer 5 (5'-ttttGTCGACGCTGAAAGACTCTTTATTGTATTCAAATCTTGTCCC-3') which does not include a stop codon and includes a C-terminal Sal1 site for insertion into pCMV-Tag 5a vector (Stratagene).

Chimera protein constructs- See Chapter 4 experimental section.

ROS Measurement- HEK 293 cells were cultured in Dulbecco's modified Eagle's medium (Gibco) (+ 4.6g/l glucose + l-glutamine) + 10% (v/v) fetal bovine serum (Atlanta Biologicals) supplemented with 100U/ml penicillin and 100µg/ml streptomycin (Gibco) in 5% CO_2 at 37ºC. Cells for ROS measurements were plated in 6-well plates, grown for

24 hours and transfected with WT or mutant human Nox4 cDNA in pcDNA3 or empty pcDNA3 using Fugene-6 (Roche) transfection system according to manufacturer's instructions. After approximately 48 hours, cells were harvested in Hank's Balanced Salt Solution (Gibco) and ROS was measured using luminol chemiluminescence with 20 μM Luminol and 0.32U horseradish peroxidase in 200 μl total volume with FluoStar™ luminometer (BMG Labtech). The mean of three separate wells is reported with standard deviation (SD). A minimum of three separate transfection experiments were repeated for each condition.

Nox4 Cell-free System- HEK 293 cells were grown and transfected as described above. To prepare cell lysates of Nox4 transfected cells, cells were suspended in lysis buffer containing 1x PBS, 0.1 mM EDTA, 0.1 PMSF, 0.2 mM FAD with a protease inhibitor cocktail. Cells in lysis buffer were sonicated twice for 10 seconds (20%, cycle duty 3) and stored on ice for 30 seconds in between pulses. Lysates were pre-incubated with 250 μM B-loop peptides for 40 minutes prior to addition of assay buffer containing 25 mM Hepes, 120 mM NaCl, 3 mM KCl, 1 mM Mg_2Cl, 100 μM amplex red, 0.032 units of horseradish peroxidase and 25 μM NADPH. Amplex red fluorescence was monitored at 37ºC by Synergy™2 Multi-Mode Microplate Reader and Gen5™ software package (Bio Tek). Amplex red reagents were excited at 540 nm wavelength with a bandwidth 25 and emission was recorded with a 620 nm filter with 40 nm bandwidth.

Co-Immunoprecipitation and Western Blot- Nox4- myc tagged constructs were transfected into HEK 293 cells grown for 24 hours in 10 cm culture dishes using Fugene-6 transfection system. Cells were harvested in HBSS and lysed in 20 mM Tris-HCl, 1% Triton-X 100, 150 mM NaCl containing protease inhibitor cocktail and EDTA (Complete

mini, Roche), 1 mM phenylmethylsulfonyl fluoride (PMSF) and 100 μM diisopropyl fluorophosphate (DFP), the latter included to improve access of the protease inhibitor to membrane compartments. Lysates were centrifuged and the protein-containing supernatant fractions were incubated with anti-myc monoclonal antibodies (Cell Signaling) overnight. Immuno-reactive proteins were precipitated with Protein G sepharose 4B beads (Sigma) and washed 10 times with Tris buffer before addition of Laemmli sample buffer (Bio-Rad) containing 5% 2-mercaptoethanol. Samples were resolved by SDS-PAGE followed by Western blot using the previous anti-myc antibody and anti-p22*phox* monoclonal antibody 44.1 (a generous gift from M. Quinn and purchased from Santa Cruz) and protein was visualized with secondary anti-mouse conjugated horseradish peroxidase (HRP) antibodies detected with enhanced chemiluminescence substrate (Pierce).

Recombinant Protein Purification- To express and purify recombinant Nox4 and Nox2 dehydrogenase domain proteins, constructs were created starting from the end of the last predicted transmembrane helix to the C-terminus consisting of residues Nox4 304-578 (GenBankTM No. NM_016931.2) and Nox2 290-570 (GenBankTM No. NM_000397) for full length dehydrogenase domains. Nox4 dehydrogenase domain truncations consisted of the following amino acid sequences: the predicted FAD-binding domain and small linker, residues 304-420; the linker region and NADPH-binding domain, residues 411-578; the N-terminal half of the NADPH-binding domain, residues 420-488; and the C-terminal half of the NADPH-binding domain, residues 489-578. The following primers were used to amplify human Nox2 or human Nox4 cDNA; Nox2 sense with BamH1 site underlined beginning with residue 290 (5’-

ttttggatccgatctcaacagaaggtgtcatca-3) and Nox2 antisense with Sal1 site underlined (5'-ttttgtcgacttagaagttttccttgttgaaaatgaaatgcac -3'); Nox4 sense beginning with residue 304 (5'-ttttggatccggagcaataagccagtcaccatca-3') and antisense primer ending with residue 578 (5'-ttttgtcgacctagctgaaagactctttattgtattc-3'); antisense primer ending with residue 420 and added stop codon (5'- ttttgtcgactcatgattcctcaaatggacttc-3'); sense primer with BamH1 site beginning with residue 411 (5'-ttttggatccggtccttttggaagtccatttgag-3'); sense primer with BamH1 site beginning with residue 420 (5'-ttttggatcctcactgaactatgaggtcagcctc -3'); antisense primer ending with residue 488 and Sal1 site (5'-ttttgtcgacttatctgttctcttgccaaaacttgttatgc-3'); sense primer beginning with residue 489 with BamH1 site (5'-ttttggatccctgactatgtcaacatccag-3'). All PCR products were digested with BamH1 and Sal1 and ligated into pGEX 4T3 (GE Healthcare) to generate glutathione S-transferase (GST) fusion proteins. Proteins were expressed in E. coli BL21 DE3 pLys and cultured at 37ºC until reaching an OD_{600} ~0.6-0.8. After addition of 200 mM IPTG, bacteria were induced for six hours at 25ºC. Cells were lysed in 50 mM Tris-HCl pH 7.5, 150 mM NaCl, 10 μM FAD, 1 mM PMSF, 100 μM DFP, 0.05% (v/v) Tween-20, 1 mM 1,4-dithiothreitol, with Complete protease inhibitor cocktail (Roche). Lysate was sonicated and centrifuged at 15,000 x g for one hour followed by incubation of the supernatant fraction with Glutathione Sepharose™ 4B (GE Healthcare). Following several washes, GST-fused proteins were eluted with reduced glutathione (Sigma) and dialyzed against 10 mM Hepes, 10 mM NaCl, 0.05% (v/v) Tween-20, 1 μM FAD, pH 7.5. All purified proteins were resolved on 12% gel by SDS-PAGE and visualized with coomassie blue staining.

Fluorescence Polarization- All proteins were freshly used following dialysis for fluorescence polarization assays. Ferredoxin-$NADP^+$ reductase was obtained from Sigma. All Nox B-loop peptides were synthesized and purified by HPLC to >98% purity by the Emory University Microchemical Facility and the correct mass was verified by mass spectroscopy. The following B-loop peptides were used for binding measurements; N-terminally conjugated fluorescein (FITC) Nox4 WT B-loop, FITC-RTLLAYLRGSQKVPSRRTRRLLDKSRTFHI-amide; Nox4 R96E B-loop, FITC-RTLLAYLRGSQKVPSRRTRELLDKSRTFHI-amide; Nox2 WT B-loop, FITC-RNLLSFLRGSSACCSTRVRRQLDRNLTFHK –amide; Nox2 R91E/R92E B-loop, FITC- RNLLSFLRGSSACCSTRVEEQLDRNLTFHK –amide; Nox5 B-loop, FITC-RRCLTWLRATWLAQVLPLDQNIQFHQ –amide. Nox4 (or Nox2) DH domain proteins in 10 mM Hepes (pH 7.5), 0.05% Tween-20, 1 μM FAD and NaCl concentration (specified in each figure legend) were titrated into a microplate and a constant 31 nM fluorescence B-loop peptide (diluted in the same buffer) was added to each well. Fluorescence polarization was measured immediately after adding protein and peptides to the plate at 25ºC in with Synergy™2 Multi-Mode Microplate Reader and Gen5™ software package (Bio Tek). The principle behind the method is as follows: the method uses plane polarized light to excite a fluorophore, and polarizing filters to monitor the difference in emitted polarized fluorescent light intensity in the parallel versus perpendicular channels. A rapid tumbling small fluorophore (i.e., the peptide) emits depolarized light, since fluorescence emission occurs on a slower time scale than the molecule's rotational relaxation time, whereas when the fluorophore is bound to a macromolecule, the rotation of the fluorophore is slowed and light remains polarized.

Thus, binding results in an increase in the polarized light channel. FAD at 1 μM did not affect the polarization readings. The Nox4 DH domain: Nox4 B-loop interaction is stable for > 1.5 hours. The fluorescence measurements were made with excitation filter 485 nm with 20 bandwidth and emission filter 528 nm bandwidth 20. Binding curves were generated by a non-linear least squares fit of the data to a four parameter binding equation (Sigmoidal dose-response curves, variable slope) using GraphPad Prism. The equation models fluorescence polarization versus Nox DH domain protein concentration using four parameters: maximum and minimum polarization values, EC_{50} and slope of the curve. The goodness of the fit for each curve was evaluated by the R^2 value. For weakly binding peptides, it was sometimes not possible to achieve saturating levels of binding. Therefore, to estimate binding constants in such cases, the maximum polarization value was constrained to that obtained from Nox4 WT B-loop peptide measurements.

Nox4 B-loop peptides lacking the FITC group were used in some experiments to compete bound FITC-labeled B-loop peptides from the dehydrogenase domains, monitoring competition by fluorescence polarization. Nox4 WT and R96E peptide sequences identical to those listed above were also synthesized without the FITC label by the Emory University Microchemical facility, and were purified and characterized as described above. Nox4 WT short peptide, NH_3^+-RRTRRLLDKSRT-COO^- were a generous gift from Dr. H. Ogawa (Fujita Health University). Un-labeled peptides of various concentrations were incubated with 60 nM GST-Nox4 DH protein with ~31 nM FITC-Nox4 WT or R96E full-length B-loop peptides. Data were fit to a one-site

competition model to obtain IC_{50} values and 95% confidence intervals. An unpaired, two-tail t-test was used to determine p values for statistical significance.

Cytochrome c reduction- Recombinant GST-Nox4 dehydrogenase domain protein or GST (100 nM each) was incubated with 300 μM FAD (Sigma) 80 μM cytochrome c (from horse heart, Sigma), and either 20 μM DPI or 0.2% DMSO in assay buffer containing 120 mM NaCl, 3 mM KCl, 1 mM $MgCl_2$, 10 mM Hepes and 0.05% Tween-20, pH 7.0. The reaction components were added to a microplate and the reaction was immediately initiated with of 250 μM NADPH (Sigma), and cytochrome c absorbance at 550nm was measured using Synergy™2 Multi-Mode Microplate Reader at 37ºC. This concentration of FAD was sufficient to nearly saturate the Nox4 DH domain resulting in ~80% of Vmax. Most of the cytochrome c reduction was confirmed to be unaffected by 100 U/ml superoxide dismutase (Sigma). The calculation of turnover number uses extinction coefficient of cytochrome c, 21.1 $mM^{-1}cm^{-1}$ at 550 nm. The reported turnover number is the average of three independent experiments.

Circular Dichroism- Nox4 WT and R96E B-loop peptides were solubilized in water and their circular dichroism was measured using a JASCO J-810 CD Spectropolarimeter.

3.3 Results

3.3.1 Conservation of the B-loop region in Vertebrate Nox Enzymes.

The boundaries between the transmembrane α-helices and B-loop were estimated using web servers that predict secondary structure. These boundaries are predicted to reside in or near the N- and C- terminal conserved regions labeled in Figure 3.1, although exact boundaries cannot be determined with certainty in the absence of a crystal structure (Hirokawa et al., 1998; Kelley and Sternberg, 2009; Rost et al., 2004). For the purposes of this dissertation, we define the B-loop as residues 77- 106 (human Nox4 sequence) according to our previously published Nox sequence alignment (Kawahara et al., 2007). This includes several additional residues at the C-terminus including histidine 105, one of the heme-iron-ligating histidine residues as a reference. Analysis of multiple sequence alignments of vertebrate Nox B-loops and surrounding regions revealed three distinct sub-regions of Nox B-loops: 1) a conserved N-terminal region, 2) a variable central region and 3) a conserved C-terminal region (Figure 3.1) (Larkin et al., 2007). The two flanking conserved regions are shared by all Nox isoforms, whereas the central variable region is characteristic of specific Nox isoforms or regulatory classes. In the case of Nox enzymes that require p22*phox* (but not calcium-regulated Noxes), the variable region contains a poly basic region (PBR) (underlined in human Nox4 sequence Figure 3.1). Some of these basic residues in Nox2 have been previously shown by mutagenesis to be necessary for activity (Biberstine-Kinkade et al., 1999; Kawahara et al., 2007).

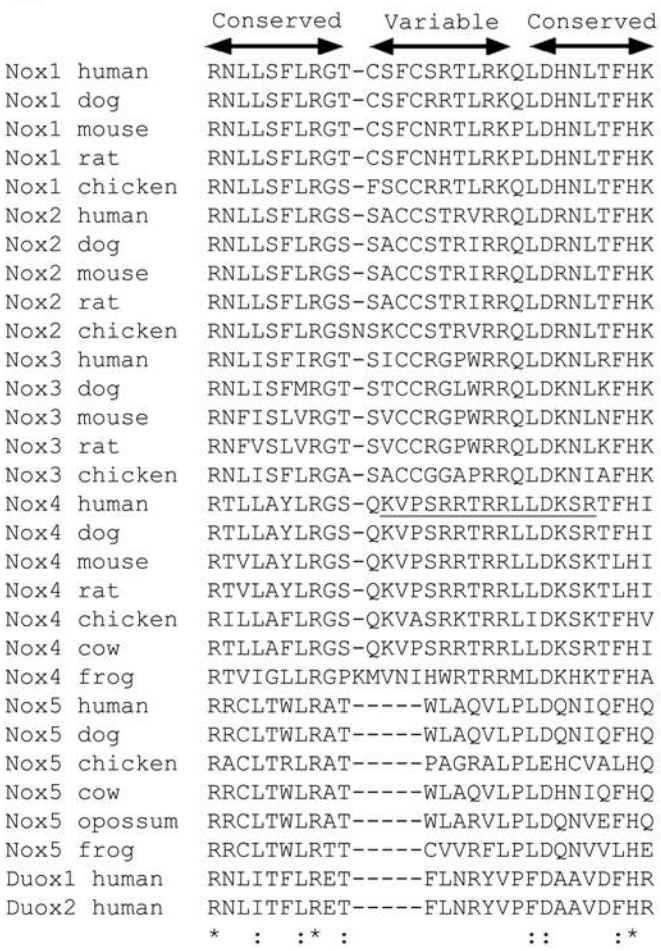

Figure 3.1. Amino acid sequence alignment of Nox/Duox B-loops.

Primary sequences of various Nox/Duox proteins were aligned using ClustalW2. Symbols below the alignment reflect level of conservation; * identical,: similar. The polybasic region of the human Nox4 sequence is underlined. This figure is from (Jackson et al., 2010).

3.3.2 Amino acids in the Nox4 B-loop are important for Nox4 Activity.

To determine the importance of the B-loop in Nox4 enzymatic activity, point substitutions of arginine residues were generated by site-directed mutagenesis (indicated in Figure 3.2A.). Mutant Nox4 was expressed in HEK 293 cells and ROS-generating activity was monitored (Figure 3.2B). Individual mutation of R84, R92, R95 and R96 to alanine all caused a decrease in Nox4 activity, ranging from 50% to <5% of wild-type (WT) activity, while the R93A mutation retained ~80% of WT activity. Individual substitution of R95 and R96 to glutamic acid resulted in nearly complete loss of ROS production (Figure 3.2B, right panel).

The expression of Nox4 WT and mutant proteins was examined by expressing mutated, myc-tagged Nox4 in HEK 293 cells, followed by immunoprecipitation and western blotting (Figure 3.2C). Similar levels of expression were detected for all Nox4 mutants compared to WT. Wild type and mutant forms of Nox4 all displayed a band at ~65 kDa, the predicted molecular weight of unprocessed Nox4 as well as a higher molecular weight band (~80 kDa), which may represent a glycosylated form of Nox4. A similar higher molecular weight Nox4 band has previously been reported in HeLa cells (Shiose et al., 2001), A549 cells (Goyal et al., 2005), vascular smooth muscle cells (Hilenski et al., 2004) and human umbilical vein endothelial cells (Hwang et al., 2005). Nox4 heterodimerizes with p22*phox*, and this binding is required for activity (Kawahara et al., 2005b). WT and all mutant forms of Nox4 co-immunoprecipitated p22*phox* (Figure 3.2C). Therefore, the decrease in activity displayed by the Nox4 mutants is not due to altered protein expression, processing or complex formation with p22*phox.*

A.

```
WT    RTLLAYLRGSQKVPSRRTRRLLDKSRTFHI
R84A  RTLLAYLAGSQKVPSRRTRRLLDKSRTFHI
R92A  RTLLAYLRGSQKVPSARTRRLLDKSRTFHI
R93A  RTLLAYLRGSQKVPSRATRRLLDKSRTFHI
R95A  RTLLAYLRGSQKVPSRRTARLLDKSRTFHI
R95E  RTLLAYLRGSQKVPSRRTERLLDKSRTFHI
R96A  RTLLAYLRGSQKVPSRRTRALLDKSRTFHI
R96E  RTLLAYLRGSQKVPSRRTRELLDKSRTFHI
```

B.

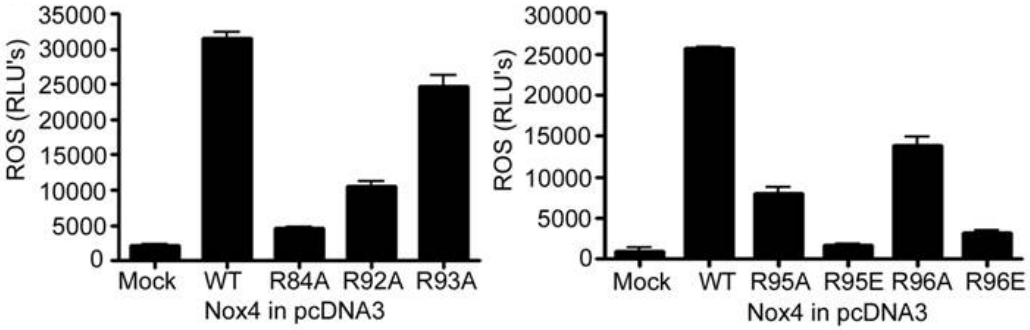

C.

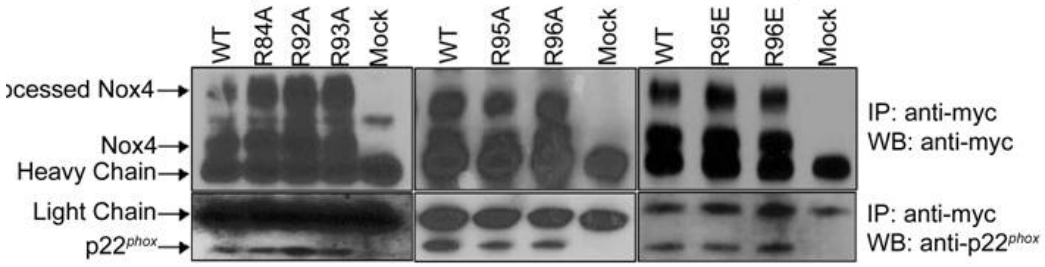

Figure 3.2. Arginine residues located in the Nox4 B-loop are important for Nox4 Activity.

A. Nox4 B-loop sequences are shown with the corresponding arginine mutation underlined. **B.** Nox4 wild type (WT), the indicated arginine mutations or empty vector (mock) were expressed in HEK 293 cells and ROS production was measured by luminol chemiluminescence. Values reported are relative light unit (RLU), mean ± S.E.M. (n=3). **C**. Nox4 expression in HEK 293 cells was determined by transfection of C-terminal myc-tagged Nox4 WT, mutant or empty vector (mock) followed by immunoprecipitation (IP) using anti-myc antibodies. Protein was resolved by SDS-PAGE and western blotting (WB) was carried out using anti-myc and anti-p22*phox* antibody as indicated. This figure is from (Jackson et al., 2010).

3.3.3 Nox4 B-loop binds to recombinant Nox4 dehydrogenase (DH) domain.

Conservation suggested and mutagenesis confirmed the importance of the B-loop in Nox4 activity. Because Nox4 does not require regulatory subunits, other than p22*phox* (and mutagenesis of the Nox4 B-loop does not affect p22*phox* -Nox4 interaction, Figure 3.2C), we hypothesized that the B-loop binds directly to the DH domain, as both of these regions reside in the cytoplasm. This interaction is also conceptually predicted by the alignment of the TM and DH domain homology models (see section 2.3.4). To test this hypothesis, fluorescence polarization was employed; this method provides a sensitive and quantitative approach to investigate protein-peptide interactions (Jameson and Seifried, 1999). Nox4 B-loop peptides conjugated to fluorescein (FITC) at their N-termini were titrated with GST-tagged recombinant Nox4 dehydrogenase domain (GST-Nox4 DH) and fluorescence polarization was monitored. GST-Nox4 DH caused a saturable increase in the fluorescence polarization of Nox4 B-loop peptide (Figure 3.3A). The polarization change was fit to a binding curve with a K_d of 58 ± 12 nM. Nox4 B-loop peptides with the R96E mutation (a mutation that inhibited Nox4 activity Figure 3.2B) showed 10-20 fold decreased affinity (e.g., see Figure 3.3A). The expressed GST domain alone failed to bind either B-loop peptide (Figure 3.3A).

As the Nox DH domains are predicted to be structurally related to the ferredoxin reductase (FNR) family (refer to Chapter 2) we tested whether the Nox4 B-loop binds the structural elements common in all DH domains or is specific for the Nox4 sequence. FNR was evaluated in the fluorescence polarization assay, and no binding of the Nox4 B-loop to this flavoprotein could be detected (Figure 3.3B).

Because of the charged nature of the B-loop and the importance of basic residue R96 in B-loop binding, the salt dependency of this interaction was investigated (Figure 3.3C). Increasing sodium chloride weakened the binding, consistent with a role for electrostatic forces in either direct binding or in stabilizing a binding conformation of the B-loop. In the presence of 10 mM NaCl, the binding constant was estimated to be less than 20 nM (this should be considered an upper limit, since accurate calculation of the very low K_d was not possible due to significant ligand depletion under this condition). No binding was detected in high salt (500 mM NaCl), while at 75 and 150 mM NaCl, respective K_d values of 59 ± 12 nM and 245 ± 71 nM were determined.

The ability of WT Nox4 and R96E B-loop peptides (not fluorescent labeled) to compete with the FITC-conjugated WT B-loop peptide for binding to the DH domain was evaluated at the 75 mM NaCl concentration. WT B-loop competes with FITC-WT B-loop for GST-Nox4 DH domain with an IC_{50} of 0.38 ± 0.08 μM while the R96E B-loop competes much less effectively, IC_{50} = 8.7 ± 1.3 μM (Figure 3.3D). A shorter peptide comprised of just the PBR of Nox4 B-loop (residues 92-103, see Figure 3.3.1) is a weaker competitor (IC_{50} = 12.5 ± 4 μM) compared with full-length B-loop peptide (residues 77-106). Therefore, while mutational data indicate the importance of the PBR for binding (Figure 3.3A), high affinity binding requires additional B-loop residues outside of this region.

The Nox4 DH domain catalyzes a relatively robust NADPH- and FAD-dependent direct reduction of cytochrome *c*, which, unlike cytochrome *c* reduction by holo-Nox enzymes, is mostly independent of superoxide since it is not inhibited by superoxide dismutase (more on this in Chapter 4). Since this reaction requires an approximately

native folding of the DH domain (i.e., FAD- and NADPH-binding sites must remain functional) it can be used to assess whether or not the expressed DH domain retains a folded structure capable of catalysis. Our purified preparations of GST-Nox4 DH (see Figure 3.3F) reduced cytochrome *c* in the presence of FAD and NADPH (turnover numbers averaged ~100 min^{-1} in 3 experiments) (Figure 3.3E) and this reduction was abrogated with the addition of the flavoprotein inhibitor, diphenyleneiodonium (DPI). These data suggest that the expressed DH domain is close to its native conformation. Purified GST displayed only a low background level of cytochrome *c* reduction that was not decreased by DPI.

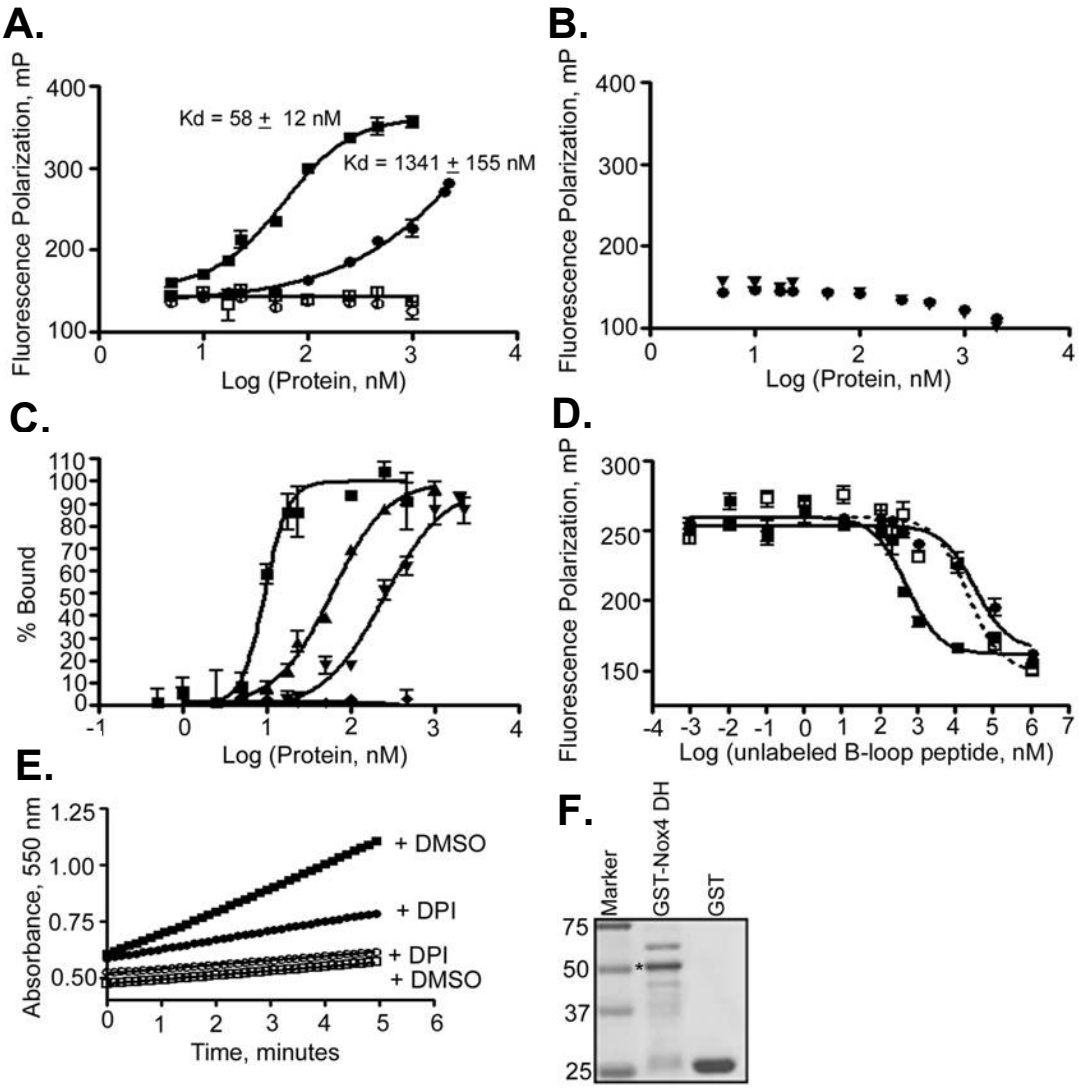
A.
Fluorescence Polarization, mP
Kd = 58 ± 12 nM
Kd = 1341 ± 155 nM
Log (Protein, nM)
B.
Fluorescence Polarization, mP
Log (Protein, nM)
C.
% Bound
Log (Protein, nM)
D.
Fluorescence Polarization, mP
Log (unlabeled B-loop peptide, nM)
E.
Absorbance, 550 nm
+ DMSO
+ DPI
+ DPI
+ DMSO
Time, minutes
F.
Marker
GST-Nox4 DH
GST
75
50
37
25

Figure 3.3. The Nox4 DH domain binds to Nox4 B-loop peptides.

A. Binding between expressed, purified recombinant proteins and FITC-conjugated Nox4 WT or R96E B-loop peptides was detected by fluorescence polarization (mP). Data were fit to sigmoidal dose-response curves using GraphPad Prism to obtain the indicated binding constants (95% confidence intervals shown). ■ GST-Nox4 DH + WT B-loop, K_d = 58 ± 12 nM; ● GST-Nox4 DH + R96E B-loop, K_d = 1341 ± 155 nM; □ GST alone + WT B-loop; ○ GST alone + R96E B-loop. **B.** Ferredoxin NADP+ reductase was incubated with Nox4 WT ▼ and R96E ● B-loop. **C.** GST-Nox4 and WT Nox4 B-loop peptides were incubated in buffer containing 10 (■), 75 (▲), 150 (▼) and 500 (♦) mM NaCl. Binding was monitored by fluorescence polarization and converted to percent bound. **D.** Unlabeled WT, R96E or PBR B-loop peptides were added to GST-Nox4 DH protein (60 nM) plus FITC-conjugated Nox4 WT B-loop. Data were fit to one-site competition curves using GraphPad Prism to obtain IC_{50} values. Reported are the mean IC_{50} of three independent experiments with standard error of the mean. ■ Holo B-loop (amino acids 77-106) IC_{50} = 0.38 ± 0.08 μM; ▲ R96E B-loop (amino acids 77-106) IC_{50} = 8.7 ± 1.3 μM; □ PBR B-loop (amino acids 92-103) IC_{50} = 12.5 ± 4 μM. The difference between IC_{50} values for unlabeled WT B-loop vs. unlabeled R96E B-loop showed $p < 0.0006$; WT B-loop vs. PBR B-loop, $p < 0.01$; no statistically significant difference was seen between binding of unlabeled R96E and unlabeled PBR B-loop. **E**. Cytochrome *c* reduction activity of ■, ● GST-Nox4 DH (100nM) or □, ○ GST (100 nM) was monitored by the absorbance increase at 550nm in the presence of 0.2% DMSO squares or 20 μM diphenyleneiodonium (DPI) circles in 0.2% DMSO. **F**. Recombinant GST-Nox4 and GST were resolved by SDS-PAGE and stained with coomassie blue.

GST-Nox4 DH (~ 5 µg) migrates at approximately 50 kDa (denoted *) and GST (~ 11 µg) at 25 kDa; molecular weight marker are shown in the first lane. This figure is from (Jackson et al., 2010).

The large difference between binding affinities of the Nox4 DH to WT or mutant peptides led us to question whether the arginine substitution in the mutant peptide was affecting the folding of the this peptide. To ensure that the wild type and mutant peptides were not folded in drastically different ways, we measured the circular dichroism (CD) spectrum for each peptide. Spectra for both the WT and mutant peptides looked identical and predict the peptides to be coiled with some slight helical character (Figure 3.4). Our model of the TM domain predicts the B-loop to be approximately 2/3 loop and 1/3 helical (see Figure 2.9). This prediction is not exactly consistent with the CD spectra however, as the peptides are only 30 amino acids in length and as they are lacking tethers at the N- and C-terminals, they may not adopt a fully native fold. Furthermore, the helical character of the B-loop is predicted based on secondary structure prediction programs (Kelley and Sternberg, 2009; Rost et al., 2004) and based on homology to cytochrome bc1. However, as there are no structural data on this region, the native fold is still unknown. Either way, the peptides do not appear to reside in solution in vastly different conformations suggesting the reduced binding with the mutant peptide is due to the DH domain not recognizing the amino acid sequence as well as WT peptide.

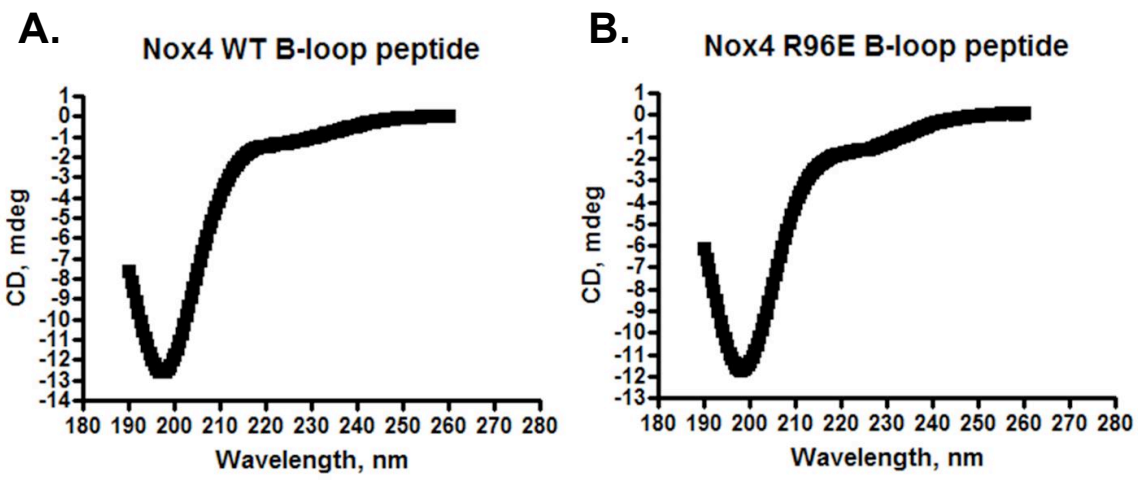

Figure 3.4. CD spectra of Nox4 WT and R96E B-loop peptides.

Circular dichroism spectra were measured for both (**A.**) WT and (**B.**) mutant B-loop peptides solubilized in water. The spectra predict both peptides to be mostly coiled.

3.3.4 Truncations of the Nox4 DH domain identify a B-loop-binding sub-domain.

To determine the region of the Nox4 DH domain responsible for B-loop binding, truncated GST-Nox4 proteins were purified and tested for binding to the Nox4 B-loop peptides (Figure 3.5A and B). Full-length DH domain (amino acids 304-578) contains both the FAD- and NADPH-binding sub-domains joined by a short connecting sequence termed the hinge region. As shown in Figure 4C, full-length Nox4 DH domain (amino acids 304-578) binds the Nox4 B-loop with the highest affinity (K_d = 49 ± 9 nM in this experiment). The expressed NADPH-binding domain (amino acids 411-578) still binds relatively tightly (K_d = 127 ± 29 nM) whereas the FAD-binding domain of Nox4 (amino acids 304-420) showed little or no binding. Approximately nine amino acids comprise the hinge region (amino acids 411-420), a stretch of residues connecting the C-terminus of the FAD-binding domain to the N-terminus of the NADPH-binding domain. This region was included in the FAD- and NADPH-binding domain truncated proteins to enhance recombinant protein expression and solubility. A less soluble form of the NADPH- binding domain without the hinge region (amino acids 420-578) also bound the Nox4 B-loop (data not shown) with similar affinity as the NADPH-binding domain truncation protein with the hinge (amino acids 411-578). Therefore, the hinge region does not contribute significantly to B-loop binding. To further delineate the B-loop binding region, the NADPH-binding sub-domain was further truncated into N-terminal (amino acids 420-488) and C-terminal (amino acids 489-578) halves. The former still showed binding to the B-loop (K_d = 404 ± 89 nM), whereas no binding to the latter was seen. Therefore, the portion of the NADPH-binding sub-domain that contributes most to binding the B-loop is contained within the 420-488 amino acid region.

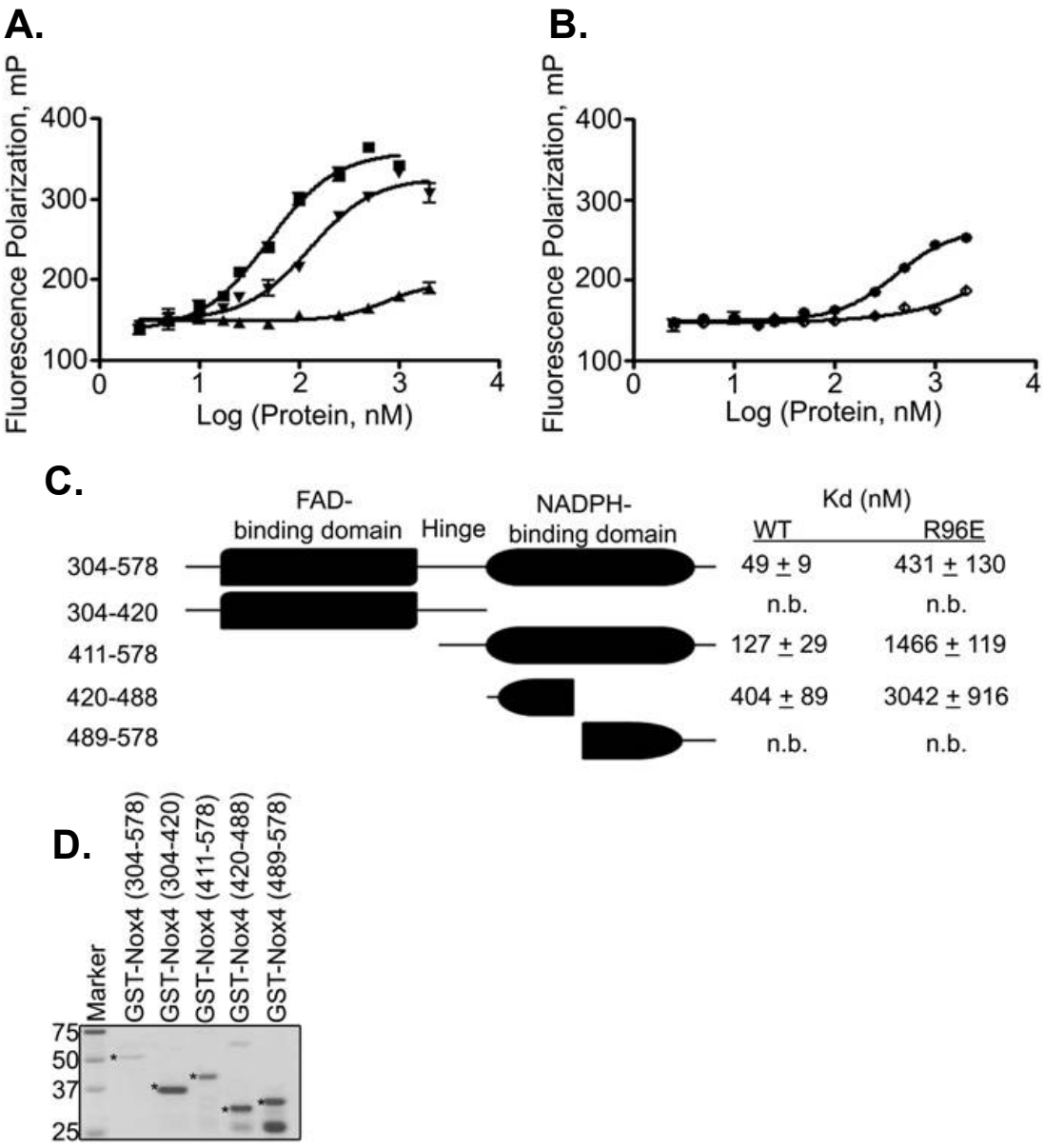
A.
Fluorescence Polarization, mP
400
300
200
100
0
1
2
3
4
Log (Protein, nM)
B.
Fluorescence Polarization, mP
400
300
200
100
0
1
2
3
4
Log (Protein, nM)
C.
FAD-
binding domain
Hinge
NADPH-
binding domain
Kd (nM)
WT
R96E
304-578
49 ± 9
431 ± 130
304-420
n.b.
n.b.
411-578
127 ± 29
1466 ± 119
420-488
404 ± 89
3042 ± 916
489-578
n.b.
n.b.
D.
Marker
GST-Nox4 (304-578)
GST-Nox4 (304-420)
GST-Nox4 (411-578)
GST-Nox4 (420-488)
GST-Nox4 (489-578)
75
50
37
25

Figure 3.5. The Nox4 B-loop preferentially binds to the NADPH- binding domain.

Fluorescence polarization was monitored as in Figure 3.3. **A.** Nox4 B-loop peptides in 75mM NaCl were titrated with: ■ GST-Nox4 DH (amino acids 304-578), ▲ GST-Nox4 (amino acids 304-420) or ▼ GST-Nox4 (amino acids 411-578). **B**. Binding between the Nox4 B-loop and NADPH-binding domain truncations: ● GST-Nox4 (amino acids 420-488) and ◊ GST-Nox4 (amino acids 489-578). **C**. Schematic of GST-tagged DH domain truncations showing residues comprising the FAD-binding domain, short connecting region (hinge) and NADPH-binding domain. Binding constants with 95% confidence intervals are summarized adjacent to the corresponding truncated protein. n.b. indicates no binding was observed. **D**. GST-Nox4 DH and truncation proteins were resolved by SDS-PAGE and stained with coomassie blue for visualization. Molecular weight markers are shown in first lane, followed by ~1 μg Nox4 (304-578), 2 μg Nox4 (304-420), 4 μg Nox4 (411-578), 4 μg Nox4 (420-488) and 16 μg Nox4 (489-578). All proteins migrated at the expected molecular weights, denoted *. This figure is from (Jackson et al., 2010).

Both the NADPH-binding domain and N-terminal half of the NADPH-binding domain bound the R96E peptide with 10-20 fold less affinity than the WT B-loop peptide, similar to the effect of this substitution on binding to the full-length DH domain (amino acids 304-578).

In an effort to further narrow down the individual residues in the Nox4 DH that bind the B-loop, we measured this interaction with various mutant Nox4 DH proteins. Twenty candidate residues were selected for mutation by three different methods; 1. based on localization in the Nox4 DH domain model, 2. conservation among Nox1-4 (due to the importance of the PBR) and 3. polarity. Our model provides some clues as to how the DH domain and TM domain interact considering the electron transfer that occurs from FAD (in DH domain) to heme A (in TM domain). Four residues were selected within the FAD-binding domain as these localized to the surface of the DH domain that we believe points towards the transmembrane region according to our homology models (Figure 3.6). The hinge region also resides on this face so we chose eight candidate residues from this region as well. Among these, three acidic residues are conserved in all the Nox/Duox isoforms that conserve the PBR in the B-loop. Ten residues from the NADPH binding domain were chosen as candidates as this region when expressed alone, retains significant binding to the B-loop (Figure 3.5). None of these mutations resulted in significant reduction in the measured binding affinity, though a few mutations led to changes in the "Bmax", or maximum fluorescence polarization signal (Table 3.7). It is not clear what exactly causes the maximum fluorescence to decrease but may suggest at least an *altered,* if not, *weaker* interaction between the B-loop and mutant Nox4 DH. Most of the mutations were tested in 150 mM NaCl buffer

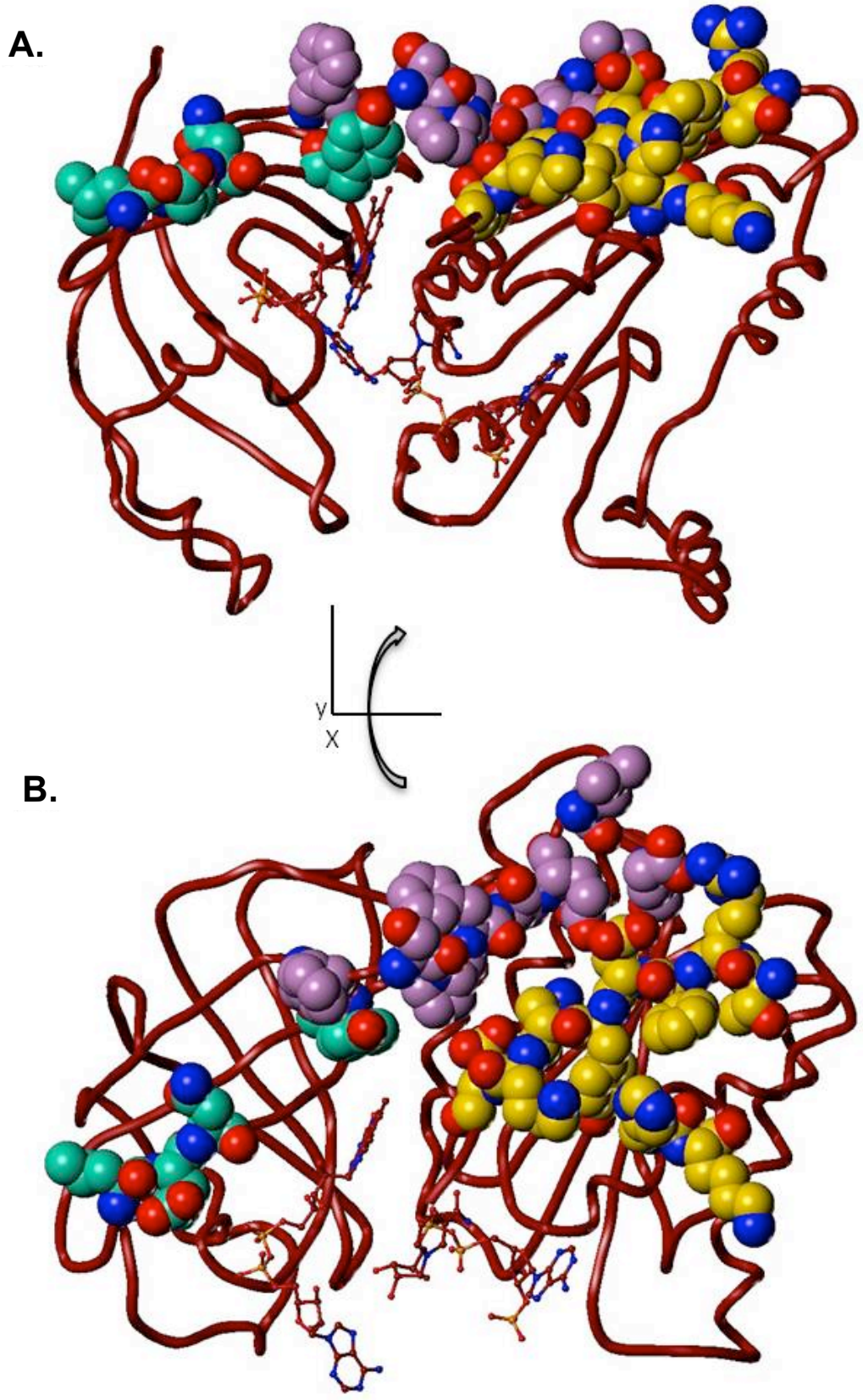
A.
y
X
B.

Figure 3.6 Candidate B-loop binding residues in the Nox4 DH domain.

The Nox4 DH domain model is shown with FAD and NADPH in ball and stick and candidate B-loop binding residues are shown in space fill. Carbons of residues in the FAD-binding domain are colored cyan, hinge region are in purple and NADPH-binding domain are in yellow. Nitrogens are colored blue and oxygens are colored red. Panel **A.** shows the domain oriented so that the dimethyl edge of FAD (edge of electron transfer) is pointed above the picture to illustrate the surface that is predicted to face the transmembrane domain. Panel **B.** shows the orientation that allows easy visualization of the β-barrel (FAD-binding domain) and Rossmann fold-like (NADPH-binding domains). Panel A. is flipped ~90º along the x-axis relative to panel B.

		Nox4 B-loop	WT		R96E		WT	R96E	WT	R96E	Comments
		DH residue range	304-578		304-578		411-578	411-578	304-420	304-420	
		Buffer [NaCl], mM	10	150	10	150	10	10	10	10	
		WT	1	1	2	6-7	1	2	1	6.4	
FAD-binding domain	1	Y338A							0.5	2.4	
	2	L349Q							1.2	9.4	
	3	E350R							0.7	0.4	
	4	N351R							3.1	2.1	
Hinge	5	F413A		1.2							Bmax 21% less
	6	S415A		1.5							
	7	P416A	1.1								Bmax 14% higher
	8	F417A	2								
	9	L421A	3.6								
	10	E418A/E419A/E424A		1.8							
	11	E418R/E419R/E424R		3.7							
NADPH-binding domain	12	H557D					0.6				
	13	K558E					2				
	14	T568A		1.6							Bmax 16% less
	15	R569A		1.5			2.1	5.3			Bmax 20% less
	16	F570A		1.1			1.6	4.2			Bmax 27% less
	17	E571A		1.5							Bmax 10% less
	18	Y572A		0.8							
	19	N573A	0.9								Bmax 11% higher
	20	K574I		1.9							Bmax 14% higher
	21	E575A	0.8								Bmax 6% higher

Table 3.7. Summary of the Binding affinity of all Nox4 DH domain point mutations.

All binding constants are normalized to the Kd of WT Nox4 DH domain: WT B-loop interaction at the indicated buffer salt concentration. Comments section shows when the maximal fluorescence value was less or higher than the WT interaction.in the full length DH domain, however in some cases, different constructs or salt concentrations were tested.

The activity of some of these mutations was measured in parallel with B-loop binding and these results are shown for reference in Figure 3.8. The hinge region mutants had drastic effects on Nox4 activity indicating a crucial function either in activation or structure. Similarly, F570 and E571 in the NADPH-binding domain are critical residues; however, the perturbation at residues R569 or T568 did not significantly affect activity. As none of these mutations resulted in decreased binding affinity to the B-loop, we do not suspect the effects on activity have to do with the B-loop interaction. Perhaps the hinge region plays a role in aligning the FAD- and NADPH-binding sub-domains. While the F570 and E571 residues located in the final β-strand are important for placement and stability of this structure. This final β-strand contains predicted active site residues, so its disturbance may have strong affects on enzyme function. The R569 and T568 residues are not located in any seemingly critical secondary structural elements, rather they reside in a surface loop that is able to accommodate for residue changes.

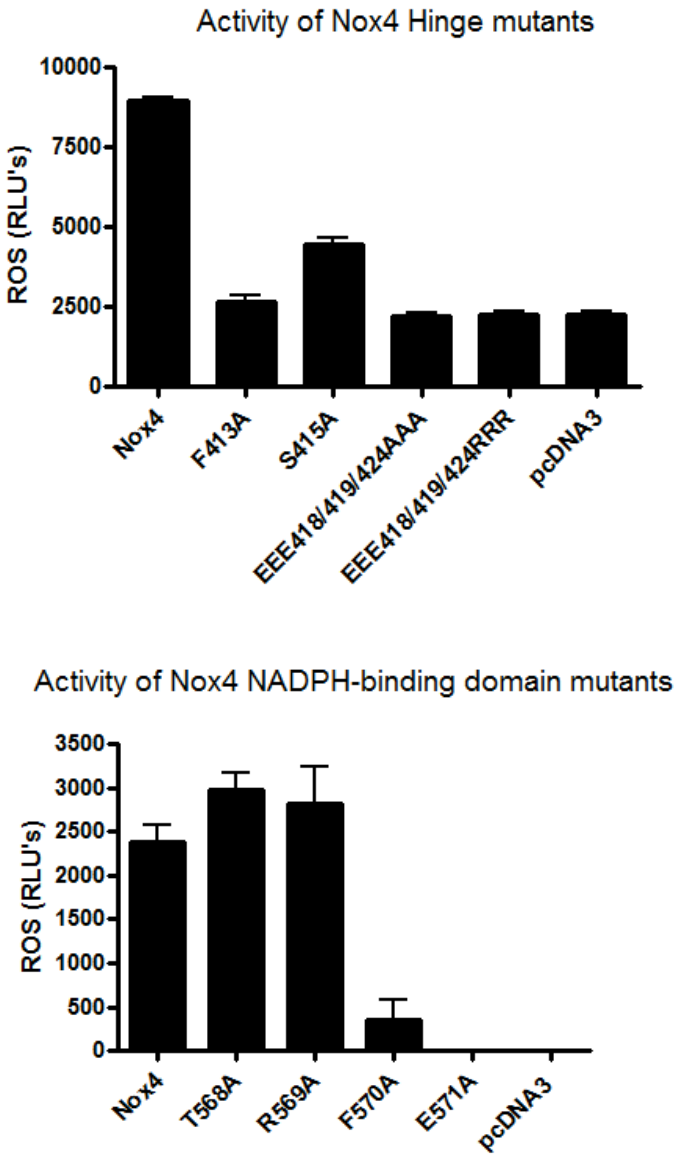

Figure 3.8. Effect of Hinge or NADPH-binding domain mutants on Nox4 ROS production.

Nox4 WT, mutants or vector alone were transiently transfected into HEK 293 cells and the ROS production was measured by luminol chemiluminscence. Average readings of relative light unit (RLU's) are reported with the SEM.

3.3.5 Isoform specificity of Nox DH domain: B-loop interaction.

The Nox2 and Nox4 B-loops including the PBR show a relatively high conservation, whereas the Nox5 B-loop is distinct (Figure 3.1). Therefore, FITC-labeled B-loop peptides from Nox2, Nox4 and Nox5 were compared with respect to binding both Nox2 and Nox4 DH domains. It was not possible to prepare the GST-Nox5 DH domain due to poor expression and solubility problems. GST-Nox2 DH bound to the B-loop peptides from both Nox4 and Nox2 with similar affinity (i.e. no statistical significant difference), K_d = 320 ± 31 nM and K_d = 622 ± 117 nM, respectively (Figure 3.8 B and C). GST-Nox4 DH also bound to B-loop peptides from Nox2 (K_d = 243 ± 49 nM) and Nox4 (K_d = 61 ± 4 nM). Therefore, in contrast to the Nox2 DH domain, which showed no significant preference for B-loop from Nox2 versus Nox4, Nox4 prefers its cognate B-loop by a factor of ~4. Also of note, the Nox4 DH domain binds its own B-loop as well as the Nox2 B-loop considerably more tightly than does Nox2 DH domain. In contrast, neither DH domain bound to either the Nox5 B-loop (which lacks the PBR) or to the Nox2 B-loop containing the double mutation corresponding to R91E/R92E (mutations that nearly abolish Nox2 activity (Biberstine-Kinkade et al., 1999)). Therefore, basic residues at these positions in the Nox2 and Nox4 B-loop peptides are necessary for high affinity binding to their DH domains.

A.

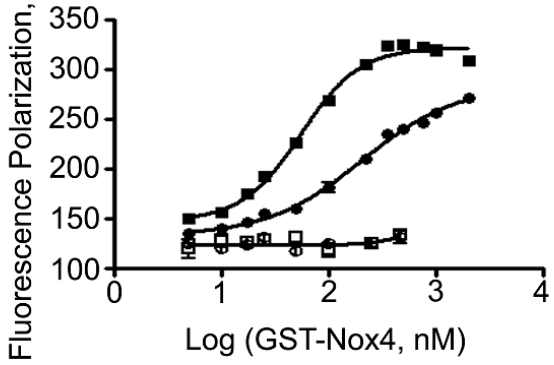

B.

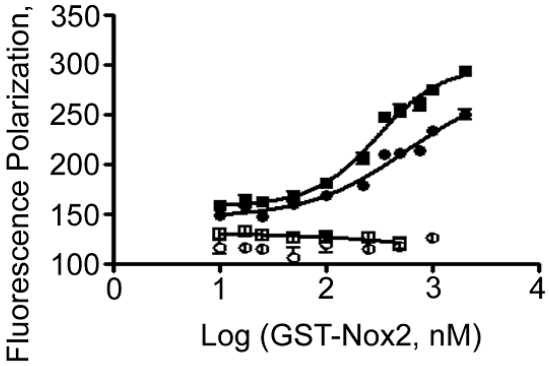

C.

	Kd (nM)
GST-Nox4	
Nox4 B-loop	61 ± 4*
Nox2 B-loop	243 ± 49
Nox2 R91E/R92E B-loop	n.b.
Nox5 B-loop	n.b.
GST-Nox2	
Nox4 B-loop	320 ± 31**
Nox2 B-loop	622 ± 117
Nox2 R91E/R92E B-loop	n.b.
Nox5 B-loop	n.b.

D.

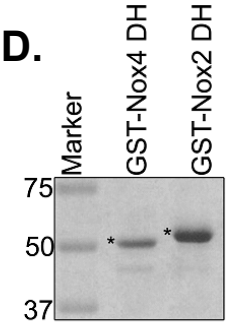

Figure 3.9. Isoform specificity of DH domain: B-loop interaction.

A. GST-Nox4 DH and, **B.** GST-Nox2 DH domains were titrated with FITC- conjugated B-loops corresponding to WT Nox4 ■, WT Nox2 ●, Nox2 R91E/R92E ○ and WT Nox5 B-loop □, and fluorescence polarization was monitored as in Figure 3 in buffer containing 75 mM NaCl. **C.** Data were fit as in Figure 3. The mean K_d of three independent experiments is reported with standard error. n.b. is no binding. * Indicates a p value < 0.02 comparing the K_d values for GST-Nox4 DH binding to Nox4 B-loop versus Nox2 B-loop. ** indicates no statistical difference between K_d values for GST-Nox2 DH binding to Nox4 B-loop versus Nox2 B-loop. **D**. Recombinant proteins GST-Nox4 DH (~ 7 µg) and GST-Nox2 DH (~ 6 µg) were resolved by SDS-PAGE and visualized by coomassie blue stain. Molecular weight markers were loaded in the first lane. Both proteins migrated at the expected molecular weights, denoted *. This figure is from (Jackson et al., 2010).

The weaker affinity of Nox2 DH domain for Nox2 B-loop peptides suggests that Nox2 may require additional regulatory components to achieve the tighter DH domain: B-loop association seen in Nox4. To test this possibility while at the same time avoiding addition of multiple regulatory proteins, we investigated the effect of the p67N/p47N chimera protein and Rac1Q61L (constitutively active mutant) on Nox2 B-loop binding to the Nox2 DH domain (Figure 3.10A). This fusion protein retains the regions of p67*phox* and p47*phox* needed to stimulate Nox2 cell-free activity (Ebisu et al., 2001). Somewhat surprisingly, we observed a significant increase in fluorescence polarization with the regulatory subunits and Nox2 B-loop even in the absence of GST-Nox2 DH and increasing amounts of DH domain did not further increase the fluorescence polarization (Figure 3.10A). Apparent binding constants between the Nox2 and Nox4 B-loop peptides and GST-Nox2 DH or regulatory subunit proteins are summarized in Table B of Figure 3.10.

The ability of the Nox2 and Nox4 B-loops to bind to both the Nox2 and Nox4 DH domains suggests these peptides share common features necessary to interact with the DH domain. The functional consequence of these mismatched B-loop:DH domain pairs can be tested with chimera proteins. Figure 3.11 shows the activity of chimera proteins constructed between Nox2 and Nox4. Chimera proteins with a Nox2 DH domain (Nox4/2), exhibit subunit regulated and PMA-stimulated activity similar to Nox2 WT. Likewise, the reverse chimera (Nox2/4) exhibits constitutive activity similar to that of WT Nox4 (the regulation of the chimera's will be discussed in Chapter 4). These data suggest a functional enzyme conformation can be achieved with a mismatched DH domain: B-loop pair. However, inserting the cognate B-loop in the Nox2/4 or Nox4/2

chimera so that the B-loop and DH domain are matched did not affect the measured ROS production.

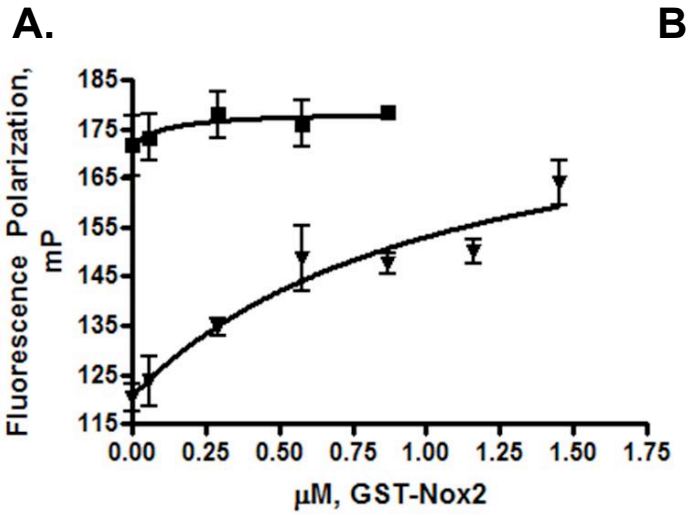

B.

	Nox2 WT	Nox4 WT
GST-Nox2	1.1	N/A
Rac1Q61L	2.2 ± 0.8	1.0 ± 0.3
Rac1 WT (GDP)	NB	NB
GST-p67phox	0.95 ± 1	NB
GST	NB	NB
p67N-p47N	4 ± 8	>7

Figure 3.10. Binding of regulatory subunits and GST-Nox2 to B-loop peptides.

A. Fluorescence polarization was measured at the 150 mM NaCl concentration of Nox2 B-loop peptide and GST-Nox2 DH domain in the absence (▼) and presence of Rac1Q61L (constitutively active mutant) and p67N/p47*phox* chimera (■). **B.** Table B displays binding constants measured between proteins listed in first column and either Nox2 or Nox4 WT B-loop peptides indicated in the first row. All binding constants are expressed in µM ± 95% confidence intervals. NB indicates binding was tested but not detected. N/A indicates binding was not tested.

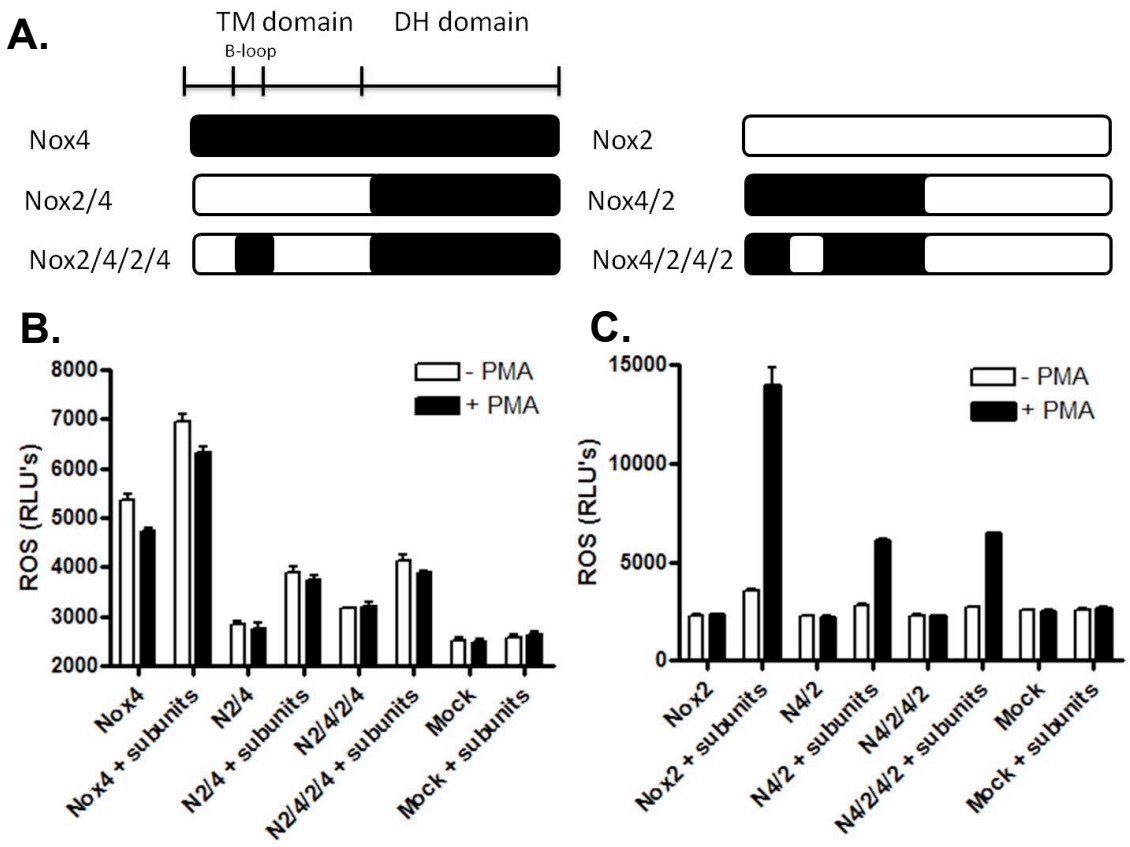

Figure 3.11 Activity of Nox2_Nox4 Chimera proteins.

A. Schematic showing identity of chimeric proteins with indicated boundaries. TM denotes the transmembrane domain and DH denotes the dehydrogenase domain. **B.,C.** Nox4, Nox2, chimeric proteins or mock (empty vector) cDNA's were transfected into HEK 293 cells with or without regulatory subunits (p67*phox*, p47*phox* and Rac1G12V). ROS production was measured by luminol chemiluminescence and averages are expressed with SEM.

3.3.6 Effect of B-loop peptides on Nox4 Activity

We have demonstrated that the Nox4 and Nox2 DH domains interact with B-loop peptides and a mutation that perturbs this binding also affects Nox4 activity in the holo-enzyme (Figure 3.3). Therefore, we hypothesize that disruption of this interaction in the holo-enzyme could inhibit Nox4 ROS production. To test this hypothesis we measured Nox4 derived ROS production in whole cells incubated with B-loop peptides. The basic sequence of tat protein (amino acids 47-57) from HIV-1 virus effectively penetrates eukaryotic cell membranes and therefore can be used as a cellular delivery mechanism when fused to such targets as peptides, liposomes or nucleic acids (Fawell et al., 1994; Green and Loewenstein, 1988; Torchilin et al., 2001).

Nox4 WT and R96E peptides were synthesized with an upstream tat sequence for cell delivery and an N-terminal 5'-6' carboxytetramethylrhodamine (TAMRA) label to monitor cellular uptake. Standard curves were created for each peptide to measure the concentration of each internalized peptide. Initial experiments suggested the peptide uptake efficiency was not equal for each peptide, so different peptide concentrations were incubated with cells to obtain relatively similar internal peptide concentrations. To monitor the viability of cells treated with peptides, we used a commercially available assay that monitors ATP concentration as a measure of metabolic activity. Administration of tat-B-loop or tat control peptides to cells expressing Nox4 HEK 293 cells all had a modest affect on ROS production and a concurrent reduction in cell viability complicating the analysis of these peptides on Nox4 activity.

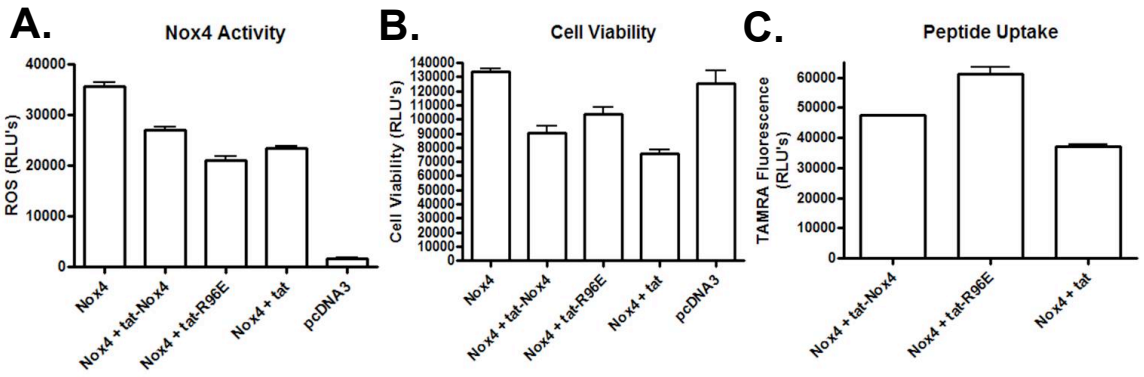

Figure 3.12. Effect of Tat-Nox4 B-loop peptides on Nox4 transfected HEK 293 cells.

Nox4 or vector alone cDNA were transiently transfected into HEK 293 cells and grown for approximately two days. Tat-Nox4, Tat-Nox4 R96E or tat alone peptides were incubated with the transfected cells and ROS production, cell viability and peptide uptake were measured. Reported are average relative light units (RLU's) with SEM. ROS production was measured by luminol chemiluminscence **(A)**; cell viability was measured with Cell TiterBlue Assay (Invitrogen) **(B.)**; and TAMRA fluorescence measured peptide uptake **(C)**.

In an effort to circumvent the cytoxicity of tat-peptides, we decided to test un-tagged B-loop peptides in a Nox4 cell-free system. This system utilizes Nox4 transiently transfected HEK 293 cells lysed by sonication and ROS is detected by Amplex red reagents. Amplex red specifically detects hydrogen peroxide in the presence of horse radish peroxidase and offers improvements over luminol chemiluminscence in sensitivity and quantification (Zhou et al., 1997). Figure 3.13A shows appreciable ROS production of Nox4 containing cell lysates. This activity like that in whole cells (Figure 3.13D) is inhibited by DPI but unlike that in whole cells requires additional NADPH, suggesting the ROS is Nox4-derived. Addition of 250 μM Nox4 WT or R96E B-loop peptides showed a modest inhibition of ROS in Nox4 lysates (28% and 35% respectively), which was only observed by pre-incubating the lysates and peptides for 40 minutes prior to ROS detection (Figure 3.13B). There was no inhibition without pre-incubation (Figure 3.13A) or with lower amounts of peptide (Figure 3.13C). Neither the Nox4 PBR B-loop nor the Nox5 B-loop peptide, (used as a negative control as this peptide showed no binding to the Nox4 DH domain Figure 3.9) showed reproducible inhibition of Nox4 ROS in lysates. Therefore, Nox4 B-loop peptides are not effective Nox4 activity inhibitors.

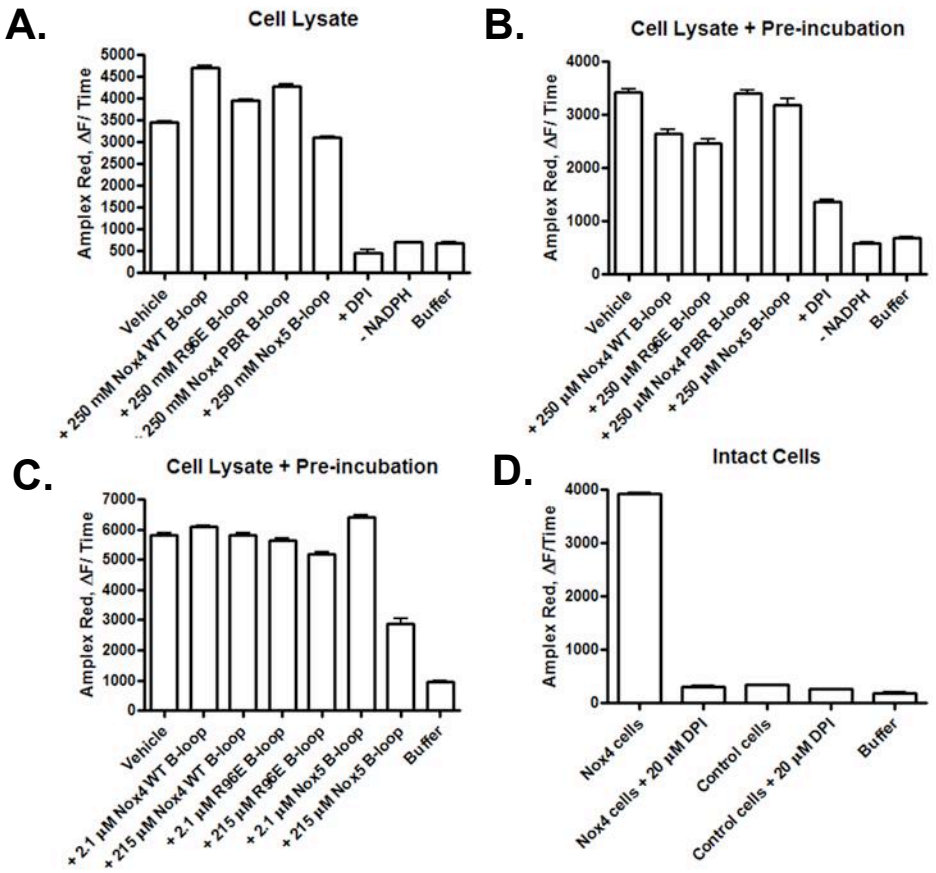

Figure 3.13. Effect of B-loop peptides on Nox4 Cell-free system.

HEK 293 cells were transiently transfected with Nox4 cDNA or un-transfected (control cells) and ROS production was monitored by amplex red fluorescence. Data are expressed as average with SEM. **A**. ROS production of Nox4 expressing HEK 293 cells lysates in the presence of NADPH, FAD and 250 μM B-loop peptides as indicated or the flavoprotein inhibitor, DPI (18 μM) and 250 μM B-loop peptides without pre-incubation. **B.** Lysates were pre-incubated with B-loop peptides for 40 minutes prior to recording fluorescence. **C.** Lysates were pre-incubated with either 2.1 μM or 215 μM B-loop peptides for 30 minutes. **D.** ROS production was measured in Nox4 or control HEK 293 cells prior to lysis with and without DPI (20 μM).

3.4 Discussion and Future Directions

Interactions involving regulatory subunits/domains and/or post-translational modifications of Nox enzymes activate ROS production in the Nox catalytic core (Vignais, 2002). Ultimately, this must involve activating one or more steps in the electron transfer from NADPH through the electron carrying groups (FAD and heme) to molecular oxygen. For Nox2, both the reduction of FAD by NADPH and the electron transfer from FAD to heme A have been proposed as steps that are activated by regulatory subunits (Diebold and Bokoch, 2001; Nisimoto et al., 1999). However, a molecular understanding of how these systems create an active conformation of Nox enzymes remains elusive. Unlike the other mammalian Nox enzymes, exogenously expressed Nox4 is constitutively active; hence, it provides a likely model for the active conformation of other Nox isoforms. In addition, because it does not require activating subunits (other than p22*phox*), Nox4 provides a more straightforward system in which to understand intra-molecular interactions that are important for activity. Investigation of Nox4 structure and function may, therefore, provide a foundation for understanding functionally important regions of Nox enzymes. However, very little is known about regions in Nox4 (other than the cofactor-binding sites) that govern its activity.

In the present study, we used mutagenesis to confirm the B-loop is an important region for Nox4 activity. Mutation of R84, R92, R95 and R96 to alanines or glutamic acids (for R95 and R96) all resulted in a marked decrease in Nox4-dependent ROS-generating activity without significantly altering Nox4 protein expression or binding to p22*phox* (Figure 3.2). These data suggest that although the B-loop PBR is a feature of p22*phox*-dependent Nox isoforms (Nox1-4), this region may not be involved in direct

p22*phox* binding. In a previous study (Kawahara et al., 2007), the Nox2 R80E mutation resulted in decreased activity, impaired Nox2 maturation to its glycosylated form and disrupted complex formation with p22*phox*. However, Nox4 mutated in the homologous residue (R84A) showed normal expression and p22*phox* binding but decreased activity, indicating that this position is also important for Nox4 activity (Figure 3.2). Dinauer and colleagues (Biberstine-Kinkade et al., 1999) mutated residues within the Nox2 B-loop including R89, R91 and R92 which are homologous to Nox4 R93, R95 and R96, respectively. For Nox2, single mutations to a neutral residue such as R89A had only a minor effect on activity, as with the effect of the homologous Nox4 R93A mutation in the present studies (Figure 3.2B left panel). For Nox2, only the double mutation of R91 and R92 significantly decreased Nox2 activity, whereas for Nox4, single mutations of either of the two homologous positions, R95 or R96, whether to alanine or glutamic acid, markedly decreased Nox4 activity (Figure 3.2). Therefore, Nox4 appears to be more sensitive than Nox2 to mutations in these positions.

While conservation in the Nox/Duox family suggested the B-loop is an important region of the enzyme and mutagenesis confirmed this hypothesis for Nox4, the homology models offer an explanation of why. The models suggest the B-loop sits under the transmembrane four helix bundle on the cytoplasmic side of the membrane in close proximity with the DH domain. In support of this model, the present studies demonstrate conclusively that the Nox4 B-loop binds directly to the Nox4 DH domain *in vitro* (Figure 3.3). Furthermore, the same B-loop mutation that markedly inhibits holo-Nox4 activity also disrupts binding of the B-loop to the DH domain indicating this interaction is functionally important for Nox4.

The B-loop:DH domain interaction may play several roles in function. First, it may help localize the FAD in close proximity to heme A, thus allowing rapid electron transfer. Calculations (Moser et al., 2008) place an upper limit on the distance between FAD and heme A of ~22 Å, since distances larger than this would result in a rate too slow to account for the observed turnover of Nox2 (Moser et al., 2008; Nisimoto et al., 1999). Consistent with this limit, in other flavocytochromes for which structures have been determined, the FAD-to-heme distances are 9.9Å for flavocytochrome c sulfide dehydrogenase and 6.3 and 5.9 Å for flavohemoglobin from *E. coli* and *A. eutrophus*, respectively (Chen et al., 1994; Ilari et al., 2002). Therefore, we suggest that the B-loop, by binding to the DH domain, can orient and localize the FAD and heme A in close proximity, allowing facile electron transfer. Furthermore, this binding occurs in such a way that the somewhat bulky B-loop itself does not sterically interfere with electron transfer. Consistent with this idea, the NADPH-binding sub-domain, rather than the FAD-binding sub-domain (Figure 3.5) contains the major determinants of B-loop binding. This is consistent with a conceptual model in which the B-loop creates the domain interface but is localized somewhat to the side, allowing close approximation of the redox centers. In addition to maintaining distance requirements for FAD-heme electron transfer, the B-loop might also affect activity more directly, for example, by modulating the midpoint potentials of electron carriers, which is also expected to affect electron transfer rates (Gunner and Honig, 1991; Moore et al., 1986).

We attempted to determine which amino acids in the Nox4 DH domain are critically important for B-loop binding by mutagenesis. The residues within the Nox4 DH domain were chosen for mutagenesis based on clues from our Nox4 DH domain

homology model, sequence conservation and polarity. However, none of the mutations resulted in significant decrease in the binding affinity, though we did observe changes in the maximum fluorescence polarization. While the model correctly predicted the feasibility of the B-loop interacting with the DH domain, it may not accurately predict the exact binding surface. Another possibility is that the B-loop peptides are binding to multiple sites on the DH domain. In this scenario, we may not observe a decrease in binding affinity if other binding sites remain intact in mutant proteins. Perhaps double or triple simultaneous mutations are needed to observe significantly perturbed binding.

The generality of the B-loop:DH domain interface to other Nox isozymes is suggested by the observed binding of Nox2 B-loop peptide to the Nox2 DH domain, an interaction that is abolished in peptides containing the inactivating (Biberstine-Kinkade et al., 1999) R91E/R92E substitutions. The B-loop:DH domain binding appears to exhibit some specificity towards regulatory classes of Nox enzymes, but only limited isoform specificity within regulatory classes. For example, the B-loop from a calcium-regulated Nox (Nox5) fails to bind to either Nox2 or Nox4 (Figure 3.8). However, within the group of p22*phox*-dependent Noxes, Nox1-4, the Nox4 DH domain binds to B-loops from both Nox2 and Nox4. Similarly, the Nox2 domain binds to B-loops from both Nox2 and Nox4, suggesting the binding regions on the two DH domains are relatively well conserved. However, while Nox2 DH does not show a statistically significant preference for the B-loops from Nox2 *versus* Nox4, Nox4 DH shows a four-fold binding preference for its own B-loop. Furthermore, Nox4 DH binds both loops more tightly than does Nox2. We speculate that the relatively tighter association in Nox4 might reflect an active, electron transferring conformation in Nox4.

We hypothesized that the Nox2DH: B-loop interaction could be enhanced in the presence of regulatory subunits necessary for Nox2 activation. However, these subunits themselves are able to interact with the Nox2 B-loop with similar affinity as the Nox2 DH complicating our attempts to test a simple cooperative binding model. The Nox2 B-loop was proposed to be a binding site for p47*phox* (DeLeo et al., 1995), consistent with the some observed binding between the p67N/p47N chimera and Nox2 B-loop or Nox4 B-loop. However these binding affinities were significantly less than those of the DH domains for their cognate B-loop peptides suggesting that in the holo-enzyme in a physiological setting, the chimera would not be able to bind the B-loop (Figure 3.9). Somewhat surprising and perplexing was that we also observed interactions between Rac1Q61L and both Nox2 and Nox4 B-loop peptides and between GST-p67*phox* and the Nox2 WT B-loop (Figure 3.9). Of note, the recently identified Rac binding site in the Nox2 DH domain is mediated by lysine residues suggesting this protein may be binding through non-specific electrostatic interactions.

The binding promiscuity of the Nox2 B-loop suggests it may present a temporary docking site for multiple factors; p47*phox*, p67*phox* or Rac1 during the course of complex assembly or the DH domain when the subunits are either not present or bound to each other. The lesser binding promiscuity of the Nox4 B-loop and support from the Nox4 homology models adds confidence that the interaction with the DH domain is legitimate and represents a reliable conformation (see Figure 2.9).

The Nox2 and Nox4 B-loops are able to bind reasonably well to their non-cognate DH domains (Figure 3.8). The functional consequence of such mismatched B-loop-DH domain pairs in an *in vivo* Nox ROS-generation system was demonstrated in experiments

using Nox2/Nox4 chimera proteins. A recent study demonstrated significant activity in a Nox4 (TM domain, including B-loop)/ Nox2 (DH domain) chimera (von Lohneysen et al., 2009). We have also observed significant activity in the reverse chimera, Nox2 (TM including B-loop)/ Nox4 DH (Figure 3.10). Taken together, both studies support the idea that the Nox2 and Nox4 B-loops can functionally compensate for each other. When the Nox4 B-loop in the Nox4 (TM domain)/Nox2 (DH domain) chimera was substituted for a Nox2 B-loop (i.e., when the Nox2 B-loop and DH domains were correctly paired), the activity was somewhat reduced in one study (von Lohneysen et al., 2010) while our data showed no change with this chimera (Nox4/2/4/2) or the reverse (Nox2/4/2/4). It is not surprising that the Nox2 DH domain based chimera's showed no change in activity upon B-loop matching as it binds both loops similarly (Figure 3.8). It was somewhat surprising that the Nox4 DH domain based chimera did not show higher activity when paired with its cognate B-loop (Nox2/4/2/4) versus the Nox2 B-loop (Nox2/4) as this domain *in vitro* showed a 3-4 fold higher binding affinity for the Nox4 B-loop. However, this prediction assumes binding affinity is directly proportional to activity output and perhaps this is simply not the case. An alternative model is that the DH domain requires interaction with the B-loop to some degree in order for activity and any combination of DH domain: B-loops that achieve this binding affinity threshold will produce activity and a tighter association would not necessarily translate to higher activity.

The theoretical isoelectric points of all B-loop peptides and recombinant protein was determined using ExPaSy proteomic server (Gasteiger et al., 2003). All B-loop peptides have a calculated pI > 8.9 and GST-Nox4 DH (full-length, NADPH-binding domain, and C-terminal half of the NADPH-binding domain) also have a calculated pI >

8. Because all of these species are positively charged at the assay pH, the interaction detected must be due to a discrete binding site rather than to non-specific electrostatic interactions. GST-Nox2 DH domain, GST-Nox4 304-420 and the N-terminal half of the Nox4 NADPH-binding site proteins all have calculated pI values of ~ 6. Although these proteins are predicted to be negatively charged, they exhibit affinities for the various B-loop peptides that do not correlate with their isoelectric points. Thus, the binding of the peptides to these Nox4 DH domains may not be explained on the basis of non-specific electrostatic effects.

Our data point to a role of the B-loop in binding the DH domain. Thus, a disruption in this interaction might be predicted to inhibit Nox enzymes. We therefore tested the effect of cell-permeable tat-fused Nox4 B-loop peptides (WT and R96E) on ROS generation in intact HEK 293 cells expressing Nox4 (Figure 3.12). Significant inhibition was seen with tat- B-loop peptides, however, these peptides also had large effects on cell viability, which confounded quantitative analysis of the data.

The effect of tat peptide alone on HEK 293 cell viability was very surprising as this peptide has been reported to be relatively non-toxic at the sub-100 micromolar range in various cell systems such as HeLa (human epithelial), A549 (human epithelial) and CHO (Chinese hamster ovarian) (Jones et al., 2005; Vives et al., 1997). Perhaps this discrepancy can be explained by cell type, viability assay, time of assay or internal peptide concentrations. These studies only report tat peptide concentrations used to incubate cells rather than internal peptide concentrations, so perhaps there is a difference in effective peptide concentrations between our studies which would make viability comparisons difficult. Additionally, their method for measuring viability was detection

of formazan dyes by metabolically active cells (i.e. MTT or WST assay) compared to our assay that determines ATP concentration. The MTT assay was performed on cells treated with peptide for 24 hours (Jones et al., 2005) and WST assay was measured after seven hours of treatment (Vives et al., 1997) and the remaining internal peptide concentration was not measured at these times making it unclear how much peptide remained in the cell at the time of the assay. By comparison, we measured viability after 15 minutes of peptide treatment at the same time we measured activity. Perhaps there is an initial stress on the cells at the time of treatment that may recover after a few hours, restoring full metabolic activity. One further difference is that the HEK 293 cells used in our studies were all transfected with Nox4 or empty vector. It was not uncommon to observe the viability of cells transfected with Nox4 as being slightly lower than the viability of those transfected with vector control or un-transfected cells. This difference, although not generally statistically significant, could be an indication of a trend towards cell stress induced by transfection that is exacerbated by the treatment of membrane penetrating peptides. The cells used in the previously reported cytotoxicity studies were not transfected. Whatever the reason may be that the tat-peptides caused loss of cell viability, these effects prevent us from making any significant conclusions about tat-B-loop peptide inhibition of Nox4 expressed in whole cells.

Unlabeled B-loop peptides were also tested in a Nox4 broken cell system and only a modest inhibition was observed (Figure 3.13). These results with Nox4 B-loop peptides are in contrast to the success of Nox2 B-loop peptides on inhibiting Nox2 activity (DeLeo et al., 1995; Rey et al., 2001). We propose that this difference could be due to two variations in these systems, 1. The Nox4 DH: B-loop interaction is stronger

than in Nox2 and may not allow a peptide to compete for DH domain binding or 2. the Nox2 B-loop peptides are disrupting complex assembly as these peptides (at least *in vitro*) have some affinity for the regulatory subunits.

In summary, the B-loop is conserved among all Nox/Duox proteins and Nox1, Nox2, Nox3 and Nox4 share a conserved PBR within this structure. Mutagenesis reveals that, like earlier studies with Nox2, the PBR is also important for Nox4 activity. Nox4 B-loop peptides bind to the Nox4 DH domain, specifically to the N-terminal half of the NADPH-binding domain. Likewise, Nox2 DH domains bind to Nox2 B-loop peptides, albeit with somewhat weaker affinity than the Nox4 association. Both of these interactions are dependent on basic residues within the Nox2 and Nox4 B-loops and neither DH domain interacts with the Nox5 B-loop peptide, which lacks a PBR. Taken together, the data support a model in which the B-loop functions as a binding sequence that links the heme-binding transmembrane domain with the FAD- and NADPH-binding DH domain. This binding is likely to affect the electron transfer between electron centers residing in both domains.

Remaining avenues of investigation include identifying the residues within the DH domain that bind the B-loop. We could not identify such residues using the homology models, so an unbiased screening approach may be more successful for this task. Identification of such residues could help to answer whether this interaction is conserved among all Nox proteins including the isoforms not directly tested in this study such as Nox5 and Duox1/2 by comparing the binding interfaces with Nox4. Furthermore, identifying whether this interaction is conserved in the EF-hand containing Noxes could also provide clues as to its function. A static, conserved interaction might

suggest a function in enzyme folding or structure whereas a dynamic, regulated interaction could provide clues to the enzyme activation mechanism. The latter scenario could be useful for designing isoform-specific inhibitory compounds. Identification of the interface residues would help to confirm or refine our current homology models while providing a starting point for computational docking experiments.

Chapter 4

The dehydrogenase domain of Nox1-4 confers subunit-dependent or independent activity

4.1 Introduction

The human Nox2 sequence is 37% identical to human Nox4 and 27% to human Nox5 (Cheng et al., 2001). All Nox/Duox proteins bind heme, FAD and NADPH and catalyze the reduction of oxygen, so the divergence in their sequences is likely manifested as different means for regulating their catalysis. As described in section 1.3, the seven mammalian Nox isoforms can be classified according to these different regulation mechanisms. The p22*phox*-dependent family consists of Nox1-4, of which Nox1-3 require additional regulatory subunits and Nox4 displays constitutive activity. And the EF-hand containing sub-family Nox5 and Duox1/2 are regulated by calcium binding.

Nox1 is activated by NOXO1, NOXA1 and GTP-bound Rac1. Nox2 is activated by p47*phox*, p67*phox* and GTP-bound Rac1/2. Nox3 can be activated by either NOXO1 alone, with NOXA1, p67*phox* alone or p47*phox*/p67*phox* in combination and possibly, Rac (Cheng et al., 2004; Ueyama et al., 2006). Nox2 and Nox1 can also be activated by combinations of NOXO1/NOXA1 or p47*phox*/p67*phox* but unlike Nox3, they require both an organizer and an activator for stimulation along with Rac1/2 (Banfi et al., 2003; Cheng et al., 2006; Cheng et al., 2004; Takeya et al., 2003). Nox4, on the other hand, is active in the absence of expressed Nox regulatory subunits (other than p22*phox*) (Martyn et al., 2006). Recently, a new protein was found to enhance Nox4 ROS production in vascular smooth muscle cells, though whether this enhancement is the effect of allosteric control of activity or another type of regulation remains to be determined (Lyle et al., 2009).

Much is known about the regulatory subunits' structure and protein-protein interactions as multiple solution and crystal structures have described these details. However, such detailed structural information on subunit interactions with the Nox1-3 catalytic units is lacking. Rather, investigators have used mutagenesis, peptide inhibition or recombinant protein binding studies to investigate the binding sites on the Nox1-3 unit for regulatory subunits. A random sequence phage display library identified three peptides corresponding to Nox2 that bind to recombinant p47*phox* protein (DeLeo et al., 1995). CGD mutations in the N-insertion and F-insertions (see section 2.3.3) result in disrupted p67*phox* and p47*phox* translocation (Leusen et al., 2000).

The remaining questions concerning Nox4 activity are whether the enzyme exists intrinsically in an active conformation or is regulated by an unknown mechanism. In the Nox1-3 subfamily, it remains to be determined whether the regulatory subunits interact and exert their effects via the DH domain, TM domain or both. This chapter chronicles a series of experiments that test the importance of the TM and DH domains in the regulation of Nox enzymes. This investigation confirms that the DH domain indeed is responsible for the spontaneous activity of Nox4 and the subunit-regulated activity in Nox1-3. Recombinant Nox4 DH domain has constitutive electron transferase activity suggesting this isoform is intrinsically active. Furthermore, protein sequence comparisons of the subunit regulated versus non-subunit regulated Nox/Duox enzymes identified novel candidate regulatory subunit binding sites.

4.2 Experimental Procedures

Generation of cDNA Encoding Chimeras and Mutant constructs- Chimera Nox2/4 consists of the TM domain of Nox2 (residues1-284) and the Nox4 DH domain (residues 298-578). Chimera Nox4/2 consists of the Nox4 TM domain (residues 1-337) and the Nox2 DH domain (residues 324-570). Chimeric constructs were created by two consecutive PCRs. The following primers were used to create Nox4/2: (1) human Nox4 sense primer with the BamHI site underlined and with a kozak sequence, 5'-ttttggatccgccaccatggctgtgtcctggaggagctggctcgccaacga-3'; (2) Nox4/2 sense primer with the Nox2 sequence underlined, 50-tttaaagcaagacctggtcagtacatttttgtcaagtgccca-3'; (3) Nox4/2 antisense primer with the Nox2 sequence underlined (reverse complement of primer 2), 5'-tgggcacttgacaaaaatgtactgaccaggtcttgctttaaa-3'; (4) Nox2 antisense primer from the end of the sequence with the NotI site underlined, 5' ttttgcggccgcttagaagttttccttgttgaaaatgaaatgcac-3'. The following primers were used to create chimera Nox2/4: (5) human Nox2 sense primer with the BamHI site underlined and with a kozak sequence, 5'-ttttggatccaccAtggggaactgggctgtgaatgaggggctc-3'; (6) Nox2/4 sense primer with the Nox2 sequence underlined, 5' ccatgtttctgtatctctgtgaaagactttacaggtatatccggagcaa-3'; (7) Nox2/4 antisense primer with the Nox2 sequence underlined, 5'-ttgctccggatatacctgtaaagtctttcacagagatacagaaacatgg-3'; (8) Nox4 antisense sequence with the NotI site underlined, 5'-ttttgcggccgcctagctgaaagactctttattgtattc-3'. PCR A used primers 1 and 3 to amplify humanNox4 TM domain cDNA, primers 5 and 7 to amplify human Nox2 TM domain cDNA, primers 2 and 4 to amplifyNox2DHdomain cDNA, and primers 6 and 8 to amplify Nox4 DH domain cDNA. PCR B used primers 1 and 4 to amplify PCR A

products of Nox4 TM and Nox2 DH domains and primers 5 and 8 to amplify PCR A products of Nox2 TM and Nox4 DH domains. PCR products from reaction B were digested with BamHI and NotI and ligated into the mammalian expression vector, pcDNA3 (Invitrogen). Sequences were confirmed by commercial DNA sequencing (Agencourt Biosciences Corp.). The B-loop:DH domain matching chimera's were constructed as follows: Primer 1 is the same Nox2 sense forward primer as above, Primer 2 is a Nox2 full length reverse primer with a Not1 site, 5'-tttgcggccgcttagaagttttccttgttgaaaatgaaatgcac-3', Primer 3 and 4 are the same Nox4 full length sense and anti-sense primers described in Chapter 3 (Page 98), Primer 5 is Nox4/2/4/2 B-loop begin forward 5'-ctt atc ctt tta ccc atg tgc cga aat ctg ctg tcc ttc -3', Primer 6 is the anti-sense of primer 5; Primer 7 is Nox4/2/4/2 B-loop end forward 5'-Agg aat ctc acc ttt cat aaa acc tgt ggt gtt act atc-3'; Primer 8 is the anti-sense of primer 7; Primer 9 is Nox2/4/2/4 B-loop begin forward 5'-ctg att ctc ttg cca gtc tgt cga aca ctc ttg gct tac-3'; Primer 10 is the anti-sense of primer 9; Primer 11 is N2/4/2/4 B-loop end forward 5'-Aaa agc aga aca ttc cat att atg gtg gca tgg atg att-3'; Primer 12 is the anti-sense of primer 11. Chimera N4/2/4/2 is made by three successive PCR reaction sets. PCR reaction set 1 includes using primers 3 and 6 with the Nox4 WT template to make product A. Primers 5 and 8 were used with the Nox2 WT template to make product B. Primers 7 and 2 were used with chimera 4 (TM)/ 2 (DH) template to make product C. The second PCR reaction set uses primers 3 and 8 with products A and B as templates to make product D. The third PCR reaction uses primers 3 and 2 with products C and D to create the full length N4/2/4/2 chimera. The same strategy was used to make N2/4/2/4

with primers 9-12. The same site-directed mutagenesis procedure outlined in section 3.2 Experimental Procedures was used to create the Nox1 and Nox2 mutant constructs.

Expressing constructs in HEK 293 cells- HEK293 cells were cultured in Dulbecco's modified Eagle's medium (Gibco) containing 4.6 mg/mL glucose, 4.6 mg/mL L-glutamate, 10% fetal serum (Atlanta Biologicals), 100 units/mL penicillin, and 0.1 mg/mL streptomycin (Gibco) in 5% CO2 at 37 _C for 24 h. Cells were transfected with cDNA encoding human full-length Nox4, full-length Nox2, the Nox2/4 chimera, the Nox4/2 chimera in vector pcDNA3, or empty pcDNA3 with and without co-expression of regulatory subunits (human Rac1G12 V, p47*phox*, and p67*phox*), using the FuGene 6 (Roche Molecular Biochemicals) transfection system according to the manufacturer's instructions. After 48 h, cells were harvested and washed twice with Hank's balanced salt solution (HBSS). Cells were centrifuged at 2000g for 5 minutes and the pellets were suspended in HBSS for the NADPH oxidase assay of intact cells and in breaking buffer for the cell-free oxidase assay.

Measurement of ROS production- ROS generation was assessed by either Luminol chemiluminescence increase or the fluorescence increase at 620 nm with a bandwidth of 40 nm (excitation wavelength of 540 nm with a bandwidth of 25 nm) due to H_2O_2-dependent Amplex Red oxidation in the presence of HRP using a Synergy 2 Multi-Mode Microplate Reader and Gen5 (Bio Tek). A standard curve of known H_2O_2 concentrations was developed using the Amplex Red assay and used to quantify H_2O_2 concentration produced in whole cells. In the whole cell assay, 10^4 cells were added to 0.1 mL of assay buffer [25 mM Hepes (pH 7.4) containing 0.12 M NaCl, 3 mM KCl, 1 mM MgCl2, 0.1 mM Amplex Red, and 0.032 unit of HRP]. The reaction was monitored at 25º C for 10

min, and the emission increase was linear during this interval. Cells were harvested in Hank's Balanced Salt Solution (Gibco) for the luminol assay and ROS was measured with 20 μM Luminol and 0.32U horseradish peroxidase in 200 μl total volume with FluoStar^{TM} luminometer (BMG Labtech). The mean of three separate wells is reported with standard deviation (SD). A minimum of three separate transfection experiments were repeated for each condition.

Expression and Purification of Nox DH Proteins- MBP fusion proteins were induced in E. coli at 37º C by addition of 0.1 mM IPTG for 2.5 h and frozen at -80º C. Thawed cells were sonicated (3 x 15 s) and solubilized in 50 mM Hepes buffer (pH 7.5) containing 0.5 M NaCl, 1 mM PMSF, 1 mM EDTA, 1 mM dithiothreitol, protease inhibitor cocktail (1 μg/mL), and 0.2 M L-arginine at 3º C. Arginine was included to improve the yield and minimize protein aggregation (Shiraki et al., 2002). Purification was conducted by amylose-agarose column chromatography (10 mm _ 15 mm) according to instructions from BioLabs, and the fusion proteins were stored at -80º C in 50 mM Hepes buffer (pH 7.5) containing 0.1 M NaCl, 0.2 M arginine, 1 mM EDTA, 0.2% Tween 20, protease inhibitor cocktail, and 0.1mM PMSF.

Pyridine Nucleotide-Dependent Electron Transferring Activity- NADPH-dependent cytochrome c, cytochrome b5, ferricyanide [K3Fe(CN)6], DCIP, INT, and NBT reductase activities were assayed at 36º C according to previously described methods (Nisimoto et al., 2004). The activities were assayed in a 1 mL volume of assay buffer [25 mM Hepes buffer (pH 7.3) containing 0.12 M NaCl, 3 mM KCl, 1 mM MgCl2, 0.25 mM FAD, and 80 μM electron acceptor]. After the mixture that included the DH domain had been pre-incubated for 1 min, the reaction was initiated by the addition of 0.25 mM

NADPH or 0.25 mM NADH. A longer pre-incubation did not affect activity. The reduction rates of electron acceptors were quantified by monitoring the absorbance changes at the appropriate wavelengths, and millimolar extinction coefficients of 21.1 $mM^{-1}cm^{-1}$ at 550 nm (cytochrome c) (Vermilion et al., 1981), 19 $mM^{-1}cm^{-1}$ at 556 nm (cytochrome b5) (Kimura et al., 2001), 1.02 $mM^{-1}cm^{-1}$ at 420 nm (ferricyanide) (Schellenberg and Hellerman, 1958), 20 $mM^{-1}cm^{-1}$ at 600 nm (DCIP) (Norager et al., 2003), 10.5 $mM^{-1}cm^{-1}$ at 490 nm (INT) (Pessach et al., 2001), and 12.6 $mM^{-1}cm^{-1}$ at 595 nm (NBT) (Mitchell et al., 1992) were used to calculate the quantity of each electron acceptor reduced. Spectrophotometric measurements were taken using a Hitachi spectrophotometer with a temperature-controlled cuvette compartment.

4.3 Results

4.3.1 ROS Generation by Nox2, Nox4, and Nox2/4 and Nox4/2 Chimeric Proteins

Nox2 activation is dependent on its assembly with cytosolic regulatory subunits, p67*phox*, p47*phox*, and the GTP-bound form of Rac, while Nox4 activity requires none of these additional proteins (reviewed, (Lambeth, 2004; Vignais, 2002)). To determine whether it is the TM domain or the DH domain that is responsible for conferring the cytosolic subunit-dependent versus constitutive activity, we created chimeric proteins by switching the TM and DH domains of Nox2 and Nox4 as shown in Figure 4.1. The cDNA encoding wild-type or chimeric proteins was expressed either with or without p67*phox*, p47*phox*, and Rac1G12V in HEK293 cells, and the resulting ROS generating activities were measured (Figure 4.1B, C). As in previous studies (Geiszt et al., 2000; Martyn et al., 2006), wild-type Nox4 exhibited constitutive activity that was unaffected

by subunits, while Nox2 activity required co-expression of regulatory subunits. Like wild-type Nox4, chimera Nox2/4 ROS generating activity was independent of regulatory subunits or PMA stimulation. In contrast, chimera Nox4/2, like wild-typeNox2, displayed activity only upon co-expression of subunits and stimulation with PMA. These data suggest the Nox2 DH domain contains the determinants that are the target of regulatory subunit binding and regulation, while the structural features necessary for constitutive activity reside in theNox4 DH domain.

Two ROS detection assays were used to ensure the measured ROS amounts were reflective of the enzyme's catalytic ability and not the type of ROS produced. Amplex Red is specific for hydrogen peroxide (Zhou et al., 1997) while luminol can be oxidized by a variety of ROS (Faulkner and Fridovich, 1993). Both assay systems use horse radish peroxidase, however the relative amounts of ROS detected between the two assays differ with respect to Nox2 and Nox4 suggesting the assays detect different species. Amplex red detects more hydrogen peroxide produced from Nox4 than Nox2 (Figure 4.1 B.), while the luminol assay detects relatively similar amounts of ROS production between the two enzymes (Figure 4.1 C). Chimera Nox 4/2 produces similar amounts of ROS as WT Nox2 in both assays, whereas chimera Nox2/4 produces relatively more ROS detected by luminol than amplex red.

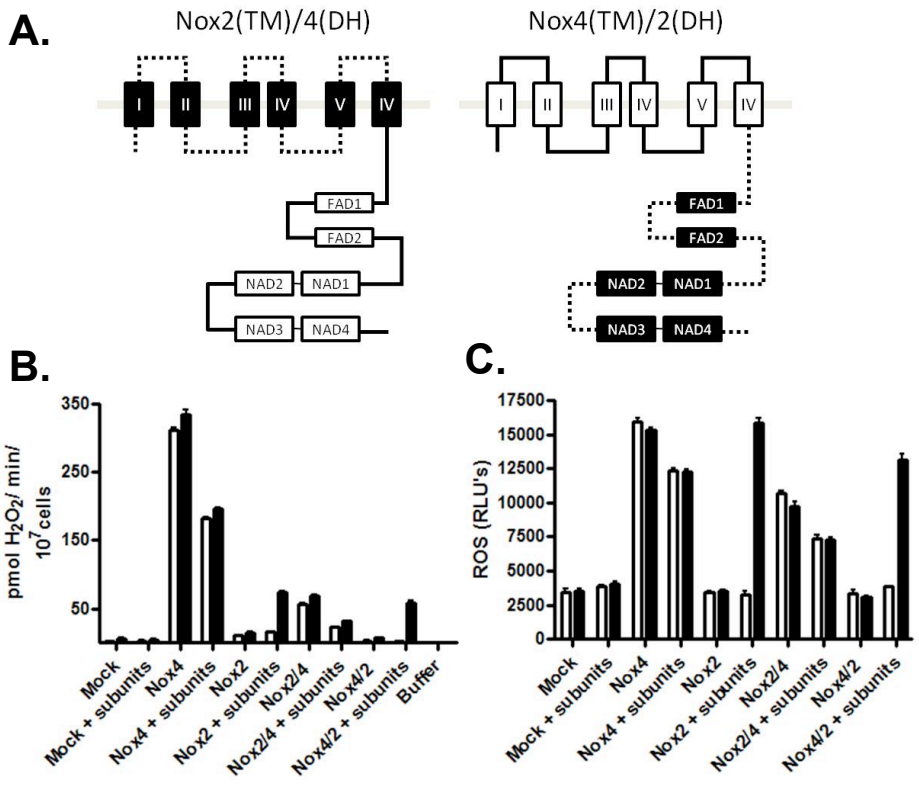

Figure 4.1 The DH domain confers subunit-dependent or independent activity in Nox2 and Nox4.

A. The schematic shows the architecture of the Nox2/4 and Nox4/2 chimeras. Boxes I-VI represent the six transmembrane helices, two boxes labeled FAD1-2 represent the two regions of the protein predicted to bind the FAD ligand, and four boxes labeled NAD1-4 represent the four regions predicted to bind the NADPH. The boundary between the chimeric proteins lies just after the sixth transmembrane helix. Chimera proteins were transfected into HEK 293 cells in the presence or absence of regulatory subunits (p47*phox*, p67*phox* and Rac1G12V) and their ROS production was measured by either Amplex Red (**B**.) or luminol chemiluminescence (**C**.). Cells were treated with (black bars) or without (white bars) PMA to stimulate regulatory subunit assembly.

4.3.2 The Nox4 DH domain displays constitutive electron transferring activity.

Experiments conducted with chimera proteins indicated that the Nox4 DH domain is necessary in order to observe the constitutive activity of Nox4. To determine whether this domain was sufficient to exhibit spontaneous electron transferase activity, Nox4 DH domain was expressed and purified as an MBP fusion protein and electron transferase activity toward several artificial electron acceptors was measured. For comparison, Nox1, Nox2 and Nox5 DH domains were also expressed and purified. The MBP fused forms of the Nox DH domains were used in this study due to poor solubility of the DH domains when the MBP tag was omitted or cleaved. Figure 4.2 shows the NADPH-dependent electron transferase activity of each isolated Nox DH domain, assayed using cytochrome *c*, cytochrome b_5, ferricyanide, 2,6-Dichlorobenzenone-indophenol sodium salt (DCIP), iodonitrotetrazolium chloride (INT) or nitrotetrazolium blue chloride (NBT) as an electron acceptor. MBP-Nox4 DH showed significant NADPH-dependent electron transferase activity towards both 1-electron acceptors and 2-electron accepting dyes, and turnover numbers varied somewhat according to the electron acceptor employed with ferricyanide being the best electron accepting substrate (470 min^{-1}), followed by DCIP (180 min^{-1}), cytochrome *c* (160 min^{1}), INT (95 min^{-1}), cytochrome b_5 (75 min^{-1}), and NBT (65 min^{-1}) being the least active. The high rate seen with ferricyanide is typical of many flavoprotein dehydrogenases, presumably due to the favorable access of this small chelated iron acceptor to the FAD. In contrast, Nox1-, Nox2- and Nox5-DH domains showed only very low NADPH-dependent electron transferase rates (< 1 min^{-1}), regardless of electron acceptor (Figure 4.2) and no activity was observed using NADH as the electron donor (data not shown). Previously, it was reported that the presence of

activating subunits stimulated diaphorase activity of the Nox2 DH domain (Nisimoto et al., 2004). The turnover, however, was still very low (< 10 min^{-1}) compared with that seen with Nox4. MBP alone showed no activity and MBP-Nox4 DH domain activity was inhibited by 70% or more with DPI for all electron acceptors. Little or no Nox4 DH-dependent activity was observed in the absence of added FAD, indicating loss of FAD during the purification. For all electron acceptors, Nox4 DH domain-dependent activities were very low using NADH rather than NADPH as an electron donor

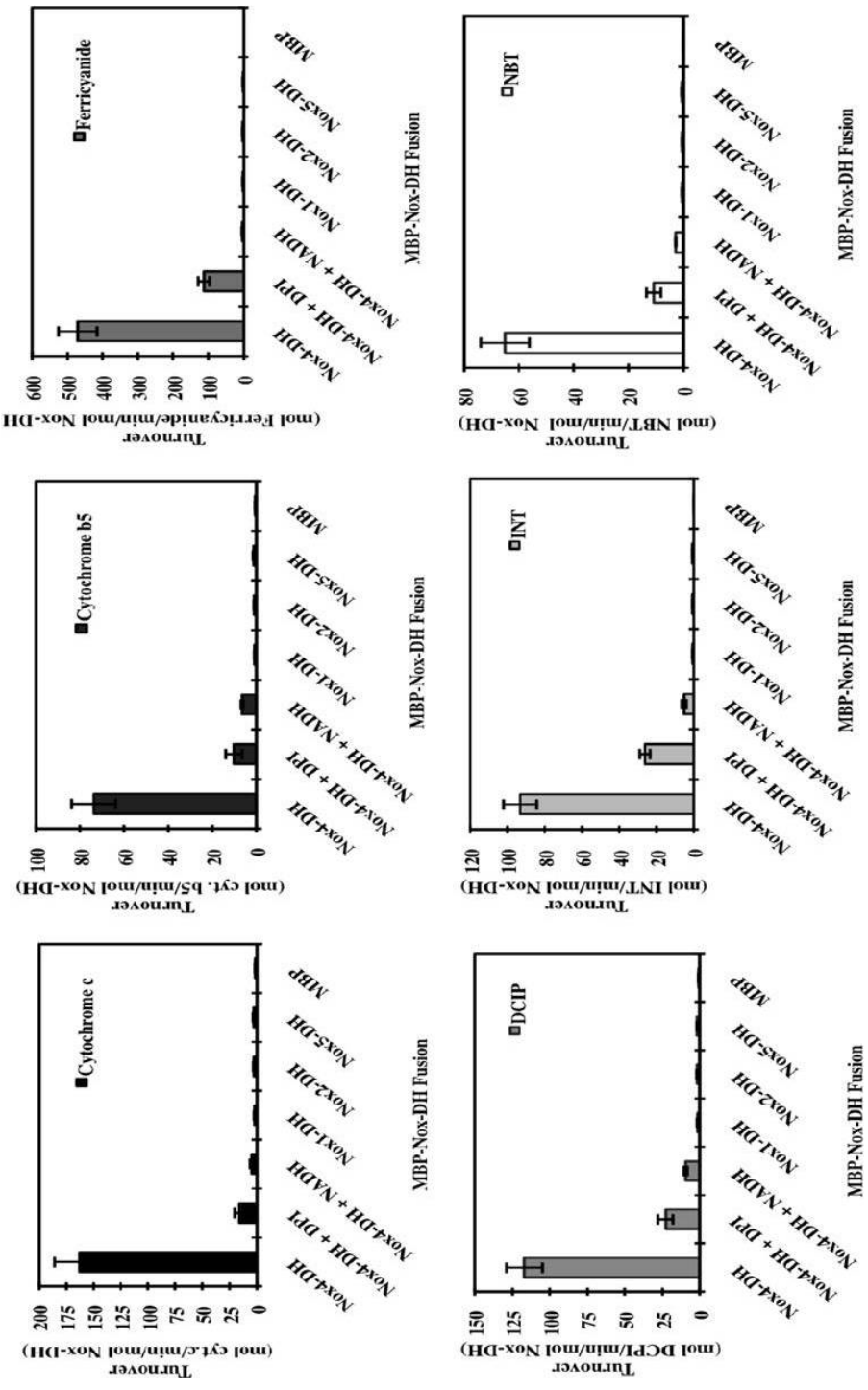
Cytochrome c
Turnover (mol cyt.c/min/mol Nox-DH)
MBP-Nox-DH Fusion
Nox4-DH
Nox4-DH + DPI
Nox4-DH + NADH
Nox1-DH
Nox2-DH
Nox5-DH
MBP
Cytochrome b5
Turnover (mol cyt. b5/min/mol Nox-DH)
MBP-Nox-DH Fusion
Nox4-DH
Nox4-DH + DPI
Nox4-DH + NADH
Nox1-DH
Nox2-DH
Nox5-DH
MBP
Ferricyanide
Turnover (mol Ferricyanide/min/mol Nox-DH
MBP-Nox-DH Fusion
Nox4-DH
Nox4-DH + DPI
Nox4-DH + NADH
Nox1-DH
Nox2-DH
Nox5-DH
MBP
DCIP
Turnover (mol DCPI/min/mol Nox-DH)
MBP-Nox-DH Fusion
Nox4-DH
Nox4-DH + DPI
Nox4-DH + NADH
Nox1-DH
Nox2-DH
Nox5-DH
MBP
INT
Turnover (mol INT/min/mol Nox-DH)
MBP-Nox-DH Fusion
Nox4-DH
Nox4-DH + DPI
Nox4-DH + NADH
Nox1-DH
Nox2-DH
Nox5-DH
MBP
NBT
Turnover (mol NBT/min/mol Nox-DH)
MBP-Nox-DH Fusion
Nox4-DH
Nox4-DH + DPI
Nox4-DH + NADH
Nox1-DH
Nox2-DH
Nox5-DH
MBP

Figure 4.2. Pyridine nucleotide-dependent electron transferase activities of Nox1 DH, Nox2 DH, Nox4 DH and Nox5 DH.

Isoforms of MBP-fused Nox-DH (approximately 25 μg) and MBP alone, were assayed for cytochrome c, cytochrome b_5, ferricyanide, DCIP, INT and NBT reductase activities. The assay was initiated by adding 0.25 mM of either NADPH or NADH. NADPH was used in all experiments, except where NADH is indicated in the third bar of each figure. The NADPH-dependent reductive reaction of Nox4 DH domain was carried out without (first column) or with (second column) 20 μM DPI pre-incubated at 36 ºC for 30 seconds. Each reductive activity indicates the turnover number mean of three independent assays, with error bars showing the S.D. This figure is reproduced with permission from Nisimoto Y, Jackson HM, Ogawa H, Kawahara T, Lambeth JD. Constitutive NADPH-dependent electron transferase activity of the Nox4 Dehydrogenase domain. Biochemistry. 2010 Mar 23;49(11):2433-42.

4.3.3 Residues conserved in Nox1-3 are important for Nox1 and Nox2 activity

The DH domain of Nox2 is sufficient to confer subunit-dependent activity. To further narrow down the binding sites of regulatory subunits on the Nox catalytic unit, we compared the sequences of the regulatory subunit dependent Nox sub-family, Nox1-3 with those of regulatory subunit-independent sub-family, Nox4, Nox5 and Duox1/2. Four residues were found to be conserved in all Nox1, Nox2 and Nox3 sequences from over 25 species (Kawahara et al., 2007). Cysteine 86 (Nox2 numbering) is located in the B-loop, while Tyr476, Trp483 and Gln507 are all located in the DH domain (Figure 4.3 A.). In order to investigate the importance of these conserved residues in Nox1 and Nox2 activity, mutated constructs were created and transfected in HEK 293 cells to measure ROS production. The Nox2 based constructs were co-expressed with the regulatory subunits, p47*phox*, p67*phox* and Rac1G12V, a constitutively active Rac1 mutant. The Nox1 constructs were co-expressed with NOXO1 and NOXA1, the respective homologues of p47*phox* and p67*phox*. These Nox1 proteins were expressed as GFP fusions due to unavailability of Nox1 antibodies for western blot. PMA treatment activates the appropriate signaling cascades required for Nox1 and Nox2 subunit assembly.

Figure 4.3 shows the activity and expression of all Nox1 and Nox2 constructs. Mutation of Cys86 to alanine did not affect the activity of Nox1 or Nox2. Interestingly, the Tyr to Phe substitution resulted in a slight increase in activity of both Nox1 and

Nox2. Though the substitution to alanine left the Nox2 activity unaffected, it decreased Nox1 activity. Substitutions of the tryptophan residues were the most dramatic, resulting in complete reduction of the measured Nox1 and Nox2 activities with alanine and more than a 50% reduction with phenylalanine. The glutamine substitution to glycine also reduced Nox1 and Nox2 activity by more than half, while the mutation to alanine did not affect Nox1 activity. None of the Nox1 and Nox2 mutations drastically effected expression or p22*phox* binding measured by co-immunoprecipitation and western blot (Figure 4.3 D, E.).

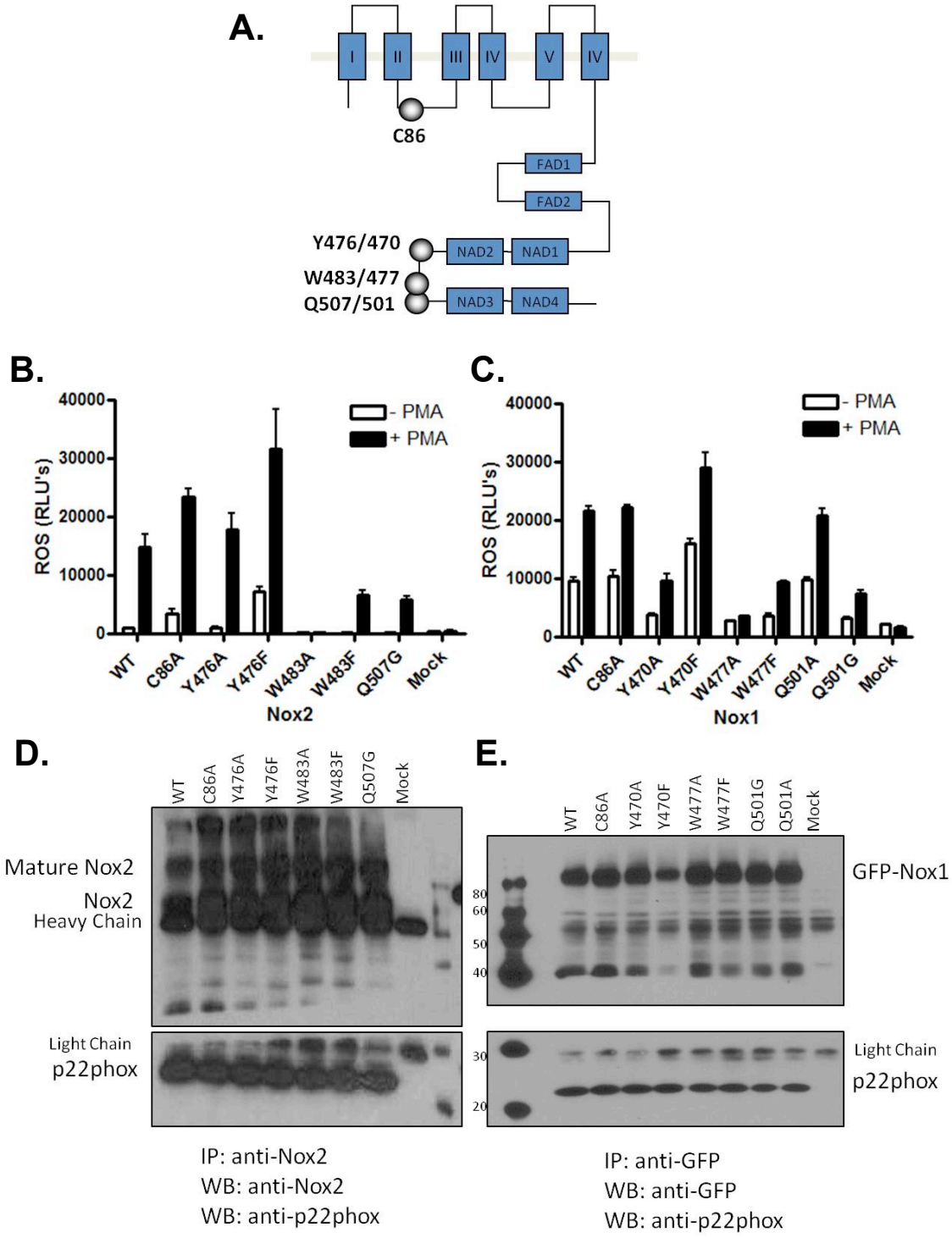
A.
I
II
III
IV
V
IV
C86
FAD1
FAD2
Y476/470
W483/477
Q507/501
NAD2
NAD1
NAD3
NAD4
B.
ROS (RLU's)
- PMA
+ PMA
WT
C86A
Y476A
Y476F
W483A
W483F
Q507G
Mock
Nox2
C.
ROS (RLU's)
- PMA
+ PMA
WT
C86A
Y470A
Y470F
W477A
W477F
Q501A
Q501G
Mock
Nox1
D.
WT
C86A
Y476A
Y476F
W483A
W483F
Q507G
Mock
Mature Nox2
Nox2
Heavy Chain
Light Chain
p22phox
IP: anti-Nox2
WB: anti-Nox2
WB: anti-p22phox
E.
WT
C86A
Y470A
Y470F
W477A
W477F
Q501G
Q501A
Mock
GFP-Nox1
Light Chain
p22phox
IP: anti-GFP
WB: anti-GFP
WB: anti-p22phox

Figure 4.3 The effect of residues conserved in Nox1-3 on Nox1 and Nox2 activity.

A. The schematic of the Nox structure shows where the conserved residues in all Nox1-3 proteins are located. Cysteine 86 is located in the B-loop, and the tyrosine, tryptophan and glutamine residues are all located between the second and third NADPH binding site. The first number listed is for Nox2 and the second corresponds to Nox1. Nox2 wild-type (WT) in pcDNA3 vector (**B.**), Nox1 WT in pEGFP vector (**C.**), the indicated mutations or empty vector (mock) were expressed in HEK 293 cells and ROS production was measured by luminol chemiluminescence. Values reported are relative light unit (RLU), mean ± S.E.M. (n=3). Nox2 (**D.**), Nox1 (**E.**) and mutant expression in HEK 293 cells was determined by transfection followed by immunoprecipitation (IP) using the indicated antibodies. Protein was resolved by SDS-PAGE and western blotting (WB) was carried out using the indicated antibodies. Bands corresponding to the glycosylated (mature) form of Nox2, Nox2, heavy chain, light chain, p22*phox* or GFP-Nox1 are all labeled.

4.4 Discussion and Future Directions

Using chimera proteins to investigate the functional importance of certain regions in proteins has been a widely embraced approach in the Nox field (Berdichevsky et al., 2007; Ebisu et al., 2001; Miyano et al., 2001). Chimera's between the regulatory subunit domains have even produced more potent enzyme activators (Ebisu et al., 2001; Miyano et al., 2001). Applying this technique to the Nox catalytic unit helped to distinguish which regions of the enzymes are important for determining the various regulation mechanisms observed in the different isoforms. The Nox2/Nox4 chimera proteins suggest the DH domain is site of regulation conferring subunit-dependency of the Nox1-3 sub-family or the constitutive activity of Nox4. These results are consistent with studies on Nox1/4 and Nox2/4 chimeras published while this work was under progress. A Nox1 TM domain/ Nox4 DH domain chimera produced ROS in the absence of co-transfected NOXO1/NOXA1 in HEK 293 cells, while the reverse chimera was inactive (Helmcke et al., 2009). Another study reported subunit-dependent activity of a Nox4 TM/ Nox2 DH chimera but their reverse chimera was inactive (von Lohneysen et al., 2010). It is difficult to explain why these studies observed some inactive chimera constructs, however it could be due to differences in chimera boundaries or ROS detection methods.

Interestingly, the relative amount of ROS produced by the Nox2/4 chimera *versus* WT Nox4 is different between the two assay systems (Figure 4.1), suggesting this chimera is producing a different reactive oxygen species. Indeed, a theory has been proposed that suggests the TM domain is responsible for determining whether hydrogen peroxide or superoxide is produced by Nox enzymes (Helmcke et al., 2009).

To investigate whether the DH domain is not only necessary but also sufficient for Nox4 constitutive activity, we expressed the DH domains from Nox1, Nox2, Nox4 and Nox5, and investigated their intrinsic activity towards non-physiological dyes or proteins. The steps in electron transfer that occur within the Nox DH domain are an initial 2-electron hydride transfer from NADPH to FAD with subsequent 1-electron transfers from the reduced and semiquinone flavin to heme (see Figure 1.1). In these experiments the heme-containing TM domain is replaced by exogenous hemoproteins (cytochrome *c*, cytochrome b_5 lacking the hydrophobic membrane-anchoring domain), the small iron-containing ferricyanide, or various dyes. The midpoint redox potentials of these acceptors ranged from +20 mV for soluble cytochrome b_5 to +360 mV of ferricyanide, all significantly higher than the redox potential of the FAD of known flavoprotein dehydrogenases (Iyanagi and Mason, 1973; Roman et al., 2003; Zhang et al., 2001). No correlation between reduction rate and redox potential of the electron acceptor was seen, indicating that other factors (e.g., the reduction of the FAD, steric access of the electron acceptor to the FAD, etc.) are more important in determining the overall rate. While the DH domains from Nox1, Nox2 and Nox5 exhibited very low activity (<1 min^{-1}), the Nox4 DH domain showed significant rates of electron transfer (65-470 min^{-1} depending on the electron acceptor), and these activities were inhibited by DPI. The most rapid rate of reduction was seen with ferricyanide as an electron acceptor, a phenomenon that has been observed with many flavoprotein dehydrogenases and which is often taken as a measure of the rate of reduction of the FAD (Olson and Massey, 1979; Takesue and Omura, 1970; Vermilion et al., 1981). The rapid reduction may be permitted due to the small size of this acceptor (allowing close approach to the reduced

FAD), the very positive redox potential, and/or additional unknown factors. For NADPH-dependent cytochrome *c* reductase activity, which is often used as a readout for superoxide generation, there was no significant decrease in activity in the presence of SOD, indicating that the DH domain of Nox4 generates little if any superoxide. Rather, the reduction of this hemoprotein must occur directly from reduced forms of the enzyme-bound FAD. Therefore, in this setting cytochrome *c* provides a model for the endogenous NADPH-to-FAD-to-heme reduction that occurs in the holo-enzyme.

Determining the binding sites of regulatory subunits on Nox2 has remained an elusive goal despite the decades of research aimed at this question. Such difficulty may be explained by the majority of these studies being conducted with peptides and recombinant proteins in *in vitro* systems or loss of function mutations *in vivo*. While the studies *in vitro* are a more direct approach, they do not provide the most physiologically relevant setting for protein-protein interactions in the absence of binding competitors, nor do they ensure native folding. In addition, it is difficult to determine whether the loss of function mutations are directly testing binding or are an affect of disrupting protein structure. We have determined with a gain of function approach that the DH domain is responsible for conferring subunit-dependent activity of Nox2. This result strongly suggests the important and unique binding sites for regulatory subunits reside in the DH domain. This hypothesis also makes practical sense given that the DH domain resides in the cytoplasm accessible to the soluble regulatory subunits, where as the majority of the TM domain is buried in the membrane or resides on the opposite side of the membrane from the cytoplasm.

The hypothesis that the DH domain is the locus of regulation in Nox2 is supported by several other lines of evidence in addition to the Nox2/4 chimera data that came out while this work was in progress. Pick and colleagues have identified three peptides within the Nox2 DH domain that can bind to recombinant p67*phox* using his "peptide walking" approach (Edgar Pick, personal communication). In the case of Rac1, residues K421, Y425 and K426 within the DH domain were found to be important for mediating binding with Nox2 (Kao et al., 2008). And a separate study showed the Nox2 DH domain expressed in whole cells without the TM domain, could still recruit p47*phox* and p67*phox* translocation (Pessach et al., 2006).

Another interpretation of the Nox4/2 chimera results is that the subunits do also bind the B-loop in the TM domain in addition to the DH domain and that the binding site is conserved in the Nox4 B-loop. While there is some sequence homology between these two loops such as the poly basic region, which has been shown important for p47*phox*/p67*phox* assembly with Nox2, we determined that the Nox4 B-loop peptide does not bind very well to the p67N/p47N chimera or p67*phox* recombinant protein (Figure 3.10). Either way, whether the subunits interact with the B-loop or not, the majority of the functional evidence suggest the DH domain is the site *under* regulation, if not the sole binding site for regulators.

To further delineate which residues within the DH domain are responsible for mediating the affects of regulatory subunits we decided to take an evolutionary approach to determine candidates. Nox1, Nox2 and Nox3 can all be activated, at least *in vitro*, by various combinations of an activator (p67*phox*/NOXA1), and organizer (p47*phox*/NOXO1) and GTP-bound Rac1/2. The fact that these subunits can be utilized

by all three Nox isoforms suggests a common binding site on the Nox catalytic unit. We hypothesize that the functional importance of the regulatory subunits would constrain evolution of their binding sites, resulting in conservation of the binding residues in all subunit-regulated Nox enzymes. To determine these residues, the sequences of all subunit-binding Nox/Duox proteins were compared (Kawahara et al., 2007). Four residues are conserved in all Nox1, Nox2 or Nox3 (subunit-regulated Nox sub-family) sequences but not Nox4, Nox5, Duox1/2. Three of the residues are located in the DH domain while one residue is located in the B-loop of the TM domain. Interestingly, none of these residues matches any of the CGD mutants or previously proposed subunit binding residues though two are located in the N-insertion, so we decided tested these novel candidates for their importance on Nox1 and Nox2 activity. Substitution of the cysteine residue located in the B-loop did not affect either Nox1 or Nox2 activity. The tyrosine residue mutated to alanine only affected Nox1 activity, while interestingly, the conservative mutation to phenylalanine slightly stimulated both Nox2 and Nox1 activity. Inspection of this position in the Nox4 DH domain model shows it is located in the middle of the third β-strand of the NADPH-binding domain. This area is buried in the domain and perhaps the mutation to the more hydrophobic phenylalanine gives a slightly more stable structure resulting in higher activity. Nevertheless, this location in the DH domain does not suggest that it is accessible to binding proteins and is unlikely to interact with the subunits. The most drastic effects on Nox1 and Nox2 activity came from mutating the conserved tryptophan residue to alanine and some activity could be restored with the more conservative mutation to phenylalanine. Mutation of the glutamine residue to alanine significantly reduced both enzymes' activities, although substitution for

glycine was tolerated very well by Nox1. Both the tryptophan and glutamine residues are located in the N-insertion, a region discussed in Chapter 2 (2.3.3 Insertions) as a possible site for regulation. Immunoprecipitation and western blot analysis show that each mutant protein is expressed and is still able to heterodimerize with p22*phox* suggesting they maintain some structural integrity.

Future studies are needed to determine whether the conserved tryptophan and glutamine residues participate directly in subunit binding. This has proved to be a difficult task technically by co-immunoprecipitation in HEK 293 cells and pull-down assay with recombinant proteins. However, there have been some successful attempts to test p67*phox*/p47*phox* binding to mutant Nox2 by translocation assays performed in transfected X-CGD PLB-985 cells (Biondа et al., 2004). Applying this paradigm to study the binding of tryptophan and glutamine residues to subunits would be useful to test this hypothesis.

A summary of the data so far point to a model of the regulatory subunit interactions with Nox such as that shown in Figure 4.4. This diagram uses the Nox4 models as a placeholder for holo-Nox2. The Nox2 regulatory subunits are shown in approximate binding positions. The Rac1 binding residues localize to the first helix of the NADPH-binding domain, which is shown pointing behind the plane of the document near the NADPH ligand in Figure 4.4. Of the three identified peptides corresponding to Nox2 that bind to recombinant p47*phox* protein (DeLeo et al., 1995), one peptide localizes to the B-loop, a second to the final loop of the NADPH-binding domain and the third to the second helix of the NADPH-binding domain (Nα2). P47*phox* is also known to interact with the C-terminal region of p22*phox* as displayed. The p47*phox*

representation in Figure 4.4 is shown to contact the B-loop, final loop of the NADPH-binding domain and p22*phox*. The definitive binding site for p22*phox* on Nox1-4 has not yet been discovered, however suggestions have been made towards it residing in the transmembrane domain.

The binding sites for p67*phox* have been suggested in both the F- and N-insertion of the Nox2 sequence. Interestingly, Trp483 and Gln507, the two mutants with the most drastic affect on Nox2 activity (section 4.3.3) also localize here in the N-insertion. Two of the peptides identified by Pick and colleagues localize to the F-insertion, while the third peptide localizes to the same region of one of the previously identified p47*phox* binding peptides located in Nα2. The p67*phox* representation in Figure 4.4 is shown contacting both the F- and N-insertions. This placement positions p67phox near the NADPH and FAD ligands for the AD to stimulate hydride transfer. The same peptide localizing to Nα2 being identified as both a p67*phox* and p47*phox* binding site may suggest either that this peptide recognizes a broad class of proteins and may not be physiologically relevant or that it is a dynamic point of contact for both of the proteins at different times during assembly. Due to this ambiguity, neither the p47*phox* nor the p67*phox* representations are shown contacting this region in Figure 4.4.

The schematic in Figure 4.4 also shows that binding between Rac and p67*phox* could still occur even when both proteins also bind the Nox unit consistent with the role of Rac in organizing p67phox for catalytic stimulation. P47*phox* and p67*phox* are also known to interact via an interaction between the C-terminal p67*phox* SH3 domain with the C-terminal PxxP motif of p47*phox* (Kami et al., 2002). However, it is not known whether this interaction occurs when both proteins are in contact with Nox2. The

schematic shows these proteins not in contact, however, given their size, it is conceivable that they could interact given their respective positions on the Nox unit. NMR and crystallographic studies of the subunit-subunit interactions have provided a lot of information on this area. However, structural studies on the Nox catalytic units in the presence of subunits are needed to fully understand the exact binding sites and how these interactions lead to enzyme activation.

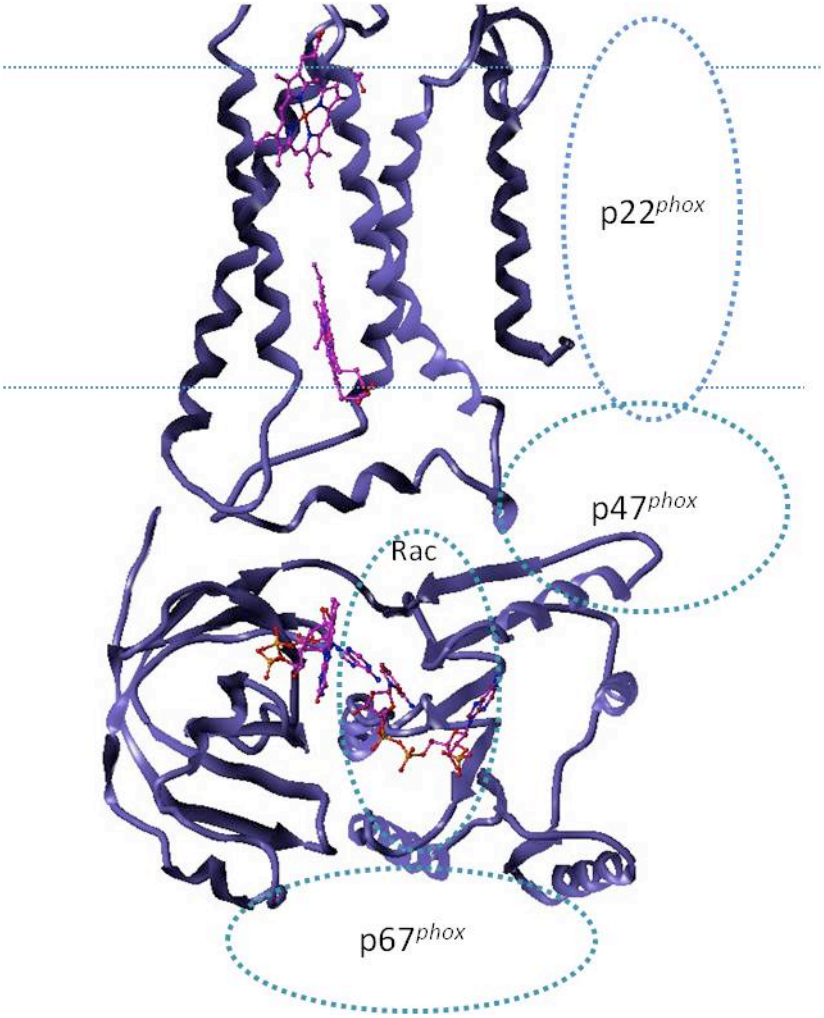

Figure 4.4 Model of regulatory subunits interactions with the Nox structure.

Models of the transmembrane and dehydrogenase domains of Nox4 was used to represent the basic Nox structure. Dotted circles represent the indicated regulatory subunits and their prospective positions relative to the Nox structure. The two dotted lines represent the membrane bilayer. FAD and NADPH are shown in ball and stick representation, with FAD on the left and NADPH on the right.

Overall Conclusions

The three chapters of this thesis have helped to describe structure-function relationships of Nox4. We chose to center most of the studies around the Nox4 isoform as a prototype for the Nox/Duox family since it is known to be spontaneously active. Prior to the beginning of this investigation, very little was known about the regions of Nox4 that are important for activity. In summary, this work described the construction and analysis of a Nox4 DH domain homology model. The B-loop was found to be an important region for Nox4 activity and consistent with the model, forms a tight interaction with the DH domain. This work also confirmed that the Nox4 DH domain has intrinsic electron transferase activity.

In addition to advancing the field with new information about the Nox4 isoform, we have also shown that many of the conclusions drawn from studying Nox4 can be broadly applied to the Nox/Duox family. The Nox4 homology models can provide a basic framework for which to understand structural features of the rest of the enzyme family. Every ligand binding residue identified in this model was conserved in all known Nox/Duox protein sequences, suggesting similar functions. The model was also used to explain the functions of highly conserved regions previously identified in a molecular evolution analysis of the Nox/Duox family. The novel role for the B-loop region identified in Nox4 was also shown to be conserved in Nox2. By swapping the different domains of Nox2 and Nox4 we were able to show that the DH domain determines the spontaneous activity of Nox4 and subunit-dependent activity of Nox2. Furthermore, through the process of building the model for Nox4 and comparing Nox/Duox sequences with other DH domain containing proteins, we identified insertions within the Nox/Duox

DH domains. These insertions could provide points of contact for the regulatory subunits or domains for Nox1-3 and Nox5, Duox1/2. Indeed residues strictly conserved in Nox1-3, located in one of these insertions is important for activity.

References

Ago, T., Kitazono, T., Kuroda, J., Kumai, Y., Kamouchi, M., Ooboshi, H., Wakisaka, M., Kawahara, T., Rokutan, K., Ibayashi, S.*, et al.* (2005). NAD(P)H oxidases in rat basilar arterial endothelial cells. Stroke *36*, 1040-1046.

Ago, T., Nunoi, H., Ito, T., and Sumimoto, H. (1999). Mechanism for phosphorylation-induced activation of the phagocyte NADPH oxidase protein p47(phox). Triple replacement of serines 303, 304, and 328 with aspartates disrupts the SH3 domain-mediated intramolecular interaction in p47(phox), thereby activating the oxidase. J Biol Chem *274*, 33644-33653.

Ambasta, R.K., Kumar, P., Griendling, K.K., Schmidt, H.H., Busse, R., and Brandes, R.P. (2004). Direct interaction of the novel Nox proteins with p22phox is required for the formation of a functionally active NADPH oxidase. J Biol Chem *279*, 45935-45941.

Ameziane-El-Hassani, R., Morand, S., Boucher, J.L., Frapart, Y.M., Apostolou, D., Agnandji, D., Gnidehou, S., Ohayon, R., Noel-Hudson, M.S., Francon, J.*, et al.* (2005). Dual oxidase-2 has an intrinsic Ca2+-dependent H2O2-generating activity. J Biol Chem *280*, 30046-30054.

Babior, B.M., and Kipnes, R.S. (1977). Superoxide-forming enzyme from human neutrophils: evidence for a flavin requirement. Blood *50*, 517-524.

Baldridge, C.W., and Gerard, R.W. (1932). The Extra Respiration of Phagocytosis. Am J Physiol *103*, 235-236.

Banfi, B., Clark, R.A., Steger, K., and Krause, K.H. (2003). Two novel proteins activate superoxide generation by the NADPH oxidase NOX1. J Biol Chem *278*, 3510-3513.

Banfi, B., Malgrange, B., Knisz, J., Steger, K., Dubois-Dauphin, M., and Krause, K.H. (2004a). NOX3, a superoxide-generating NADPH oxidase of the inner ear. J Biol Chem *279*, 46065-46072.

Banfi, B., Maturana, A., Jaconi, S., Arnaudeau, S., Laforge, T., Sinha, B., Ligeti, E., Demaurex, N., and Krause, K.H. (2000). A mammalian H+ channel generated through alternative splicing of the NADPH oxidase homolog NOH-1. Science *287*, 138-142.

Banfi, B., Molnar, G., Maturana, A., Steger, K., Hegedus, B., Demaurex, N., and Krause, K.H. (2001). A Ca(2+)-activated NADPH oxidase in testis, spleen, and lymph nodes. J Biol Chem *276*, 37594-37601.

Banfi, B., Tirone, F., Durussel, I., Knisz, J., Moskwa, P., Molnar, G.Z., Krause, K.H., and Cox, J.A. (2004b). Mechanism of Ca2+ activation of the NADPH oxidase 5 (NOX5). J Biol Chem *279*, 18583-18591.

Bedard, K., and Krause, K.H. (2007). The NOX family of ROS-generating NADPH oxidases: physiology and pathophysiology. Physiol Rev *87*, 245-313.

Beevers, L.a.H., R.H. (1969). Nitrate reduction in higher plants. Annu Rev Plant Physiol *20*, 494-522.

BelAiba, R.S., Djordjevic, T., Petry, A., Diemer, K., Bonello, S., Banfi, B., Hess, J., Pogrebniak, A., Bickel, C., and Gorlach, A. (2007). NOX5 variants are functionally active in endothelial cells. Free Radic Biol Med *42*, 446-459.

Berdichevsky, Y., Mizrahi, A., Ugolev, Y., Molshanski-Mor, S., and Pick, E. (2007). Tripartite chimeras comprising functional domains derived from the cytosolic NADPH oxidase components p47phox, p67phox, and Rac1 elicit activator-independent superoxide production by phagocyte membranes: an essential role for anionic membrane phospholipids. J Biol Chem *282*, 22122-22139.

Berthier, S., Paclet, M.H., Lerouge, S., Roux, F., Vergnaud, S., Coleman, A.W., and Morel, F. (2003). Changing the conformation state of cytochrome b558 initiates NADPH oxidase activation: MRP8/MRP14 regulation. J Biol Chem *278*, 25499-25508.

Bewley, M.C., Marohnic, C.C., and Barber, M.J. (2001). The structure and biochemistry of NADH-dependent cytochrome b5 reductase are now consistent. Biochemistry *40*, 13574-13582.

Biberstine-Kinkade, K.J., DeLeo, F.R., Epstein, R.I., LeRoy, B.A., Nauseef, W.M., and Dinauer, M.C. (2001). Heme-ligating histidines in flavocytochrome b(558): identification of specific histidines in gp91(phox). J Biol Chem *276*, 31105-31112.

Biberstine-Kinkade, K.J., Yu, L., and Dinauer, M.C. (1999). Mutagenesis of an arginine- and lysine-rich domain in the gp91(phox) subunit of the phagocyte NADPH-oxidase flavocytochrome b558. J Biol Chem *274*, 10451-10457.

Bionda, C., Li, X.J., van Bruggen, R., Eppink, M., Roos, D., Morel, F., and Stasia, M.J. (2004). Functional analysis of two-amino acid substitutions in gp91 phox in a patient with X-linked flavocytochrome b558-positive chronic granulomatous disease by means of transgenic PLB-985 cells. Hum Genet *115*, 418-427.

Block, K., Gorin, Y., and Abboud, H.E. (2009). Subcellular localization of Nox4 and regulation in diabetes. Proc Natl Acad Sci U S A *106*, 14385-14390.

Bokoch, G.M. (2005). Regulation of innate immunity by Rho GTPases. Trends Cell Biol *15*, 163-171.

Bortolotti, A., Perez-Dorado, I., Goni, G., Medina, M., Hermoso, J.A., Carrillo, N., and Cortez, N. (2009). Coenzyme binding and hydride transfer in Rhodobacter capsulatus ferredoxin/flavodoxin NADP(H) oxidoreductase. Biochim Biophys Acta *1794*, 199-210.

Brar, S.S., Corbin, Z., Kennedy, T.P., Hemendinger, R., Thornton, L., Bommarius, B., Arnold, R.S., Whorton, A.R., Sturrock, A.B., Hueckstead, T.P*., et al.* (2003). NOX5 NAD(P)H oxidase regulates growth and apoptosis in DU 145 prostate cancer cells. Am J Physiol Cell Physiol *285*, C353-369.

Bravo, J., Karathanassis, D., Pacold, C.M., Pacold, M.E., Ellson, C.D., Anderson, K.E., Butler, P.J., Lavenir, I., Perisic, O., Hawkins, P.T.*, et al.* (2001). The crystal structure of the PX domain from p40(phox) bound to phosphatidylinositol 3-phosphate. Mol Cell *8*, 829-839.

Bruns, C.M., and Karplus, P.A. (1995). Refined crystal structure of spinach ferredoxin reductase at 1.7 A resolution: oxidized, reduced and 2'-phospho-5'-AMP bound states. J Mol Biol *247*, 125-145.

Buettner, G.R. (1993). The pecking order of free radicals and antioxidants: lipid peroxidation, alpha-tocopherol, and ascorbate. Arch Biochem Biophys *300*, 535-543.

Burritt, J.B., DeLeo, F.R., McDonald, C.L., Prigge, J.R., Dinauer, M.C., Nakamura, M., Nauseef, W.M., and Jesaitis, A.J. (2001). Phage display epitope mapping of human neutrophil flavocytochrome b558. Identification of two juxtaposed extracellular domains. J Biol Chem *276*, 2053-2061.

Burritt, J.B., Foubert, T.R., Baniulis, D., Lord, C.I., Taylor, R.M., Mills, J.S., Baughan, T.D., Roos, D., Parkos, C.A., and Jesaitis, A.J. (2003). Functional epitope on human neutrophil flavocytochrome b558. J Immunol *170*, 6082-6089.

Carnesecchi, S., Carpentier, J.L., Foti, M., and Szanto, I. (2006). Insulin-induced vascular endothelial growth factor expression is mediated by the NADPH oxidase NOX3. Exp Cell Res *312*, 3413-3424.

Ceccarelli, E.A., Arakaki, A.K., Cortez, N., and Carrillo, N. (2004). Functional plasticity and catalytic efficiency in plant and bacterial ferredoxin-NADP(H) reductases. Biochim Biophys Acta *1698*, 155-165.

Chamulitrat, W., Schmidt, R., Tomakidi, P., Stremmel, W., Chunglok, W., Kawahara, T., and Rokutan, K. (2003). Association of gp91phox homolog Nox1 with anchorage-independent growth and MAP kinase-activation of transformed human keratinocytes. Oncogene *22*, 6045-6053.

Chavez, V., Mohri-Shiomi, A., and Garsin, D.A. (2009). Ce-Duox1/BLI-3 generates reactive oxygen species as a protective innate immune mechanism in Caenorhabditis elegans. Infect Immun *77*, 4983-4989.

Chen, Z.W., Koh, M., Van Driessche, G., Van Beeumen, J.J., Bartsch, R.G., Meyer, T.E., Cusanovich, M.A., and Mathews, F.S. (1994). The structure of flavocytochrome c sulfide dehydrogenase from a purple phototrophic bacterium. Science *266*, 430-432.

Cheng, G., Cao, Z., Xu, X., van Meir, E.G., and Lambeth, J.D. (2001). Homologs of gp91phox: cloning and tissue expression of Nox3, Nox4, and Nox5. Gene *269*, 131-140.

Cheng, G., Diebold, B.A., Hughes, Y., and Lambeth, J.D. (2006). Nox1-dependent reactive oxygen generation is regulated by Rac1. J Biol Chem *281*, 17718-17726.

Cheng, G., and Lambeth, J.D. (2004). NOXO1, regulation of lipid binding, localization, and activation of Nox1 by the Phox homology (PX) domain. J Biol Chem *279*, 4737-4742.

Cheng, G., Ritsick, D., and Lambeth, J.D. (2004). Nox3 regulation by NOXO1, p47phox, and p67phox. J Biol Chem *279*, 34250-34255.

Cheret, C., Gervais, A., Lelli, A., Colin, C., Amar, L., Ravassard, P., Mallet, J., Cumano, A., Krause, K.H., and Mallat, M. (2008). Neurotoxic activation of microglia is promoted by a nox1-dependent NADPH oxidase. J Neurosci *28*, 12039-12051.

Clark, R.A., Volpp, B.D., Leidal, K.G., and Nauseef, W.M. (1990). Two cytosolic components of the human neutrophil respiratory burst oxidase translocate to the plasma membrane during cell activation. J Clin Invest *85*, 714-721.

Clempus, R.E., Sorescu, D., Dikalova, A.E., Pounkova, L., Jo, P., Sorescu, G.P., Schmidt, H.H., Lassegue, B., and Griendling, K.K. (2007). Nox4 is required for maintenance of the differentiated vascular smooth muscle cell phenotype. Arterioscler Thromb Vasc Biol *27*, 42-48.

Correll, C.C., Batie, C.J., Ballou, D.P., and Ludwig, M.L. (1992). Phthalate dioxygenase reductase: a modular structure for electron transfer from pyridine nucleotides to [2Fe-2S]. Science *258*, 1604-1610.

Cross, A.R., Jones, O.T., Harper, A.M., and Segal, A.W. (1981). Oxidation-reduction properties of the cytochrome b found in the plasma-membrane fraction of human neutrophils. A possible oxidase in the respiratory burst. Biochem J *194*, 599-606.

Cross, A.R., Parkinson, J.F., and Jones, O.T. (1984). The superoxide-generating oxidase of leucocytes. NADPH-dependent reduction of flavin and cytochrome b in solubilized preparations. Biochem J *223*, 337-344.

Cucoranu, I., Clempus, R., Dikalova, A., Phelan, P.J., Ariyan, S., Dikalov, S., and Sorescu, D. (2005). NAD(P)H oxidase 4 mediates transforming growth factor-beta1-induced differentiation of cardiac fibroblasts into myofibroblasts. Circ Res *97*, 900-907.

Dai, X., Cao, X., and Kreulen, D.L. (2006). Superoxide anion is elevated in sympathetic neurons in DOCA-salt hypertension via activation of NADPH oxidase. Am J Physiol Heart Circ Physiol *290*, H1019-1026.

Dandliker, W.B., and De Saussure, V.A. (1970). Fluorescence polarization in immunochemistry. Immunochemistry *7*, 799-828.

Datla, S.R., Peshavariya, H., Dusting, G.J., Mahadev, K., Goldstein, B.J., and Jiang, F. (2007). Important role of Nox4 type NADPH oxidase in angiogenic responses in human microvascular endothelial cells in vitro. Arterioscler Thromb Vasc Biol *27*, 2319-2324.

De Deken, X., Wang, D., Many, M.C., Costagliola, S., Libert, F., Vassart, G., Dumont, J.E., and Miot, F. (2000). Cloning of two human thyroid cDNAs encoding new members of the NADPH oxidase family. J Biol Chem *275*, 23227-23233.

de Mochel, N.S., Seronello, S., Wang, S.H., Ito, C., Zheng, J.X., Liang, T.J., Lambeth, J.D., and Choi, J. (2010). Hepatocyte NAD(P)H oxidases as an endogenous source of reactive oxygen species during hepatitis C virus infection. Hepatology *52*, 47-59.

Debeurme, F., Picciocchi, A., Dagher, M.C., Grunwald, D., Beaumel, S., Fieschi, F., and Stasia, M.J. (2010). Regulation of NADPH oxidase activity in phagocytes - Relationship between FAD/NADPH binding and oxidase complex assembly. J Biol Chem.

DeLeo, F.R., Yu, L., Burritt, J.B., Loetterle, L.R., Bond, C.W., Jesaitis, A.J., and Quinn, M.T. (1995). Mapping sites of interaction of p47-phox and flavocytochrome b with random-sequence peptide phage display libraries. Proc Natl Acad Sci U S A *92*, 7110-7114.

Deng, Z., Aliverti, A., Zanetti, G., Arakaki, A.K., Ottado, J., Orellano, E.G., Calcaterra, N.B., Ceccarelli, E.A., Carrillo, N., and Karplus, P.A. (1999). A productive NADP+ binding mode of ferredoxin-NADP + reductase revealed by protein engineering and crystallographic studies. Nat Struct Biol *6*, 847-853.

Denu, J.M., and Tanner, K.G. (1998). Specific and reversible inactivation of protein tyrosine phosphatases by hydrogen peroxide: evidence for a sulfenic acid intermediate and implications for redox regulation. Biochemistry *37*, 5633-5642.

Diaz, B., Shani, G., Pass, I., Anderson, D., Quintavalle, M., and Courtneidge, S.A. (2009). Tks5-dependent, nox-mediated generation of reactive oxygen species is necessary for invadopodia formation. Sci Signal *2*, ra53.

Diebold, B.A., and Bokoch, G.M. (2001). Molecular basis for Rac2 regulation of phagocyte NADPH oxidase. Nat Immunol *2*, 211-215.

Dinauer, M.C., Orkin, S.H., Brown, R., Jesaitis, A.J., and Parkos, C.A. (1987). The glycoprotein encoded by the X-linked chronic granulomatous disease locus is a component of the neutrophil cytochrome b complex. Nature *327*, 717-720.

Doussiere, J., Brandolin, G., Derrien, V., and Vignais, P.V. (1993). Critical assessment of the presence of an NADPH binding site on neutrophil cytochrome b558 by photoaffinity and immunochemical labeling. Biochemistry *32*, 8880-8887.

Doussiere, J., Gaillard, J., and Vignais, P.V. (1996). Electron transfer across the O2-generating flavocytochrome b of neutrophils. Evidence for a transition from a low-spin state to a high-spin state of the heme iron component. Biochemistry *35*, 13400-13410.

Dupuy, C., Ohayon, R., Valent, A., Noel-Hudson, M.S., Deme, D., and Virion, A. (1999). Purification of a novel flavoprotein involved in the thyroid NADPH oxidase. Cloning of the porcine and human cdnas. J Biol Chem *274*, 37265-37269.

Dupuy, C., Virion, A., De Sandro, V., Ohayon, R., Kaniewski, J., Pommier, J., and Deme, D. (1992). Activation of the NADPH-dependent H2O2-generating system in pig thyroid particulate fraction by limited proteolysis and Zn2+ treatment. Biochem J *283 (Pt 2)*, 591-595.

Dym, O., and Eisenberg, D. (2001). Sequence-structure analysis of FAD-containing proteins. Protein Sci *10*, 1712-1728.

Ebisu, K., Nagasawa, T., Watanabe, K., Kakinuma, K., Miyano, K., and Tamura, M. (2001). Fused p47phox and p67phox truncations efficiently reconstitute NADPH oxidase with higher activity and stability than the individual components. J Biol Chem *276*, 24498-24505.

Edens, W.A., Sharling, L., Cheng, G., Shapira, R., Kinkade, J.M., Lee, T., Edens, H.A., Tang, X., Sullards, C., Flaherty, D.B.*, et al.* (2001). Tyrosine cross-linking of extracellular matrix is catalyzed by Duox, a multidomain oxidase/peroxidase with homology to the phagocyte oxidase subunit gp91phox. J Cell Biol *154*, 879-891.

El Hassani, R.A., Benfares, N., Caillou, B., Talbot, M., Sabourin, J.C., Belotte, V., Morand, S., Gnidehou, S., Agnandji, D., Ohayon, R.*, et al.* (2005). Dual oxidase2 is expressed all along the digestive tract. Am J Physiol Gastrointest Liver Physiol *288*, G933-942.

Enoch, H.G., and Strittmatter, P. (1979). Cytochrome b5 reduction by NADPH-cytochrome P-450 reductase. J Biol Chem *254*, 8976-8981.

Ermler, U., Siddiqui, R.A., Cramm, R., and Friedrich, B. (1995). Crystal structure of the flavohemoglobin from Alcaligenes eutrophus at 1.75 A resolution. EMBO J *14*, 6067-6077.

Faulkner, K., and Fridovich, I. (1993). Luminol and lucigenin as detectors for O2. Free Radic Biol Med *15*, 447-451.

Fawell, S., Seery, J., Daikh, Y., Moore, C., Chen, L.L., Pepinsky, B., and Barsoum, J. (1994). Tat-mediated delivery of heterologous proteins into cells. Proc Natl Acad Sci U S A *91*, 664-668.

Finan, P., Shimizu, Y., Gout, I., Hsuan, J., Truong, O., Butcher, C., Bennett, P., Waterfield, M.D., and Kellie, S. (1994). An SH3 domain and proline-rich sequence mediate an interaction between two components of the phagocyte NADPH oxidase complex. J Biol Chem *269*, 13752-13755.

Flocco, M.M., and Mowbray, S.L. (1994). Planar stacking interactions of arginine and aromatic side-chains in proteins. J Mol Biol *235*, 709-717.

Flores, M.V., Crawford, K.C., Pullin, L.M., Hall, C.J., Crosier, K.E., and Crosier, P.S. (2010). Dual oxidase in the intestinal epithelium of zebrafish larvae has anti-bacterial properties. Biochem Biophys Res Commun.

Frankel, A.D., and Pabo, C.O. (1988). Cellular uptake of the tat protein from human immunodeficiency virus. Cell *55*, 1189-1193.

Freeman, J.L., Abo, A., and Lambeth, J.D. (1996). Rac "insert region" is a novel effector region that is implicated in the activation of NADPH oxidase, but not PAK65. J Biol Chem *271*, 19794-19801.

Fukuyama, M., Rokutan, K., Sano, T., Miyake, H., Shimada, M., and Tashiro, S. (2005). Overexpression of a novel superoxide-producing enzyme, NADPH oxidase 1, in adenoma and well differentiated adenocarcinoma of the human colon. Cancer Lett *221*, 97-104.

Gao, D., Nong, S., Huang, X., Lu, Y., Zhao, H., Lin, Y., Man, Y., Wang, S., Yang, J., and Li, J. (2010). The effects of palmitate on hepatic insulin resistance are mediated by NADPH oxidase 3-derived reactive oxygen species through JNK and p38MAPK pathways. J Biol Chem.

Gasteiger, E., Gattiker, A., Hoogland, C., Ivanyi, I., Appel, R.D., and Bairoch, A. (2003). ExPASy: The proteomics server for in-depth protein knowledge and analysis. Nucleic Acids Res *31*, 3784-3788.

Gavazzi, G., Banfi, B., Deffert, C., Fiette, L., Schappi, M., Herrmann, F., and Krause, K.H. (2006). Decreased blood pressure in NOX1-deficient mice. FEBS Lett *580*, 497-504.

Geiszt, M., Kopp, J.B., Varnai, P., and Leto, T.L. (2000). Identification of renox, an NAD(P)H oxidase in kidney. Proc Natl Acad Sci U S A *97*, 8010-8014.

Geiszt, M., Lekstrom, K., Brenner, S., Hewitt, S.M., Dana, R., Malech, H.L., and Leto, T.L. (2003). NAD(P)H oxidase 1, a product of differentiated colon epithelial cells, can partially replace glycoprotein 91phox in the regulated production of superoxide by phagocytes. J Immunol *171*, 299-306.

Gianni, D., Diaz, B., Taulet, N., Fowler, B., Courtneidge, S.A., and Bokoch, G.M. (2009). Novel p47(phox)-related organizers regulate localized NADPH oxidase 1 (Nox1) activity. Sci Signal *2*, ra54.

Gianni, D., Taulet, N., Zhang, H., Dermardirossian, C., Kister, J., Martinez, L., Roush, W.R., Brown, S.J., Bokoch, G., and Rosen, H. (2010). A novel and specific NADPH oxidase-1 (Nox1) small-molecule inhibitor blocks the formation of functional invadopodia in human colon cancer cells. ACS Chem Biol.

Gorzalczany, Y., Sigal, N., Itan, M., Lotan, O., and Pick, E. (2000). Targeting of Rac1 to the phagocyte membrane is sufficient for the induction of NADPH oxidase assembly. J Biol Chem *275*, 40073-40081.

Goyal, P., Weissmann, N., Grimminger, F., Hegel, C., Bader, L., Rose, F., Fink, L., Ghofrani, H.A., Schermuly, R.T., Schmidt, H.H.*, et al.* (2004). Upregulation of

NAD(P)H oxidase 1 in hypoxia activates hypoxia-inducible factor 1 via increase in reactive oxygen species. Free Radic Biol Med *36*, 1279-1288.

Goyal, P., Weissmann, N., Rose, F., Grimminger, F., Schafers, H.J., Seeger, W., and Hanze, J. (2005). Identification of novel Nox4 splice variants with impact on ROS levels in A549 cells. Biochem Biophys Res Commun *329*, 32-39.

Grasberger, H., and Refetoff, S. (2006). Identification of the maturation factor for dual oxidase. Evolution of an eukaryotic operon equivalent. J Biol Chem *281*, 18269-18272.

Green, M., and Loewenstein, P.M. (1988). Autonomous functional domains of chemically synthesized human immunodeficiency virus tat trans-activator protein. Cell *55*, 1179-1188.

Groemping, Y., Lapouge, K., Smerdon, S.J., and Rittinger, K. (2003). Molecular basis of phosphorylation-induced activation of the NADPH oxidase. Cell *113*, 343-355.

Gunner, M.R., and Honig, B. (1991). Electrostatic control of midpoint potentials in the cytochrome subunit of the Rhodopseudomonas viridis reaction center. Proc Natl Acad Sci U S A *88*, 9151-9155.

Ha, E.M., Oh, C.T., Bae, Y.S., and Lee, W.J. (2005). A direct role for dual oxidase in Drosophila gut immunity. Science *310*, 847-850.

Haataja, L., Groffen, J., and Heisterkamp, N. (1997). Characterization of RAC3, a novel member of the Rho family. J Biol Chem *272*, 20384-20388.

Hall, T.A. (1999). BioEdit: a user-friendly biological sequence alignment editor and analysis program for Windows 95/98/NT. . Nucl Acids Symp Ser *41*, 95-98.

Han, C.H., Freeman, J.L., Lee, T., Motalebi, S.A., and Lambeth, J.D. (1998). Regulation of the neutrophil respiratory burst oxidase. Identification of an activation domain in p67(phox). J Biol Chem *273*, 16663-16668.

Harrigan, T.J., Abdullaev, I.F., Jourd'heuil, D., and Mongin, A.A. (2008). Activation of microglia with zymosan promotes excitatory amino acid release via volume-regulated anion channels: the role of NADPH oxidases. J Neurochem *106*, 2449-2462.

Harrison, J.E., and Schultz, J. (1976). Studies on the chlorinating activity of myeloperoxidase. J Biol Chem *251*, 1371-1374.

Helmcke, I., Heumuller, S., Tikkanen, R., Schroder, K., and Brandes, R.P. (2009). Identification of structural elements in Nox1 and Nox4 controlling localization and activity. Antioxid Redox Signal *11*, 1279-1287.

Hermoso, J.A., Mayoral, T., Faro, M., Gomez-Moreno, C., Sanz-Aparicio, J., and Medina, M. (2002). Mechanism of coenzyme recognition and binding revealed by crystal

structure analysis of ferredoxin-NADP+ reductase complexed with NADP+. J Mol Biol *319*, 1133-1142.

Heyworth, P.G., Bohl, B.P., Bokoch, G.M., and Curnutte, J.T. (1994). Rac translocates independently of the neutrophil NADPH oxidase components p47phox and p67phox. Evidence for its interaction with flavocytochrome b558. J Biol Chem *269*, 30749-30752.

Heyworth, P.G., Cross, A.R., and Curnutte, J.T. (2003). Chronic granulomatous disease. Curr Opin Immunol *15*, 578-584.

Heyworth, P.G., Curnutte, J.T., Nauseef, W.M., Volpp, B.D., Pearson, D.W., Rosen, H., and Clark, R.A. (1991). Neutrophil nicotinamide adenine dinucleotide phosphate oxidase assembly. Translocation of p47-phox and p67-phox requires interaction between p47-phox and cytochrome b558. J Clin Invest *87*, 352-356.

Hildebrandt, A., and Estabrook, R.W. (1971). Evidence for the participation of cytochrome b 5 in hepatic microsomal mixed-function oxidation reactions. Arch Biochem Biophys *143*, 66-79.

Hilenski, L.L., Clempus, R.E., Quinn, M.T., Lambeth, J.D., and Griendling, K.K. (2004). Distinct subcellular localizations of Nox1 and Nox4 in vascular smooth muscle cells. Arterioscler Thromb Vasc Biol *24*, 677-683.

Hirokawa, T., Boon-Chieng, S., and Mitaku, S. (1998). SOSUI: classification and secondary structure prediction system for membrane proteins. Bioinformatics *14*, 378-379.

Holm, L., and Rosenstrom, P. (2010). Dali server: conservation mapping in 3D. Nucleic Acids Res *38 Suppl*, W545-549.

Honbou, K., Minakami, R., Yuzawa, S., Takeya, R., Suzuki, N.N., Kamakura, S., Sumimoto, H., and Inagaki, F. (2007). Full-length p40phox structure suggests a basis for regulation mechanism of its membrane binding. EMBO J *26*, 1176-1186.

Honore, S., Kovacic, H., Pichard, V., Briand, C., and Rognoni, J.B. (2003). Alpha2beta1-integrin signaling by itself controls G1/S transition in a human adenocarcinoma cell line (Caco-2): implication of NADPH oxidase-dependent production of ROS. Exp Cell Res *285*, 59-71.

Hubbard, P.A., Shen, A.L., Paschke, R., Kasper, C.B., and Kim, J.J. (2001). NADPH-cytochrome P450 oxidoreductase. Structural basis for hydride and electron transfer. J Biol Chem *276*, 29163-29170.

Hultquist, D.E., and Passon, P.G. (1971). Catalysis of methaemoglobin reduction by erythrocyte cytochrome B5 and cytochrome B5 reductase. Nat New Biol *229*, 252-254.

Hwang, J., Kleinhenz, D.J., Lassegue, B., Griendling, K.K., Dikalov, S., and Hart, C.M. (2005). Peroxisome proliferator-activated receptor-gamma ligands regulate endothelial membrane superoxide production. Am J Physiol Cell Physiol *288*, C899-905.

Ibi, M., Matsuno, K., Shiba, D., Katsuyama, M., Iwata, K., Kakehi, T., Nakagawa, T., Sango, K., Shirai, Y., Yokoyama, T.*, et al.* (2008). Reactive oxygen species derived from NOX1/NADPH oxidase enhance inflammatory pain. J Neurosci *28*, 9486-9494.

Ilari, A., Bonamore, A., Farina, A., Johnson, K.A., and Boffi, A. (2002). The X-ray structure of ferric Escherichia coli flavohemoglobin reveals an unexpected geometry of the distal heme pocket. J Biol Chem *277*, 23725-23732.

Imajoh-Ohmi, S., Tokita, K., Ochiai, H., Nakamura, M., and Kanegasaki, S. (1992). Topology of cytochrome b558 in neutrophil membrane analyzed by anti-peptide antibodies and proteolysis. J Biol Chem *267*, 180-184.

Infanger, D.W., Sharma, R.V., and Davisson, R.L. (2006). NADPH oxidases of the brain: distribution, regulation, and function. Antioxid Redox Signal *8*, 1583-1596.

Ingelman, M., Bianchi, V., and Eklund, H. (1997). The three-dimensional structure of flavodoxin reductase from Escherichia coli at 1.7 A resolution. J Mol Biol *268*, 147-157.

Ismail, S., Sturrock, A., Wu, P., Cahill, B., Norman, K., Huecksteadt, T., Sanders, K., Kennedy, T., and Hoidal, J. (2009). NOX4 mediates hypoxia-induced proliferation of human pulmonary artery smooth muscle cells: the role of autocrine production of transforming growth factor-{beta}1 and insulin-like growth factor binding protein-3. Am J Physiol Lung Cell Mol Physiol *296*, L489-499.

Isogai, Y., Iizuka, T., and Shiro, Y. (1995). The mechanism of electron donation to molecular oxygen by phagocytic cytochrome b558. J Biol Chem *270*, 7853-7857.

Iyanagi, T., and Mason, H.S. (1973). Some properties of hepatic reduced nicotinamide adenine dinucleotide phosphate-cytochrome c reductase. Biochemistry *12*, 2297-2308.

Jackson, H.M., Kawahara, T., Nisimoto, Y., Smith, S.M., and Lambeth, J.D. (2010). Nox4 B-loop creates an interface between the transmembrane and dehydrogenase domains. J Biol Chem *285*, 10281-10290.

Jagnandan, D., Church, J.E., Banfi, B., Stuehr, D.J., Marrero, M.B., and Fulton, D.J. (2007). Novel mechanism of activation of NADPH oxidase 5. calcium sensitization via phosphorylation. J Biol Chem *282*, 6494-6507.

Jameson, D.M., and Seifried, S.E. (1999). Quantification of protein-protein interactions using fluorescence polarization. Methods *19*, 222-233.

Jay, D.B., Papaharalambus, C.A., Seidel-Rogol, B., Dikalova, A.E., Lassegue, B., and Griendling, K.K. (2008). Nox5 mediates PDGF-induced proliferation in human aortic smooth muscle cells. Free Radic Biol Med *45*, 329-335.

Jones, S.W., Christison, R., Bundell, K., Voyce, C.J., Brockbank, S.M., Newham, P., and Lindsay, M.A. (2005). Characterisation of cell-penetrating peptide-mediated peptide delivery. Br J Pharmacol *145*, 1093-1102.

Kami, K., Takeya, R., Sumimoto, H., and Kohda, D. (2002). Diverse recognition of non-PxxP peptide ligands by the SH3 domains from p67(phox), Grb2 and Pex13p. EMBO J *21*, 4268-4276.

Kanai, F., Liu, H., Field, S.J., Akbary, H., Matsuo, T., Brown, G.E., Cantley, L.C., and Yaffe, M.B. (2001). The PX domains of p47phox and p40phox bind to lipid products of PI(3)K. Nat Cell Biol *3*, 675-678.

Kaneda, M., Sakuraba, H., Ohtake, A., Nishida, A., Kiryu, C., and Kakinuma, K. (1999). Missense mutations in the gp91-phox gene encoding cytochrome b558 in patients with cytochrome b positive and negative X-linked chronic granulomatous disease. Blood *93*, 2098-2104.

Kao, Y.Y., Gianni, D., Bohl, B., Taylor, R.M., and Bokoch, G.M. (2008). Identification of a conserved Rac-binding site on NADPH oxidases supports a direct GTPase regulatory mechanism. J Biol Chem *283*, 12736-12746.

Karathanassis, D., Stahelin, R.V., Bravo, J., Perisic, O., Pacold, C.M., Cho, W., and Williams, R.L. (2002). Binding of the PX domain of p47(phox) to phosphatidylinositol 3,4-bisphosphate and phosphatidic acid is masked by an intramolecular interaction. EMBO J *21*, 5057-5068.

Karlsson, A., Beharry, Z.M., Matthew Eby, D., Coulter, E.D., Neidle, E.L., Kurtz, D.M., Jr., Eklund, H., and Ramaswamy, S. (2002). X-ray crystal structure of benzoate 1,2-dioxygenase reductase from Acinetobacter sp. strain ADP1. J Mol Biol *318*, 261-272.

Karplus, P.A., Daniels, M.J., and Herriott, J.R. (1991). Atomic structure of ferredoxin-NADP+ reductase: prototype for a structurally novel flavoenzyme family. Science *251*, 60-66.

Kawahara, T., Kohjima, M., Kuwano, Y., Mino, H., Teshima-Kondo, S., Takeya, R., Tsunawaki, S., Wada, A., Sumimoto, H., and Rokutan, K. (2005a). Helicobacter pylori lipopolysaccharide activates Rac1 and transcription of NADPH oxidase Nox1 and its organizer NOXO1 in guinea pig gastric mucosal cells. Am J Physiol Cell Physiol *288*, C450-457.

Kawahara, T., and Lambeth, J.D. (2007). Molecular evolution of Phox-related regulatory subunits for NADPH oxidase enzymes. BMC Evol Biol *7*, 178.

Kawahara, T., and Lambeth, J.D. (2008). Phosphatidylinositol (4,5)-bisphosphate modulates Nox5 localization via an N-terminal polybasic region. Mol Biol Cell *19*, 4020-4031.

Kawahara, T., Quinn, M.T., and Lambeth, J.D. (2007). Molecular evolution of the reactive oxygen-generating NADPH oxidase (Nox/Duox) family of enzymes. BMC Evol Biol *7*, 109.

Kawahara, T., Ritsick, D., Cheng, G., and Lambeth, J.D. (2005b). Point mutations in the proline-rich region of p22phox are dominant inhibitors of Nox1- and Nox2-dependent reactive oxygen generation. J Biol Chem *280*, 31859-31869.

Kelley, L.A., and Sternberg, M.J. (2009). Protein structure prediction on the Web: a case study using the Phyre server. Nat Protoc *4*, 363-371.

Keyes, S.R., and Cinti, D.L. (1980). Biochemical properties of cytochrome b5-dependent microsomal fatty acid elongation and identification of products. J Biol Chem *255*, 11357-11364.

Kikuchi, H., Hikage, M., Miyashita, H., and Fukumoto, M. (2000). NADPH oxidase subunit, gp91(phox) homologue, preferentially expressed in human colon epithelial cells. Gene *254*, 237-243.

Kim, S., Suga, M., Ogasahara, K., Ikegami, T., Minami, Y., Yubisui, T., and Tsukihara, T. (2007). Structure of Physarum polycephalum cytochrome b5 reductase at 1.56 A resolution. Acta Crystallogr Sect F Struct Biol Cryst Commun *63*, 274-279.

Kimura, S., Nishida, H., and Iyanagi, T. (2001). Effects of flavin-binding motif amino acid mutations in the NADH-cytochrome b5 reductase catalytic domain on protein stability and catalysis. J Biochem *130*, 481-490.

Kiss, P.J., Knisz, J., Zhang, Y., Baltrusaitis, J., Sigmund, C.D., Thalmann, R., Smith, R.J., Verpy, E., and Banfi, B. (2006). Inactivation of NADPH oxidase organizer 1 results in severe imbalance. Curr Biol *16*, 208-213.

Knaus, U.G., Heyworth, P.G., Evans, T., Curnutte, J.T., and Bokoch, G.M. (1991). Regulation of phagocyte oxygen radical production by the GTP-binding protein Rac 2. Science *254*, 1512-1515.

Kobayashi, S., Nojima, Y., Shibuya, M., and Maru, Y. (2004). Nox1 regulates apoptosis and potentially stimulates branching morphogenesis in sinusoidal endothelial cells. Exp Cell Res *300*, 455-462.

Kreck, M.L., Freeman, J.L., Abo, A., and Lambeth, J.D. (1996). Membrane association of Rac is required for high activity of the respiratory burst oxidase. Biochemistry *35*, 15683-15692.

Kumar, S., Molina-Cruz, A., Gupta, L., Rodrigues, J., and Barillas-Mury, C. (2010). A peroxidase/dual oxidase system modulates midgut epithelial immunity in Anopheles gambiae. Science *327*, 1644-1648.

Kumar, S., and Weaver, V.M. (2009). Mechanics, malignancy, and metastasis: the force journey of a tumor cell. Cancer Metastasis Rev *28*, 113-127.

Kuroda, J., Nakagawa, K., Yamasaki, T., Nakamura, K., Takeya, R., Kuribayashi, F., Imajoh-Ohmi, S., Igarashi, K., Shibata, Y., Sueishi, K.*, et al.* (2005). The superoxide-producing NAD(P)H oxidase Nox4 in the nucleus of human vascular endothelial cells. Genes Cells *10*, 1139-1151.

Lambeth, J.D. (2004). NOX enzymes and the biology of reactive oxygen. Nat Rev Immunol *4*, 181-189.

Lambeth, J.D., Cheng, G., Arnold, R.S., and Edens, W.A. (2000). Novel homologs of gp91phox. Trends Biochem Sci *25*, 459-461.

Lambeth, J.D., Krause, K.H., and Clark, R.A. (2008). NOX enzymes as novel targets for drug development. Semin Immunopathol *30*, 339-363.

Lapouge, K., Smith, S.J., Walker, P.A., Gamblin, S.J., Smerdon, S.J., and Rittinger, K. (2000). Structure of the TPR domain of p67phox in complex with Rac.GTP. Mol Cell *6*, 899-907.

Larkin, M.A., Blackshields, G., Brown, N.P., Chenna, R., McGettigan, P.A., McWilliam, H., Valentin, F., Wallace, I.M., Wilm, A., Lopez, R.*, et al.* (2007). Clustal W and Clustal X version 2.0. Bioinformatics *23*, 2947-2948.

Laskowski, R.A., MacArthur M. W., Moss, D.S., Thornton, J. M. (1993). PROCHECK - a program to check the stereochemical quality of protein structures. Journal of Applied Crystallography *26*, 283-291.

Lassegue, B., and Griendling, K.K. (2010). NADPH oxidases: functions and pathologies in the vasculature. Arterioscler Thromb Vasc Biol *30*, 653-661.

Lassegue, B., Sorescu, D., Szocs, K., Yin, Q., Akers, M., Zhang, Y., Grant, S.L., Lambeth, J.D., and Griendling, K.K. (2001). Novel gp91(phox) homologues in vascular smooth muscle cells : nox1 mediates angiotensin II-induced superoxide formation and redox-sensitive signaling pathways. Circ Res *88*, 888-894.

Laurent, E., McCoy, J.W., 3rd, Macina, R.A., Liu, W., Cheng, G., Robine, S., Papkoff, J., and Lambeth, J.D. (2008). Nox1 is over-expressed in human colon cancers and correlates with activating mutations in K-Ras. Int J Cancer *123*, 100-107.

Lee, M.Y., San Martin, A., Mehta, P.K., Dikalova, A.E., Garrido, A.M., Datla, S.R., Lyons, E., Krause, K.H., Banfi, B., Lambeth, J.D.*, et al.* (2009). Mechanisms of vascular smooth muscle NADPH oxidase 1 (Nox1) contribution to injury-induced neointimal formation. Arterioscler Thromb Vasc Biol *29*, 480-487.

Leusen, J.H., Meischl, C., Eppink, M.H., Hilarius, P.M., de Boer, M., Weening, R.S., Ahlin, A., Sanders, L., Goldblatt, D., Skopczynska, H.*, et al.* (2000). Four novel

mutations in the gene encoding gp91-phox of human NADPH oxidase: consequences for oxidase assembly. Blood *95*, 666-673.

Li, J., Stouffs, M., Serrander, L., Banfi, B., Bettiol, E., Charnay, Y., Steger, K., Krause, K.H., and Jaconi, M.E. (2006). The NADPH oxidase NOX4 drives cardiac differentiation: Role in regulating cardiac transcription factors and MAP kinase activation. Mol Biol Cell *17*, 3978-3988.

Li, S., Tabar, S.S., Malec, V., Eul, B.G., Klepetko, W., Weissmann, N., Grimminger, F., Seeger, W., Rose, F., and Hanze, J. (2008). NOX4 regulates ROS levels under normoxic and hypoxic conditions, triggers proliferation, and inhibits apoptosis in pulmonary artery adventitial fibroblasts. Antioxid Redox Signal *10*, 1687-1698.

Li, X., Marchal, C.C., Stull, N.D., Stahelin, R.V., and Dinauer, M.C. (2010). p47phox PX domain regulates plasma membrane but not phagosome neutrophil NADPH oxidase activation. J Biol Chem.

Li, X.J., Grunwald, D., Mathieu, J., Morel, F., and Stasia, M.J. (2005). Crucial role of two potential cytosolic regions of Nox2, 191TSSTKTIRRS200 and 484DESQANHFAVHHDEEKD500, on NADPH oxidase activation. J Biol Chem *280*, 14962-14973.

Lim, S.D., Sun, C., Lambeth, J.D., Marshall, F., Amin, M., Chung, L., Petros, J.A., and Arnold, R.S. (2005). Increased Nox1 and hydrogen peroxide in prostate cancer. Prostate *62*, 200-207.

Lu, G., Lindqvist, Y., Schneider, G., Dwivedi, U., and Campbell, W. (1995). Structural studies on corn nitrate reductase: refined structure of the cytochrome b reductase fragment at 2.5 A, its ADP complex and an active-site mutant and modeling of the cytochrome b domain. J Mol Biol *248*, 931-948.

Lyle, A.N., Deshpande, N.N., Taniyama, Y., Seidel-Rogol, B., Pounkova, L., Du, P., Papaharalambus, C., Lassegue, B., and Griendling, K.K. (2009). Poldip2, a novel regulator of Nox4 and cytoskeletal integrity in vascular smooth muscle cells. Circ Res *105*, 249-259.

Maehara, Y., Miyano, K., and Sumimoto, H. (2009). Role for the first SH3 domain of p67phox in activation of superoxide-producing NADPH oxidases. Biochem Biophys Res Commun *379*, 589-593.

Mahadev, K., Motoshima, H., Wu, X., Ruddy, J.M., Arnold, R.S., Cheng, G., Lambeth, J.D., and Goldstein, B.J. (2004). The NAD(P)H oxidase homolog Nox4 modulates insulin-stimulated generation of H2O2 and plays an integral role in insulin signal transduction. Mol Cell Biol *24*, 1844-1854.

Malec, V., Gottschald, O.R., Li, S., Rose, F., Seeger, W., and Hanze, J. (2010). HIF-1 alpha signaling is augmented during intermittent hypoxia by induction of the Nrf2

pathway in NOX1-expressing adenocarcinoma A549 cells. Free Radic Biol Med *48*, 1626-1635.

Marcoux, J., Man, P., Petit-Haertlein, I., Vives, C., Forest, E., and Fieschi, F. (2010). p47phox Molecular Activation for Assembly of the Neutrophil NADPH Oxidase Complex. J Biol Chem *285*, 28980-28990.

Martyn, K.D., Frederick, L.M., von Loehneysen, K., Dinauer, M.C., and Knaus, U.G. (2006). Functional analysis of Nox4 reveals unique characteristics compared to other NADPH oxidases. Cell Signal *18*, 69-82.

Massenet, C., Chenavas, S., Cohen-Addad, C., Dagher, M.C., Brandolin, G., Pebay-Peyroula, E., and Fieschi, F. (2005). Effects of p47phox C terminus phosphorylations on binding interactions with p40phox and p67phox. Structural and functional comparison of p40phox and p67phox SH3 domains. J Biol Chem *280*, 13752-13761.

McCord, J.M., and Fridovich, I. (1969). Superoxide dismutase. An enzymic function for erythrocuprein (hemocuprein). J Biol Chem *244*, 6049-6055.

Medina, M., Luquita, A., Tejero, J., Hermoso, J., Mayoral, T., Sanz-Aparicio, J., Grever, K., and Gomez-Moreno, C. (2001). Probing the determinants of coenzyme specificity in ferredoxin-NADP+ reductase by site-directed mutagenesis. J Biol Chem *276*, 11902-11912.

Meitzler, J.L., and Ortiz de Montellano, P.R. (2009). Caenorhabditis elegans and human dual oxidase 1 (DUOX1) "peroxidase" domains: insights into heme binding and catalytic activity. J Biol Chem *284*, 18634-18643.

Meng, D., Lv, D.D., and Fang, J. (2008). Insulin-like growth factor-I induces reactive oxygen species production and cell migration through Nox4 and Rac1 in vascular smooth muscle cells. Cardiovasc Res *80*, 299-308.

Miller, F.J., Jr., Filali, M., Huss, G.J., Stanic, B., Chamseddine, A., Barna, T.J., and Lamb, F.S. (2007). Cytokine activation of nuclear factor kappa B in vascular smooth muscle cells requires signaling endosomes containing Nox1 and ClC-3. Circ Res *101*, 663-671.

Mitchell, J.A., Kohlhaas, K.L., Matsumoto, T., Pollock, J.S., Forstermann, U., Warner, T.D., Schmidt, H.H., and Murad, F. (1992). Induction of NADPH-dependent diaphorase and nitric oxide synthase activity in aortic smooth muscle and cultured macrophages. Mol Pharmacol *41*, 1163-1168.

Miyano, K., Koga, H., Minakami, R., and Sumimoto, H. (2009). The insert region of the Rac GTPases is dispensable for activation of superoxide-producing NADPH oxidases. Biochem J *422*, 373-382.

Miyano, K., Ogasawara, S., Han, C.H., Fukuda, H., and Tamura, M. (2001). A fusion protein between rac and p67phox (1-210) reconstitutes NADPH oxidase with higher activity and stability than the individual components. Biochemistry *40*, 14089-14097.

Mizrahi, A., Berdichevsky, Y., Ugolev, Y., Molshanski-Mor, S., Nakash, Y., Dahan, I., Alloul, N., Gorzalczany, Y., Sarfstein, R., Hirshberg, M.*, et al.* (2006). Assembly of the phagocyte NADPH oxidase complex: chimeric constructs derived from the cytosolic components as tools for exploring structure-function relationships. J Leukoc Biol *79*, 881-895.

Mochizuki, T., Furuta, S., Mitsushita, J., Shang, W.H., Ito, M., Yokoo, Y., Yamaura, M., Ishizone, S., Nakayama, J., Konagai, A.*, et al.* (2006). Inhibition of NADPH oxidase 4 activates apoptosis via the AKT/apoptosis signal-regulating kinase 1 pathway in pancreatic cancer PANC-1 cells. Oncogene *25*, 3699-3707.

Mofarrahi, M., Brandes, R.P., Gorlach, A., Hanze, J., Terada, L.S., Quinn, M.T., Mayaki, D., Petrof, B., and Hussain, S.N. (2008). Regulation of proliferation of skeletal muscle precursor cells by NADPH oxidase. Antioxid Redox Signal *10*, 559-574.

Moore, G.R., Pettigrew, G.W., and Rogers, N.K. (1986). Factors influencing redox potentials of electron transfer proteins. Proc Natl Acad Sci U S A *83*, 4998-4999.

Morand, S., Ueyama, T., Tsujibe, S., Saito, N., Korzeniowska, A., and Leto, T.L. (2009). Duox maturation factors form cell surface complexes with Duox affecting the specificity of reactive oxygen species generation. FASEB J *23*, 1205-1218.

Moreno, J.C., Bikker, H., Kempers, M.J., van Trotsenburg, A.S., Baas, F., de Vijlder, J.J., Vulsma, T., and Ris-Stalpers, C. (2002). Inactivating mutations in the gene for thyroid oxidase 2 (THOX2) and congenital hypothyroidism. N Engl J Med *347*, 95-102.

Moser, C.C., Chobot, S.E., Page, C.C., and Dutton, P.L. (2008). Distance metrics for heme protein electron tunneling. Biochim Biophys Acta *1777*, 1032-1037.

Nagamani, S.C., Erez, A., Eng, C., Ou, Z., Chinault, C., Workman, L., Coldwell, J., Stankiewicz, P., Patel, A., Lupski, J.R.*, et al.* (2009). Interstitial deletion of 6q25.2-q25.3: a novel microdeletion syndrome associated with microcephaly, developmental delay, dysmorphic features and hearing loss. Eur J Hum Genet *17*, 573-581.

Nakano, Y., Longo-Guess, C.M., Bergstrom, D.E., Nauseef, W.M., Jones, S.M., and Banfi, B. (2008). Mutation of the Cyba gene encoding p22phox causes vestibular and immune defects in mice. J Clin Invest *118*, 1176-1185.

Nisimoto, Y., Freeman, J.L., Motalebi, S.A., Hirshberg, M., and Lambeth, J.D. (1997). Rac binding to p67(phox). Structural basis for interactions of the Rac1 effector region and insert region with components of the respiratory burst oxidase. J Biol Chem *272*, 18834-18841.

Nisimoto, Y., Jackson, H.M., Ogawa, H., Kawahara, T., and Lambeth, J.D. (2010). Constitutive NADPH-dependent electron transferase activity of the Nox4 dehydrogenase domain. Biochemistry *49*, 2433-2442.

Nisimoto, Y., Motalebi, S., Han, C.H., and Lambeth, J.D. (1999). The p67(phox) activation domain regulates electron flow from NADPH to flavin in flavocytochrome b(558). J Biol Chem *274*, 22999-23005.

Nisimoto, Y., Ogawa, H., Miyano, K., and Tamura, M. (2004). Activation of the flavoprotein domain of gp91phox upon interaction with N-terminal p67phox (1-210) and the Rac complex. Biochemistry *43*, 9567-9575.

Nisimoto, Y., Tsubouchi, R., Diebold, B.A., Qiao, S., Ogawa, H., Ohara, T., and Tamura, M. (2008). Activation of NADPH oxidase 1 in tumour colon epithelial cells. Biochem J *415*, 57-65.

Norager, S., Arent, S., Bjornberg, O., Ottosen, M., Lo Leggio, L., Jensen, K.F., and Larsen, S. (2003). Lactococcus lactis dihydroorotate dehydrogenase A mutants reveal important facets of the enzymatic function. J Biol Chem *278*, 28812-28822.

Olson, S.T., and Massey, V. (1979). Purification and properties of the flavoenzyme D-lactate dehydrogenase from Megasphaera elsdenii. Biochemistry *18*, 4714-4724.

Pacher, P., Beckman, J.S., and Liaudet, L. (2007). Nitric oxide and peroxynitrite in health and disease. Physiol Rev *87*, 315-424.

Paffenholz, R., Bergstrom, R.A., Pasutto, F., Wabnitz, P., Munroe, R.J., Jagla, W., Heinzmann, U., Marquardt, A., Bareiss, A., Laufs, J.*, et al.* (2004). Vestibular defects in head-tilt mice result from mutations in Nox3, encoding an NADPH oxidase. Genes Dev *18*, 486-491.

Pao, M., Wiggs, E.A., Anastacio, M.M., Hyun, J., DeCarlo, E.S., Miller, J.T., Anderson, V.L., Malech, H.L., Gallin, J.I., and Holland, S.M. (2004). Cognitive function in patients with chronic granulomatous disease: a preliminary report. Psychosomatics *45*, 230-234.

Park, M.Y., Imajoh-Ohmi, S., Nunoi, H., and Kanegasaki, S. (1997). Synthetic peptides corresponding to various hydrophilic regions of the large subunit of cytochrome b558 inhibit superoxide generation in a cell-free system from neutrophils. Biochem Biophys Res Commun *234*, 531-536.

Parkos, C.A., Allen, R.A., Cochrane, C.G., and Jesaitis, A.J. (1987). Purified cytochrome b from human granulocyte plasma membrane is comprised of two polypeptides with relative molecular weights of 91,000 and 22,000. J Clin Invest *80*, 732-742.

Pedruzzi, E., Guichard, C., Ollivier, V., Driss, F., Fay, M., Prunet, C., Marie, J.C., Pouzet, C., Samadi, M., Elbim, C.*, et al.* (2004). NAD(P)H oxidase Nox-4 mediates 7-ketocholesterol-induced endoplasmic reticulum stress and apoptosis in human aortic smooth muscle cells. Mol Cell Biol *24*, 10703-10717.

Perrin, F. (1926). Polarization de la lumiere de fluorescence.Vie moyenne de molecules dans l'etat excite. J Phys Radium *7*.

Pessach, I., Leto, T.L., Malech, H.L., and Levy, R. (2001). Essential requirement of cytosolic phospholipase A(2) for stimulation of NADPH oxidase-associated diaphorase activity in granulocyte-like cells. J Biol Chem *276*, 33495-33503.

Pessach, I., Shmelzer, Z., Leto, T.L., Dinauer, M.C., and Levy, R. (2006). The C-terminal flavin domain of gp91phox bound to plasma membranes of granulocyte-like X-CGD PLB-985 cells is sufficient to anchor cytosolic oxidase components and support NADPH oxidase-associated diaphorase activity independent of cytosolic phospholipase A2 regulation. J Leukoc Biol *80*, 630-639.

Petry, A., Djordjevic, T., Weitnauer, M., Kietzmann, T., Hess, J., and Gorlach, A. (2006). NOX2 and NOX4 mediate proliferative response in endothelial cells. Antioxid Redox Signal *8*, 1473-1484.

Ponting, C.P. (1996). Novel domains in NADPH oxidase subunits, sorting nexins, and PtdIns 3-kinases: binding partners of SH3 domains? Protein Sci *5*, 2353-2357.

Rao, S.T., and Rossmann, M.G. (1973). Comparison of super-secondary structures in proteins. J Mol Biol *76*, 241-256.

Reddy, V.V., Kupfer, D., and Caspi, E. (1977). Mechanism of C-5 double bond introduction in the biosynthesis of cholesterol by rat liver microsomes. J Biol Chem *252*, 2797-2801.

Rey, F.E., Cifuentes, M.E., Kiarash, A., Quinn, M.T., and Pagano, P.J. (2001). Novel competitive inhibitor of NAD(P)H oxidase assembly attenuates vascular O(2)(-) and systolic blood pressure in mice. Circ Res *89*, 408-414.

Richardson, J.S., and Richardson, D.C. (1988). Amino acid preferences for specific locations at the ends of alpha helices. Science *240*, 1648-1652.

Rigutto, S., Hoste, C., Grasberger, H., Milenkovic, M., Communi, D., Dumont, J.E., Corvilain, B., Miot, F., and De Deken, X. (2009). Activation of dual oxidases Duox1 and Duox2: differential regulation mediated by camp-dependent protein kinase and protein kinase C-dependent phosphorylation. J Biol Chem *284*, 6725-6734.

Ritsick, D.R., Edens, W.A., Finnerty, V., and Lambeth, J.D. (2007). Nox regulation of smooth muscle contraction. Free Radic Biol Med *43*, 31-38.

Roman, L.J., McLain, J., and Masters, B.S. (2003). Chimeric enzymes of cytochrome P450 oxidoreductase and neuronal nitric-oxide synthase reductase domain reveal structural and functional differences. J Biol Chem *278*, 25700-25707.

Rost, B., Yachdav, G., and Liu, J. (2004). The PredictProtein server. Nucleic Acids Res *32*, W321-326.

Rotrosen, D., Yeung, C.L., Leto, T.L., Malech, H.L., and Kwong, C.H. (1992). Cytochrome b558: the flavin-binding component of the phagocyte NADPH oxidase. Science *256*, 1459-1462.

Roy, A., Kucukural, A., and Zhang, Y. (2010). I-TASSER: a unified platform for automated protein structure and function prediction. Nat Protoc *5*, 725-738.

Royer-Pokora, B., Kunkel, L.M., Monaco, A.P., Goff, S.C., Newburger, P.E., Baehner, R.L., Cole, F.S., Curnutte, J.T., and Orkin, S.H. (1986). Cloning the gene for an inherited human disorder--chronic granulomatous disease--on the basis of its chromosomal location. Nature *322*, 32-38.

Sali, A., and Blundell, T.L. (1993). Comparative protein modelling by satisfaction of spatial restraints. J Mol Biol *234*, 779-815.

Salmeen, A., Park, B.O., and Meyer, T. (2010). The NADPH oxidases NOX4 and DUOX2 regulate cell cycle entry via a p53-dependent pathway. Oncogene *29*, 4473-4484.

Sarfstein, R., Gorzalczany, Y., Mizrahi, A., Berdichevsky, Y., Molshanski-Mor, S., Weinbaum, C., Hirshberg, M., Dagher, M.C., and Pick, E. (2004). Dual role of Rac in the assembly of NADPH oxidase, tethering to the membrane and activation of p67phox: a study based on mutagenesis of p67phox-Rac1 chimeras. J Biol Chem *279*, 16007-16016.

Schacter, B.A., Nelson, E.B., Marver, H.S., and Masters, B.S. (1972). Immunochemical evidence for an association of heme oxygenase with the microsomal electron transport system. J Biol Chem *247*, 3601-3607.

Schapiro, B.L., Newburger, P.E., Klempner, M.S., and Dinauer, M.C. (1991). Chronic granulomatous disease presenting in a 69-year-old man. N Engl J Med *325*, 1786-1790.

Schellenberg, K.A., and Hellerman, L. (1958). Oxidation of reduced diphosphopyridine nucleotide. J Biol Chem *231*, 547-556.

Schilder, Y.D., Heiss, E.H., Schachner, D., Ziegler, J., Reznicek, G., Sorescu, D., and Dirsch, V.M. (2009). NADPH oxidases 1 and 4 mediate cellular senescence induced by resveratrol in human endothelial cells. Free Radic Biol Med *46*, 1598-1606.

Segal, A.W. (1981). The antimicrobial role of the neutrophil leukocyte. J Infect *3*, 3-17.

Segal, A.W., and Jones, O.T. (1978). Novel cytochrome b system in phagocytic vacuoles of human granulocytes. Nature *276*, 515-517.

Segal, A.W., West, I., Wientjes, F., Nugent, J.H., Chavan, A.J., Haley, B., Garcia, R.C., Rosen, H., and Scrace, G. (1992). Cytochrome b-245 is a flavocytochrome containing FAD and the NADPH-binding site of the microbicidal oxidase of phagocytes. Biochem J *284 (Pt 3)*, 781-788.

Serrander, L., Cartier, L., Bedard, K., Banfi, B., Lardy, B., Plastre, O., Sienkiewicz, A., Forro, L., Schlegel, W., and Krause, K.H. (2007). NOX4 activity is determined by mRNA levels and reveals a unique pattern of ROS generation. Biochem J *406*, 105-114.

Shatwell, K.P., Dancis, A., Cross, A.R., Klausner, R.D., and Segal, A.W. (1996). The FRE1 ferric reductase of Saccharomyces cerevisiae is a cytochrome b similar to that of NADPH oxidase. J Biol Chem *271*, 14240-14244.

Shin, M., and Arnon, D.I. (1965). Enzymic Mechanisms of Pyridine Nucleotide Reduction in Chloroplasts. J Biol Chem *240*, 1405-1411.

Shiose, A., Kuroda, J., Tsuruya, K., Hirai, M., Hirakata, H., Naito, S., Hattori, M., Sakaki, Y., and Sumimoto, H. (2001). A novel superoxide-producing NAD(P)H oxidase in kidney. J Biol Chem *276*, 1417-1423.

Shiraki, K., Kudou, M., Fujiwara, S., Imanaka, T., and Takagi, M. (2002). Biophysical effect of amino acids on the prevention of protein aggregation. J Biochem *132*, 591-595.

Shmelzer, Z., Karter, M., Eisenstein, M., Leto, T.L., Hadad, N., Ben-Menahem, D., Gitler, D., Banani, S., Wolach, B., Rotem, M*., et al.* (2008). Cytosolic phospholipase A2alpha is targeted to the p47phox-PX domain of the assembled NADPH oxidase via a novel binding site in its C2 domain. J Biol Chem *283*, 31898-31908.

Si, J., Fu, X., Behar, J., Wands, J., Beer, D.G., Souza, R.F., Spechler, S.J., Lambeth, D., and Cao, W. (2007). NADPH oxidase NOX5-S mediates acid-induced cyclooxygenase-2 expression via activation of NF-kappaB in Barrett's esophageal adenocarcinoma cells. J Biol Chem *282*, 16244-16255.

Sorce, S., and Krause, K.H. (2009). NOX enzymes in the central nervous system: from signaling to disease. Antioxid Redox Signal *11*, 2481-2504.

Sorescu, G.P., Song, H., Tressel, S.L., Hwang, J., Dikalov, S., Smith, D.A., Boyd, N.L., Platt, M.O., Lassegue, B., Griendling, K.K*., et al.* (2004). Bone morphogenic protein 4 produced in endothelial cells by oscillatory shear stress induces monocyte adhesion by stimulating reactive oxygen species production from a nox1-based NADPH oxidase. Circ Res *95*, 773-779.

Spencer, J.P., Wong, J., Jenner, A., Aruoma, O.I., Cross, C.E., and Halliwell, B. (1996). Base modification and strand breakage in isolated calf thymus DNA and in DNA from human skin epidermal keratinocytes exposed to peroxynitrite or 3-morpholinosydnonimine. Chem Res Toxicol *9*, 1152-1158.

Sridhar Prasad, G., Kresge, N., Muhlberg, A.B., Shaw, A., Jung, Y.S., Burgess, B.K., and Stout, C.D. (1998). The crystal structure of NADPH:ferredoxin reductase from Azotobacter vinelandii. Protein Sci *7*, 2541-2549.

Stahelin, R.V., Burian, A., Bruzik, K.S., Murray, D., and Cho, W. (2003). Membrane binding mechanisms of the PX domains of NADPH oxidase p40phox and p47phox. J Biol Chem *278*, 14469-14479.

Suh, Y.A., Arnold, R.S., Lassegue, B., Shi, J., Xu, X., Sorescu, D., Chung, A.B., Griendling, K.K., and Lambeth, J.D. (1999). Cell transformation by the superoxide-generating oxidase Mox1. Nature *401*, 79-82.

Sumimoto, H. (2008). Structure, regulation and evolution of Nox-family NADPH oxidases that produce reactive oxygen species. FEBS J *275*, 3249-3277.

Sumimoto, H., Sakamoto, N., Nozaki, M., Sakaki, Y., Takeshige, K., and Minakami, S. (1992). Cytochrome b558, a component of the phagocyte NADPH oxidase, is a flavoprotein. Biochem Biophys Res Commun *186*, 1368-1375.

Szanto, I., Rubbia-Brandt, L., Kiss, P., Steger, K., Banfi, B., Kovari, E., Herrmann, F., Hadengue, A., and Krause, K.H. (2005). Expression of NOX1, a superoxide-generating NADPH oxidase, in colon cancer and inflammatory bowel disease. J Pathol *207*, 164-176.

Takesue, S., and Omura, T. (1970). Solubilization of NADH-cytochrome b5 reductase from liver microsomes by lysosomal digestion. J Biochem *67*, 259-266.

Takeya, R., Ueno, N., Kami, K., Taura, M., Kohjima, M., Izaki, T., Nunoi, H., and Sumimoto, H. (2003). Novel human homologues of p47phox and p67phox participate in activation of superoxide-producing NADPH oxidases. J Biol Chem *278*, 25234-25246.

Taylor, W.R., Jones, D.T., and Segal, A.W. (1993). A structural model for the nucleotide binding domains of the flavocytochrome b-245 beta-chain. Protein Sci *2*, 1675-1685.

Teahan, C., Rowe, P., Parker, P., Totty, N., and Segal, A.W. (1987). The X-linked chronic granulomatous disease gene codes for the beta-chain of cytochrome b-245. Nature *327*, 720-721.

Thrasher, A.J., Keep, N.H., Wientjes, F., and Segal, A.W. (1994). Chronic granulomatous disease. Biochim Biophys Acta *1227*, 1-24.

Tirone, F., and Cox, J.A. (2007). NADPH oxidase 5 (NOX5) interacts with and is regulated by calmodulin. FEBS Lett *581*, 1202-1208.

Tirone, F., Radu, L., Craescu, C.T., and Cox, J.A. (2010). Identification of the binding site for the regulatory calcium-binding domain in the catalytic domain of NOX5. Biochemistry *49*, 761-771.

Tobar, N., Guerrero, J., Smith, P.C., and Martinez, J. (2010). NOX4-dependent ROS production by stromal mammary cells modulates epithelial MCF-7 cell migration. Br J Cancer.

Torchilin, V.P., Rammohan, R., Weissig, V., and Levchenko, T.S. (2001). TAT peptide on the surface of liposomes affords their efficient intracellular delivery even at low temperature and in the presence of metabolic inhibitors. Proc Natl Acad Sci U S A *98*, 8786-8791.

Touyz, R.M., Chen, X., Tabet, F., Yao, G., He, G., Quinn, M.T., Pagano, P.J., and Schiffrin, E.L. (2002). Expression of a functionally active gp91phox-containing neutrophil-type NAD(P)H oxidase in smooth muscle cells from human resistance arteries: regulation by angiotensin II. Circ Res *90*, 1205-1213.

Tsunawaki, S., Mizunari, H., Nagata, M., Tatsuzawa, O., and Kuratsuji, T. (1994). A novel cytosolic component, p40phox, of respiratory burst oxidase associates with p67phox and is absent in patients with chronic granulomatous disease who lack p67phox. Biochem Biophys Res Commun *199*, 1378-1387.

Tybulewicz, V.L., and Henderson, R.B. (2009). Rho family GTPases and their regulators in lymphocytes. Nat Rev Immunol *9*, 630-644.

Ueno, N., Takeya, R., Miyano, K., Kikuchi, H., and Sumimoto, H. (2005). The NADPH oxidase Nox3 constitutively produces superoxide in a p22phox-dependent manner: its regulation by oxidase organizers and activators. J Biol Chem *280*, 23328-23339.

Ueyama, T., Geiszt, M., and Leto, T.L. (2006). Involvement of Rac1 in activation of multicomponent Nox1- and Nox3-based NADPH oxidases. Mol Cell Biol *26*, 2160-2174.

Ushio-Fukai, M., Tang, Y., Fukai, T., Dikalov, S.I., Ma, Y., Fujimoto, M., Quinn, M.T., Pagano, P.J., Johnson, C., and Alexander, R.W. (2002). Novel role of gp91(phox)-containing NAD(P)H oxidase in vascular endothelial growth factor-induced signaling and angiogenesis. Circ Res *91*, 1160-1167.

Valko, M., Leibfritz, D., Moncol, J., Cronin, M.T., Mazur, M., and Telser, J. (2007). Free radicals and antioxidants in normal physiological functions and human disease. Int J Biochem Cell Biol *39*, 44-84.

Van Buul, J.D., Fernandez-Borja, M., Anthony, E.C., and Hordijk, P.L. (2005). Expression and localization of NOX2 and NOX4 in primary human endothelial cells. Antioxid Redox Signal *7*, 308-317.

Vermilion, J.L., Ballou, D.P., Massey, V., and Coon, M.J. (1981). Separate roles for FMN and FAD in catalysis by liver microsomal NADPH-cytochrome P-450 reductase. J Biol Chem *256*, 266-277.

Vignais, P.V. (2002). The superoxide-generating NADPH oxidase: structural aspects and activation mechanism. Cell Mol Life Sci *59*, 1428-1459.

Vigone, M.C., Fugazzola, L., Zamproni, I., Passoni, A., Di Candia, S., Chiumello, G., Persani, L., and Weber, G. (2005). Persistent mild hypothyroidism associated with novel sequence variants of the DUOX2 gene in two siblings. Hum Mutat *26*, 395.

Vives, E., Brodin, P., and Lebleu, B. (1997). A truncated HIV-1 Tat protein basic domain rapidly translocates through the plasma membrane and accumulates in the cell nucleus. J Biol Chem *272*, 16010-16017.

von Lohneysen, K., Noack, D., Wood, M.R., Friedman, J.S., and Knaus, U.G. (2009). Structural Insights into Nox4 and Nox2 - Motifs Involved in Function and Cellular Localization. Mol Cell Biol.

von Lohneysen, K., Noack, D., Wood, M.R., Friedman, J.S., and Knaus, U.G. (2010). Structural insights into Nox4 and Nox2: motifs involved in function and cellular localization. Mol Cell Biol *30*, 961-975.

Wang, M., Roberts, D.L., Paschke, R., Shea, T.M., Masters, B.S., and Kim, J.J. (1997). Three-dimensional structure of NADPH-cytochrome P450 reductase: prototype for FMN- and FAD-containing enzymes. Proc Natl Acad Sci U S A *94*, 8411-8416.

Weber, G. (1953). Rotational Brownian motion and polarization of the fluorescence of solutions. Adv Protein Chem *8*, 415-459.

Wilmot, C.M., and Thornton, J.M. (1988). Analysis and prediction of the different types of beta-turn in proteins. J Mol Biol *203*, 221-232.

Wilson, M.I., Gill, D.J., Perisic, O., Quinn, M.T., and Williams, R.L. (2003). PB1 domain-mediated heterodimerization in NADPH oxidase and signaling complexes of atypical protein kinase C with Par6 and p62. Mol Cell *12*, 39-50.

Winterbourn, C.C. (2008). Reconciling the chemistry and biology of reactive oxygen species. Nat Chem Biol *4*, 278-286.

Wong, J.L., Creton, R., and Wessel, G.M. (2004). The oxidative burst at fertilization is dependent upon activation of the dual oxidase Udx1. Dev Cell *7*, 801-814.

Yoshida, L.S., Saruta, F., Yoshikawa, K., Tatsuzawa, O., and Tsunawaki, S. (1998). Mutation at histidine 338 of gp91(phox) depletes FAD and affects expression of cytochrome b558 of the human NADPH oxidase. J Biol Chem *273*, 27879-27886.

Yu, L., Zhen, L., and Dinauer, M.C. (1997). Biosynthesis of the phagocyte NADPH oxidase cytochrome b558. Role of heme incorporation and heterodimer formation in maturation and stability of gp91phox and p22phox subunits. J Biol Chem *272*, 27288-27294.

Yuzawa, S., Ogura, K., Horiuchi, M., Suzuki, N.N., Fujioka, Y., Kataoka, M., Sumimoto, H., and Inagaki, F. (2004). Solution structure of the tandem Src homology 3 domains of p47phox in an autoinhibited form. J Biol Chem *279*, 29752-29760.

Zhang, H., Whitelegge, J.P., and Cramer, W.A. (2001). Ferredoxin:NADP+ oxidoreductase is a subunit of the chloroplast cytochrome b6f complex. J Biol Chem *276*, 38159-38165.

Zhang, Y. (2008). I-TASSER server for protein 3D structure prediction. BMC Bioinformatics *9*, 40.

Zhang, Y. (2009). I-TASSER: fully automated protein structure prediction in CASP8. Proteins *77 Suppl 9*, 100-113.

Zhou, M., Diwu, Z., Panchuk-Voloshina, N., and Haugland, R.P. (1997). A stable nonfluorescent derivative of resorufin for the fluorometric determination of trace hydrogen peroxide: applications in detecting the activity of phagocyte NADPH oxidase and other oxidases. Anal Biochem *253*, 162-168.